Université de Liège
Faculté des Sciences
Département de Physique

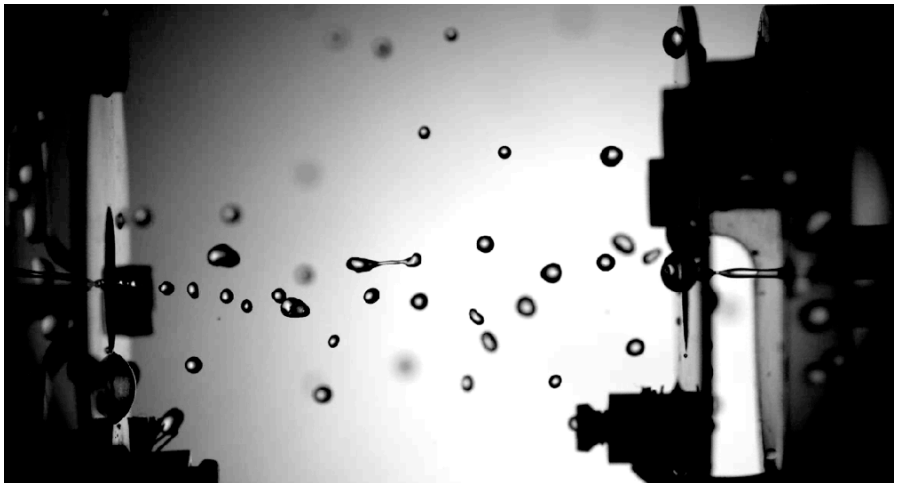

Influences of electric charges on an isolated drop

Brandenbourger Martin

Thèse présentée en vue de l'obtention du grade de Docteur en Sciences Physiques

Année académique 2015-2016

Université de Liège
Faculté des Sciences
Département de physique
GRASP

Thesis advisor: Dr. Stéphane Dorbolo

Université de Liège
Faculté des Sciences

Group for Research and Applications in Statistical Physics
Allée du 6 août, 19 B-4000 Liège, Belgium

email: martin.brandenbourger@gmail.com

Cette Thèse a été réalisée dans le cadre d'une bourse de doctorat fournie par le Fonds pour la formation à la Recherche dans l'Industrie et dans l'Agriculture (FRIA) financé par le Fonds de la Recherche Scientifique - FNRS (FRS - FNRS).

Thèse présentée en vue de l'obtention du grade
de Docteur en Sciences Physiques
Année académique 2015-2016

Remerciements

En premier lieu, je tiens à remercier les professeurs Álvaro Marín, Antonin Eddi, Benoît Scheid, Hervé Caps et John Martin d'avoir accepté de faire partie de mon Jury de thèse. C'est une grande joie pour moi que chacun d'eux aient accepté de prendre le temps de juger mon travail.

En second lieu, j'aimerais remercier la personne qui m'a fait aimer la recherche, Stéphane Dorbolo. Stéphane, ton style unique et ton approche de la recherche m'ont toujours impressionnés. Cette façon de toujours trouver de nouveaux angles d'approches et de monter de magnifiques projets a été très inspirante. Au-delà de cela, ton écoute et ton intarissable flot d'idées m'ont toujours motivés. Ta façon de toujours apporter de la bonne humeur et surtout de la bonne entente au sein du laboratoire n'a pas de prix. Enfin, ta patiente et ta sincérité ont constitués le terreau fertile qui m'amène aujourd'hui à présenter ce manuscrit. En somme, merci pour ton aide et tous ces chouettes moments partagés.

Bien entendu, cette thèse ne fut pas qu'un échange bilatéral, beaucoup d'autres intervenants ont contribué à la réalisation de ce travail. Cette thèse a été réalisée au sein du laboratoire GRASP. Je suis profondément convaincu que l'ambiance d'innovation, d'amitié et d'échange permanent ont énormément contribué à mon travail. En particulier, j'aimerais tout d'abord remercier Laurent Maquet, Baptiste Darbois-Texier, Hervé Caps et Pierre-Brice Bintein.

Laurent, nos habitudes de vieux couple lors de nos sessions de mesures m'ont beaucoup appris. C'est en faisant nos premiers pas d'expérimentateurs que nous nous sommes rencontrés et c'est en vrais potes que l'on finit notre thèse à quelques mois d'intervalle. Qui aime bien châtie bien, je crois que ce dicton nous va incroyablement bien. Surtout ne change pas, sauf si ton médecin te le recommande.

Baptiste, tu es une personne incroyable, aussi bien dans le laboratoire qu'en dehors. Ta motivation et ton optimisme m'ont ouvert les yeux à de nombreuses reprises. Tes deux ans passés au laboratoire ont sans aucun doute contribué à forger le chercheur que je suis aujourd'hui. Il va falloir trouver de nouvelles excuses pour encore travailler ensemble !

Hervé, tes compétences en matière de transfert de connaissance ont construit le physicien que je suis. Evidemment, cette phrase doit être présente dans la majorité des thèses du GRASP, mais ce qui est pour moi particulier, c'est que j'ai découvert l'université de Liège grâce à ta capacité à retirer une nappe d'une table sans faire bouger des assiettes. Grâce à toi, Science et Culture a donc été le catalyseur de ma passion pour la physique. Au-delà de ton instruction, je tiens à te remercier pour tous ces bons moments passés ensemble, en particulier dans la région de Bordeaux !

Pierre-Brice, le petit nouveau, je pense qu'on a beaucoup de point de ressemblance. Je regrette terriblement de n'avoir pas eu plus de temps pour maniper avec toi. Occupe-toi bien de Stéphane après notre départ à Laurent et moi. Enfin, merci pour tes conseils avisés et pour avoir trouvé un titre à cette thèse.

Mes chers voisins de bureau, pour ne pas les citer Nicolas, Charles, Alexis et Sofiene, nos petites discussions et les photos de Charles vont me manquer. Un merci tout particulier à Alexis pour ses relectures éclairées et éclairantes.

Je remercie également Geoffroy, Eric, Médéric et presque tous ceux cités plus haut pour les moments Pavé et Minus. Ces moments de pure détente ont aussi permis de forger un fort esprit d'équipe et de belles amitiés.

Dans le top des contributeurs de cette thèse, je me dois également de citer Médéric, Samuel, Jean-Claude, Florian et Chouaib. Les gars, vous avez des mains en or et des compétences que je rêverais d'avoir. Ces deux dons ont permis de réaliser une bonne partie des montages présentés dans cette thèse et pour cela, je vous remercie. J'ajouterais une note toute particulière pour Médéric et Sam, avec qui j'ai passé de supers moments à l'ESTEC aux Pays-Bas. J'aurais voulu que ces moments se reproduisent plus souvent.

Bien entendu, le GRASP est constitué de beaucoup d'autres membres incroyables. Nicolas Vandewalle, Julien, Martial, Alexis Darras, François Ludwig, Maxime, Arianne, Boris, Florianne, Martin Poty, Galien et Sébastien, je vous remercie pour chacun des longs ou brefs moments passés avec vous. En particulier, Nicolas, merci pour ton incroyable soutien et Julien, merci pour tes incroyables blagues. De la même manière, je remercie Maryam, Florian Moreau, Felipe, Jérôme, Louis, Guillaume, Antonella et Eline. Même si vos passages ont été trop brefs pour certains d'entre vous, j'ai vraiment apprécié chacune de vos personnalités.

I would like to extent a special thank to Tadd Truscott and his two PhD students Zhao and Nathan. Tadd, thank for your stay in Belgium. I think I never learned so many things in such a small period of time. You are an amazing person, not only in research, but also in everyday life. I am really impressed by the way you are always driven by passion. Zhao, I love your efficiency and Nathan it was a real pleasure to have you in the lab.

Durant ma première année de thèse, j'ai également eu l'occasion de passer trois mois au laboratoire de la compagnie des interfaces, sous l'encadrement de David Quéré. David, merci de m'avoir ouvert la porte de ce laboratoire exceptionnel. Durant mon séjour, j'ai eu l'occasion de rencontrer des gens passionnants. Certains, sans que le hasard y soit pour quelque chose, ont déjà été cités plus haut. Ainsi, Eline, Philippe, Pierre-Brice, Baptiste, Dan, Guillaume, Timothée, Caroline et Adrien, merci pour tous ces chouettes moments partagés. Un remerciement spécial à Loïc, un Français de plus en Belgique !

Enfin, cette thèse a bénéficié de nombreuses aides gouvernementales et européennes. J'aimerais remercier chacun des organismes qui ont contribué aux résultats présentés dans ce manuscrit. Je remercie tout d'abord le projet Micromast, financé par Belspo, ainsi que le FRIA, financé par le FNRS, pour m'avoir accordé le financement de 4 ans d'études doctorales. Je remercie également L'ARD de l'Université de Liège, pour le financement de plusieurs voyages, ainsi que l'ESA pour le financement

d'études en hyper et micro gravité.

Je voudrais également profiter de cette section pour remercier toute ma famille : Papa, maman, Alix, vous avez forgé l'homme qui je suis aujourd'hui et pour cela, merci. Parrain, merci pour nos longues conversations et ton insatiable intérêt à m'ouvrir les yeux sur de nouvelles choses. Marraine, merci pour tout l'amour que tu m'as apporté. Chers Touristes, merci pour toutes nos aventures. Virginie, source intarissable de mes passions, c'est ton soutien inébranlable qui m'a conduit jusqu'ici. Merci pour ton amour, l'éternité n'est pas suffisante pour exprimer a quel point je t'aime.

Merci...

Liège, Septembre 2016
Martin Brandenbourger

Table of Contents

Publications

Parts of this manuscript have been published in peer reviewed revues, others are submitted. Those publications are listed below.

1. M. Brandenbourger, N. Vandewalle, and S. Dorbolo, *Displacement of an electrically charged drop on a vibrating bath*, PRL, **116**, 044501 (2016).

2. M. Brandenbourger, H. Caps, J. Hardouin, Y. Vitry, and S. Dorbolo, Electrically charged droplets in microgravity : Impact and Trajectories, Submitted to Icarus (2016).

3. L. Maquet, B. Darbois-Texier, A. Duchesne, M. Brandenbourger, B. Sobac, A. Rednikov, P. Colinet, and S. Dorbolo, *Leidenfrost drops on a heated liquid pool*, accepted in PRF (2016).

4. M. Brandenbourger, S. Dorbolo, *Electrically charged droplet: case study of a simple generator*, J. Can. Phys. **92**, 1203 (2014).

Sometimes it is good to step back to better assess a situation. During my PhD thesis, I had the opportunity to work on other projects. Projects that led to a publication are listed below:

1. M. Brandenbourger, S. Dorbolo, and B. Darbois-Texier, *Physics of a Toy Geyser*, Submitted to PRF (2016).

2. L. Maquet, M. Brandenbourger, B. Sobac, A.-L. Biance, P. Colinet, S. Dorbolo, *Leidenfrost drops : Effect of gravity*, EPL **110**, 24001 (2015).

3. S. Dorbolo, L. Maquet, M. Brandenbourger, F. Ludewig, G. Lumay, H. Caps, N. Vandewalle, S. Rondia, M. Melard, J. van Loon, A. Dowson, and S. Vincent-Bonnieu, *Influence of the gravity on the discharge of a silo*, Granular Matter. 15, 263 (2013).

4. S. Dorbolo, M. Brandenbourger, F. Damanet, H. Dister, F. Ludewig, D. Terwagne, G. Lumay, and N. Vandewalle, *Granular gas in a periodic lattice*, European Journal of Physics **32**, 1465 (2011).

Résumé
–Summary in French–

La célèbre expérience de Millikan, ainsi que l'étude des nuages d'orages, ont montré qu'un excès de charges électriques dans une goutte peut considérablement influencer son comportement. D'une part, l'excès de charges électriques influence les propriétés des gouttes, telles que sa fréquence d'oscillation ou sa pression interne. D'autre part, les charges au sein de la goutte peuvent interagir avec des champs électriques extérieurs. Dans cette thèse, on s'est intéressé à l'influence d'un excès de charges électriques sur une goutte millimétrique isolée électriquement.

Les précédentes recherches sur des gouttes chargées isolées ont souvent été cantonnées à l'étude de gouttes micrométriques. Ceci s'explique par la difficulté d'isoler électriquement cette goutte. Pour répondre à cette problématique, nous nous sommes intéressé à trois dispositifs permettant d'éviter la décharge d'une goutte : la microgravité, l'expérience du bain vibrant et l'effet Leidenfrost. A travers ces trois systèmes, nous avons étudié l'influence des charges électriques sur les propriétés physiques de la goutte ainsi que sur son interaction avec les systèmes de stockages utilisés. En outre, nous nous sommes également intéressé à l'interaction d'une goutte chargée avec un champ électrique extérieur. Ainsi, nous avons examiné l'interaction entre deux gouttes chargées et l'interaction entre une goutte chargée et un champ électrique homogène.

L'ensemble de ces études nous a permis de mieux décrire le processus de migration de charges au sein d'un liquide ainsi que le processus de perte de charges d'une goutte. En particulier, nous avons pu identifier et modéliser un nouveau mécanisme de pertes de charges se produisant en un temps caractéristique de plusieurs minutes. Nous avons également pu confirmer l'influence de la charge électrique sur l'énergie de surface d'une goutte. Quant à l'utilisation de trois systèmes de stockages, nos études en microgravité nous ont permis de décrire l'influence de la répulsion ou de l'attraction électrique sur l'impact entre deux gouttes chargées. L'éventail de comportements observés a été comparé au cas d'impacts entre deux gouttes neutres. Dans un autre registre, l'étude d'une goutte chargée se déplaçant à la surface d'un bain vibrant grâce à l'action d'un champ électrique extérieur nous a permis d'en apprendre plus sur l'interaction entre une goutte et la surface d'un bain visqueux. Par exemple, nous avons observé un régime “go-stop" dans lequel la goutte chargée se déplace durant son rebond et est stoppée durant son interaction avec le bain vibrant. Nous avons pu montrer qu'un tel régime apparait pour une goutte de volume important influencée par une force électrique faible. Dans cette configuration, la goutte se déplace avec une vitesse moyenne constante, ce qui la rend facilement manipulable. En conséquence, cette étude a menée

au développement d'un prototype de microfludique permettant de contrôler le déplacement de gouttes en évitant toutes pollutions par contact. Dans cette optique, nous nous sommes également intéressé à l'interaction entre deux gouttes chargées stockées sur un bain vibrant. Cette étude a permis d'affiner notre compréhension de l'interaction entre deux gouttes chargées. Ainsi, nous avons pu montrer que deux gouttes de même charges se déplacent jusqu'à atteindre une distance d'équilibre. Cet équilibre est dû à la compensation de l'attraction capillaire par la répulsion électrique. Enfin, notre étude de gouttes chargées en Leidenfrost sur un bain liquide a démontré que la présence de charges électriques produit une coalescence prématurée de la goutte avec le bain liquide. Plus généralement, nos mesures nous ont amené à mieux comprendre comment la présence de charges électriques à la surface de deux interfaces liquides séparées d'une fine couche de gaz tend à générer une forte attraction entre ces deux interfaces.

A la vue de nos résultats, nous pouvons conclure que la présence de charges au sein de gouttes millimétriques influence de façon visible leurs comportements intrinsèques ainsi que leurs interactions avec leur environnement. En outre, chacun des systèmes de stockages étudiés a apporté des réponses à différentes problématiques. L'étude en microgravité de l'impact entre deux gouttes chargées ébauche de nouvelles explications quant au comportement des nuages d'orages. Les résultats accumulés quant à la manipulation de gouttes chargées sur bain vibrant ouvrent la voie à de nouveaux systèmes microfluidiques. Enfin, l'analyse d'une goutte chargée en Leidenfrost décrit un nouveau moyen d'étudier l'influence de charges électriques sur l'interaction entre interfaces liquides.

English summary

Research such as the famous Millikan experiment or the studies concerning thunderclouds have shown that droplets can be considerably influenced by an excess of electric charges. Indeed, an excess of charges can affect the intrinsic properties of a droplet, such as its natural oscillation frequency or its internal pressure. Moreover, the electric charges in excess in droplets can also interact with external electric fields. In this thesis, we investigated the influence of electric charges on millimetric droplets that are electrically isolated.

In literature, research on isolated charged droplets are mainly focused on droplets with a micrometric size. The lack of studies concerning millimetric charged droplets is explained by the difficulty storing them while avoiding charge leakage. In order to answer to this issue, we examined three storage systems limiting the charge leakage: the microgravity, the vibrating bath method and the Leidenfrost effect. Through these systems, we studied the influence of electric charges on the droplet physical properties, but also the interaction between the charged droplet and its storage system. Furthermore, we investigated the interaction of charged droplets with external electric fields. More precisely, we studied the interaction between two electrically charged droplets and the interaction between one charged droplet and an external homogeneous electric field.

A first set of experiments on electrically charged droplets allowed us modeling the charge migration process in liquids and the charge leakage from a millimetric droplet. In particular, we identified and modeled a new mechanism of charges leakage occurring at a time scale of several minutes. Moreover, we confirmed the influence of the electric charges on the droplet surface energy previously deduced from experiments on micrometric droplets. Concerning the three storage systems, the experiments performed in microgravity allowed us describing the influence of the electric interaction on the impact between two charged droplets. The diverse behaviors observed were compared to the cases of impacts between two neutral drops. On a different note, the study of a charged droplet moving on the surface of a vibrating bath because of the influence of an external electric field gave new insights on the interaction between a bouncing droplet and a viscous liquid bath. For example, we observed a “go-stop" motion during which the droplet horizontally moves when it bounces away and is stopped during its interaction with the liquid bath. We showed that this motion occurs when large droplets are influenced by a weak electric field. Droplets with this kind of motion move with a constant average speed, which makes them easily manoeuvrable. Therefore, the control of the droplet motion led to the development of a new microfluidic prototype. Via this new setup, basic microfluidic tasks can be performed

without polluting droplet via contacts with solids or liquids. With these results in mind, we also examined the interaction between two charged droplets bouncing on the vibrating bath. This study brought new insights on the interaction between two charged droplets. Indeed, we observed that two drops with the same charges tend to remain at an equilibrium distance. Our study showed that this equilibrium distance is due to the compensation of the electric repulsion by capillary attraction at the surface of the vibrating bath. Finally, our study of charged droplet in Leidenfrost state on a liquid bath led to a better understanding of the interaction between charged liquid interfaces. Indeed, we showed that electric charges cause the early coalescence of charged droplet because of an increase in the vapor layer drainage.

We conclude from our results that an excess of electric charges influences ostensibly the intrinsic behavior of a droplet and its interaction with the environment. Furthermore, each storage system studied brought answers to specific issues. The study of the impact between charged droplets in microgravity outlines new explanations on the behavior of thunderclouds. The results accumulated on the micromanipulation of charged droplet bouncing on a vibrating bath opens the way to a new kind of microfluidic system. Finally, the study on the charged Leidenfrost droplets describes new ways to investigate the influence of electric charges on liquid interfaces.

1 Introduction

This thesis aims at studying electrically charged drops (which will also be called charged droplets). The next Chapters are dedicated to the description of the obtained results and the validation of these results compared to the state of the art. But before studying in detail the behavior of electrically charged droplets, we have to define what they are.

Droplets, neutral or charged, can be simply described as being small volumes of liquid (typically, few cubic millimeters). These small quantities of liquid are present everywhere on Earth and we encounter them every day of our lives. While waking up, we feel few drops of sweat due to the heat of the night. Once out of bed, we feel again droplets falling from the shower. It is now time to take the breakfast and while pouring a glass of fresh orange juice, few droplets splash out of our glass. We wipe these droplets with paper towel and we go quickly to work. On our way, we complain about the rain that announces a non-sunny day. The day has not yet begun, but droplets have already been everywhere.

What do differentiate small quantities of liquids from large ones? At the scale of a droplet, the surface forces become more effective than volume forces. Typically, the droplet surface tension overcomes the gravity force. Therefore, droplet does not answer to the same laws as larger quantities of liquids. Volumes of liquids are generally considered small when they have a characteristic length equal or smaller than the capillary length $l_c = \sqrt{\gamma/\rho g}$, where γ is the surface tension, ρ is the droplet density and g is the acceleration of gravity. Water has a capillary length $l_c \approx 3$ mm. At this scale, because the surface forces overcome the volume forces, the physics of liquids varies compared to observations made at the scale of a bowl or a pool filled with

water. For example, liquids tend to reduce their surface rather than spread out. As a consequence, droplets tend to take a spherical shape. The droplets studied during this thesis were composed of various liquids (essentially water and silicone oil), but had a characteristic size $l \leq l_c$.

In our case, we study droplets that have an excess of positive or negative electric charges. The interest in the study of charged drops is two fold.

1. The excess of electric charges in the droplet affects its fundamental behavior. Indeed, charges in excess in the droplets influences the droplet natural frequency, intern pressure,...

2. The excess of charges in droplets also means that the droplet reacts differently to external electric fields. The excess of electric charges may move in the droplet and affect its surface according to the applied electric field. In the same way, the droplet can be set in motion by the electric forces applied on the electric charges.

Both aspects are studied throughout this manuscript. Because of the predominance of its surface force, a droplet, charged or not, may take various shapes according to its environment. As shown in Fig. 1.1, droplets may spread on a solid surface according to its wettability. On the contrary, droplets take a lens shape at the surface of a fluid. Finally, a droplet can also be in contact only with gas. In such configurations, the droplet minimizes its volume because of the surface tension. Therefore, the droplet takes a spherical shape. The three cited configurations are subject to different research. For example, in the case neutral droplets in contact with a solid, research investigated the angle of contact θ of the droplet as a function of the solid and liquid properties. In the same way, in the case of charged droplets in contact with solids, studies investigated how the charge of the droplet varies this angle of contact θ. This last research topic is commonly named electrowetting.

In our case, we chose to stay away from these configurations and consider droplets in contact only with gas. In particular, we studied droplets in contact with ambient air or in contact with their own vapor. In such configurations, there is no wetting. The charged droplet is only influenced by its surface tension, the air motion and eventually external forces. Moreover, given the low viscosity of air, the droplet deformation is not damped by external interactions. Furthermore, gases are relatively good electrical insulators. As a consequence, we can make the assumption that the droplet charge loss is highly limited while the droplets are in contact only with gas. In other words, we can assume that the droplet is electrically isolated. Of course, this hypothesis has to be checked throughout the thesis.

In short, our subject of research can be defined as the investigation of the behavior of a liquid droplet with an excess of electric charges, the droplet being only in contact with ambient air. Naturally, electric charges are

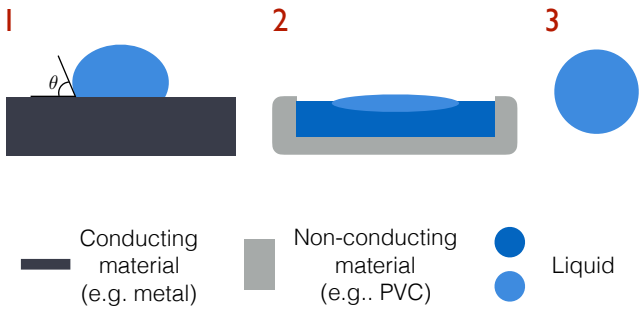

Figure 1.1: Examples of droplets in contact with a solid, with a liquid and with a gas. Note that the colors used on the schema define the color coding used for the entire of this manuscript.

not observable by the naked eye. Therefore, it is not easy to differentiate a neutral droplet from a charged droplet. Yet, charged droplets are present in Nature.

The Fig. 1.2 shows three natural spots where electrically charged droplets only in contact with ambiant air can be found. The thunderclouds are the most common example. Actually, thunderclouds can be defined as clusters of water droplets that acquired an excess of electric charges. They are mostly recognized by their lightnings, occurring when the thundercloud discharge on the earth. Since Benjamin Franklin [1], numerous studies tried to describe the thunderclouds behavior. The state of understanding is well summarized by Leblanc *et al* [2]. The difficulty resides in the fact that charged clouds are difficult to reproduce. Studies approached the problem by simulating the process [3] or by direct measurements in thunderclouds [4]. Nowadays, thunderclouds are described as complex structures with different layers of electric charges alternating in polarity [4]. Beyond the description of the interaction between several charged droplets, the interaction between two charged droplets is not fully understood [5].

Clouds are not the only droplets concerned by electric charges. Naturally, raindrops produced by a thundercloud are also charged [5, 6]. Charged droplets are also observable in waterfalls [7] and in droplets at the surface of ocean [8, 9]. They correspond to sprays of small droplet visible on the Fig 1.2. The same questions as the ones about thunderclouds arise when looking at these charged droplets.

Given their ability to influence the droplet properties and interact with electric

Image Credit: Robert Arn

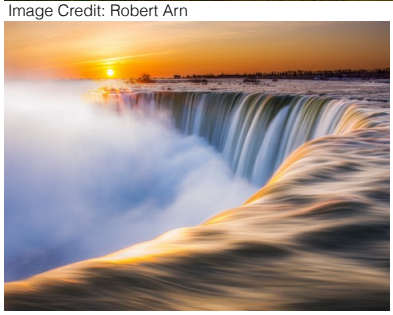

Image Credit: Derek Kind

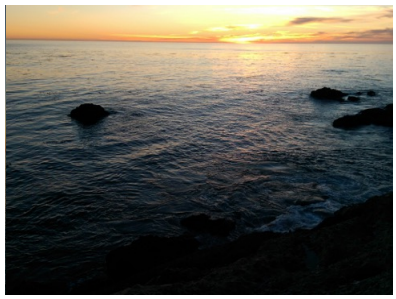

Image Credit: Laure Thibaut

Figure 1.2: Thunderclouds, waterfalls and droplets emitted from ocean are three examples of the natural presence of electrically charged droplets.

fields, charged droplets also play a role in industry. They are used in various domains such as agriculture research (pesticide spreading [10]), spectrometry (electrospray ionization technique [11]), satellite research (electric propulsion rocket engine [12]) or microfluidics [13]. These domains will be cited along the manuscript, but, as physicist, we primarily focus our attention on the droplet behavior itself and not their industrial applications.

Now that the object “electrically charged droplet" has been defined, it remains to describe in detail its behavior. In the next Chapter, we introduce the concept of charges excess and the major discoveries made about charged droplets in contact only with gas. Then, we highlight the remaining gray areas where understanding still needs to gain ground. Finally, we expose our strategy to take a part in this dialogue.

2

Research context

Contents

In this Chapter, we summarize the state of knowledge on the behavior of electrically charged droplets. Firstly, we outline the different mechanisms describing how droplets may acquire an excess of electric charges. Secondly, we explain results of studies investigating the influence of electric charges on the intrinsic behavior of droplets. Thirdly, we introduce different experiments that allowed understanding the influence of an external electric field on a charged droplet. Finally, we detail two research domains that directly derive from the study of electrically charged droplets: the electrosprays and the digital microfluidics. Through all these research we identify shadow zones that require further investigations. Once these lacks of understanding identified, we construct the strategy of our research.

2.1 How does the droplet acquire an excess of charges?

The occurrence of an excess of charges in a liquid droplet may take many forms. In the following lines, we summarize the main phenomena leading to an excess of charges in droplets. Each mechanism is schematized in Fig 2.1.

1. **Chemical reactions** - Chemical reactions such as reduction-oxidation reactions induce ions in liquid (e.g. reductant $\rightarrow$ product + e^-). A redox reaction can happen, for example, at a solid/liquid interface during the formation of a droplet. The droplet then takes away the charge excess when it detaches from the interface.

2. **Ionizing radiations** - Ionizing particles, such as beta particles, may hit the liquid droplet with enough kinetic energy to free electrons from molecules composing the droplet. Indeed, when the ionizing particle hits the molecule, it produces Bremsstrahlung or secondary electrons. Both phenomena generate the emission of an electron from the molecule.

3. **Triboelectricity** - The friction between two solids may remove charges from one material to the other. The phenomenon leads to negative or positive charge excess in both bodies. The experiment can be easily performed by rubbing a balloon on hairs. The charge by triboelectricity works in the same way for the friction between one liquid and one solid or the friction between two liquids.

4. **Charges migration** - Under the influence of an external electric field, charges may migrate inside liquids. As a consequence, parts of the liquid acquire an excess of electric charges. If a droplet detaches from the liquid, it takes away this excess of electric charges.

Each of these mechanisms may occur separately or work together to charge a droplet. The understanding of the charge mechanism is essential to explain how a droplet may or may not acquire a charge. Indeed, those mechanisms may be spontaneous, generating charge in liquid without controls. For example, there is still no agreement on the processes generating charge excess in thunderclouds. The current models suppose a charging process triggered by ionizing radiation and raised up by triboelectricity [2]. A precise understanding of the underlying charge process would allow predicting the thundercloud formation.

In the same way, in laboratories, excess of charges in droplets may be generated unconsciously. For example, Choi *et al* [14] reported the uncontrolled charge of droplet produced by conventional pipetting. Such a process turns out to be potentially catastrophic for numerous biological studies. For example, it may affect the combination and localization of charged bio-molecules. In this case, it seems essential to understand how to reduce the different charge mechanisms.

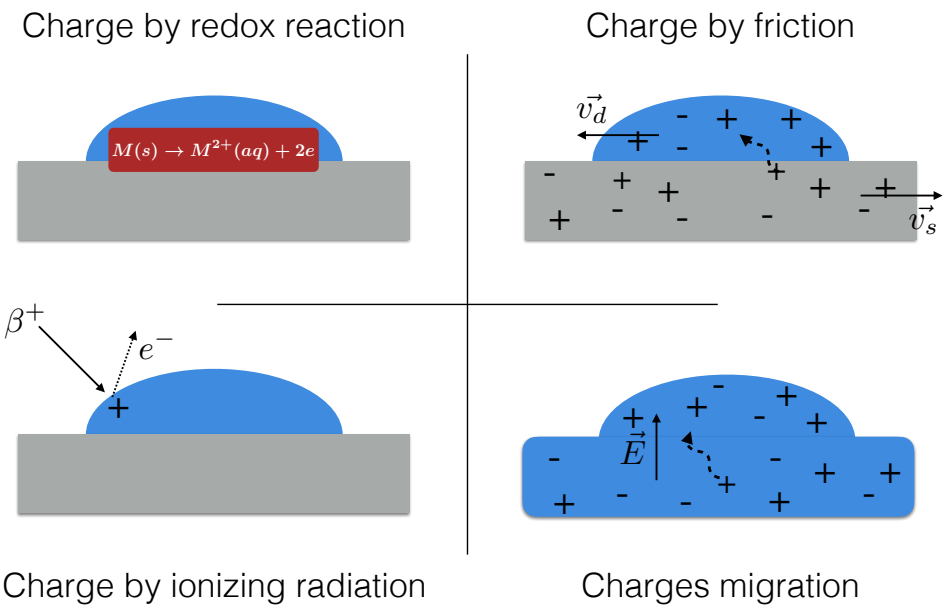

Figure 2.1: Description of four different ways for a droplet to accumulate an excess of charges. The top left schema describes the droplet charge via redox reaction. The bottom left schema describes the charge by ionizing radiation. The top right schema describes the triboelectricity process. The bottom right schema describes the charge migration mechanism. Once the excess of charges is induced in the droplet, the droplet may detach from its substrate. When the droplet detaches from the substrate, a free electrically charged droplet has been created.

Finally, the excess of charges in a droplet can be desired. In this case, the amount of charges induced in droplets is more or less difficult to control, depending on the charging method. For example, the charge by friction does not induce the same amount of charges from one experiment to the other. On the contrary, the charge migration can be controlled by applying controlled electric fields. Each of the properties of the four charging methods is summarized in Tab. 2.1. We detail in each case if the charging mechanisms is reproducible, if it is easy to implement, if it exists in nature and if it is used in industry.

	Reproducible	Easy to implement	In Nature	In industry
Chemical reaction	Y	N	Y	N
Ionizing radiation	Y	N	Y	N
Triboelectricity	N	Y	Y	N
Charges migration	Y	Y	Y	Y

Table 2.1: Summary of the different properties of each charging mechanisms.

The approach of this thesis is to induce a well-known amount of charges in a droplet and study the influence of these charges on the droplet behavior. As the Consequence, the charge by migration is the only mechanism that was used to generate charged droplets. The detail of the charge by migration processes is described in Section 3.1. Once the droplet is charged, it remains to study its behavior. In the next Section, we examine how scientists have studied the behavior of electrically charged droplets.

2.2 How does the charge affect the droplet?

As stated above, liquids may gather electric charges through various ways, meaning that the question of the charge influence can be asked on almost all experiments involving droplets. The present section does not aim at describing the entire bibliography around the influence of electric charges on droplets. In the next lines we focus our attention on specific discoveries that revolutionized the approach on the influence of electric charges on the droplet behavior.

2.2.1 Influence of the charge on the droplet interface

One of the most cited article on electrically charged droplets is the study entitled *On the Equilibrium of Liquid Conducting Masses Charged with Electricity* by Lord Rayleigh in 1882 [15]. In his study, Lord Rayleigh described mathematically how electric charges influence the droplet interface. Droplets are described as deformable objects with a surface energy linked to their surface tension. The electric charges are supposed to spread uniformly on the droplet surface due to their repulsion. This

basic model of a charged droplet is schematized in Fig. 2.2. In his study, Lord Rayleigh theoretically describes how a liquid with an excess of electric charges reacts to small perturbations. By comparing the electric potential to the cohesion energy of the system, he deduced the oscillation frequency for the normal modes of a spherical mass of liquids:

$$f^2 = \frac{l(l-1)}{4\pi^2\rho r^3}\left(\gamma(l+2) - \frac{q^2}{16\pi^2\epsilon_0 r^3}\right) \tag{2.1}$$

where f is the oscillation frequency of the spherical mass of liquid, l determines the oscillating mode of the liquid, ρ is the liquid density, r is the sphere radius, ϵ_0 is the vacuum permittivity and q is the surface charge of the liquid. Typically, a droplet possesses a charge between 1 pC and 100 pC. Note that from Eq. 2.1, the oscillation frequency of a neutral droplet is expressed by $f_0 = l(l-1)(l+2)\gamma/4\pi^2\rho r^3$.

In the case of a neutral water droplet with $r = 0.5$ mm, $\rho = 1000$ kg/m^3 and $\gamma = 72$ mN/m oscillating in its natural mode ($l = 2$), the droplet oscillates with a frequency $f = 342$ Hz. If the same droplet possess a charge $q = 100$ pC, the droplet natural oscillation frequency corresponds to $f = 306$ Hz.

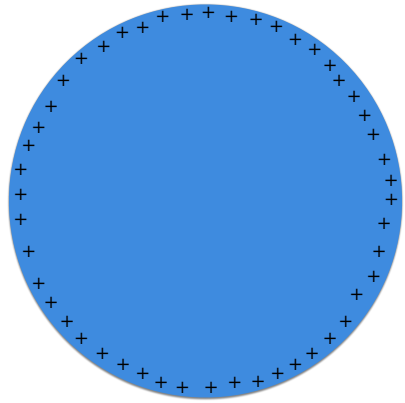

Figure 2.2: Basic model of a charged droplet: A conductive and deformable charged sphere. Because of the charge repulsion, the charges in excess are spread homogeneously on the surface of the sphere.

From this study at small perturbations, Lord Rayleigh also deduced the limit of stability for a charged liquid sphere. When the electric repulsion between charges overcomes the cohesion energy of the liquid, it becomes unstable. If Eq. 2.1 can be expressed in real numbers, the liquid sphere is stable. On the contrary, a frequency expressed by complex numbers corresponds to an unstable liquid sphere. As a consequence, the critical charge for the instability to occur can be directly deduced from Eq. 2.1:

$$q_c = \sqrt{64\pi^2 r^3 \gamma \epsilon_0} \tag{2.2}$$

The theoretical predictions of Lord Rayleigh were proven to be exceptionally accurate. The oscillation frequency has been successfully validated via experimental setups using pendant droplets [16] or levitating droplets [17] methods. In particular, Hill and Eaves [18] have successfully measured the frequency shift of a charged droplet for several charges and oscillating modes thanks to diamagnetical levitation of a water droplet.

Of course, electric charges inside the droplet can also be influenced by an external electric field. As a consequence, the droplet oscillation frequency can be influenced by an external electric field. The oscillation frequency, theoretically deduced from the balance of pressures applied on the droplet, was calculated by Brazier-Smith *et al* [16]. The frequency shift was found to be in good agreement with their measurements.

The stability limit predicted by Lord Rayleigh was also experimentally studied. The charged droplet instability is now commonly named Coulomb instability or Coulomb explosion. Duft *et al.* [19, 20], have been able to precisely measure the limit of the instability. For this purpose, they used an electrodynamic trap to levitate a charged ethylene glycol droplet. The electric field generated by the electrodynamic trap is adjusted in order to not affect the charged droplet oscillation. During the droplet evaporation, the radius decreased until a critical size corresponding to the droplet instability. They were able to observe microscopic images of the droplet deformation resulting from this instability. The Fig. 2.3 shows the reproduction of the image sequence obtained by Duft et al. [20]. The first image (a) was taken at $t(a) = 0$ ms. The following images was taken at $t(b) = 10$ ms, $t(c) = 15$ ms, $t(d) = 20$ ms, $t(e) = 40$ ms and $t(f) = 70$ ms. The droplet was composed of ethylene glycol and had an initial radius and charge of respectively 58 μm and 3.3 pC. From image (a) to image (c), the droplet elongates until ejecting a fine jet of micro-droplets. These droplets are highly charged. After the emission of the droplet jet, from image (d) to image (f), the droplet stabilizes and goes back to a steady oscillation.

Since this major breakthrough, several studies have been focused on the description of the dynamic of the Coulomb instability [21–24]. With Rayleigh work and the following studies, the understanding of the charge influence on the interface between gas and droplet is almost fully complete. However, as we will see in the Section 2.4, these studies do not answer to all the questions asked about the influence of charges on droplets. Typically, the droplet can lose its charges via other mechanisms than the Coulomb explosion.

Finally, note that the surface energy of a charged droplet is the only intrinsic property that is significantly affected by the presence of electric charges. Other properties, such as the droplet density or the droplet viscosity only slightly vary with the droplet charge.

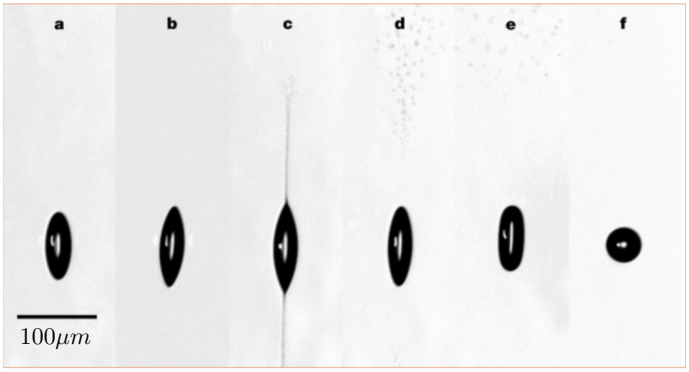

Figure 2.3: Image sequence of a Coulomb explosion observed by Duft et al [20]. The first image (a) was taken at $t(a) = 0$ ms. The following images was taken at $t(b) = 10$ ms, $t(c) = 15$ ms, $t(d) = 20$ ms, $t(e) = 40$ ms and $t(f) = 70$ ms. The droplet was composed of ethylene glycol and had an initial radius and charge of respectively 58 μm and 3.3 pC.

2.2.2 Charged droplets influenced by an external electric field

The study of the interaction between electric fields and charged droplets has evolved in the same way as the study of the interaction between electric fields and electric charges. Basically, When an electric field $\vec{E}$ is applied on the charged droplet, it generates an electric force $q\vec{E}$ on the electric charges in the droplet. This electric force can displace the electric charges inside the droplet or displace the droplet itself.

Before looking at the influence of electric fields on charged droplets, we have to precise that a non-charged droplet can be influenced by electric fields. Indeed, polar liquids or liquids with free charges, such as water, can be influenced by non-homogeneous electric fields. When an electric field is applied on the liquid, polarized molecules (or free charges) tend to align in the direction of the electric field. If the electric field is non-homogenous, the electric force change in intensity along the liquid. As a consequence, polar molecules (or free charges) endure a total force in the direction of the electric field gradient. Because of this net force, the liquid can be deformed or set in motion. The phenomenon is called dielectrophoresis. A droplet influenced by a non-homogneous electric field is schematized in Fig. 2.4. The dielectrophoresis is itself an important scientific domain, but is not directly linked to the behavior of an excess of electric charges in a droplet.

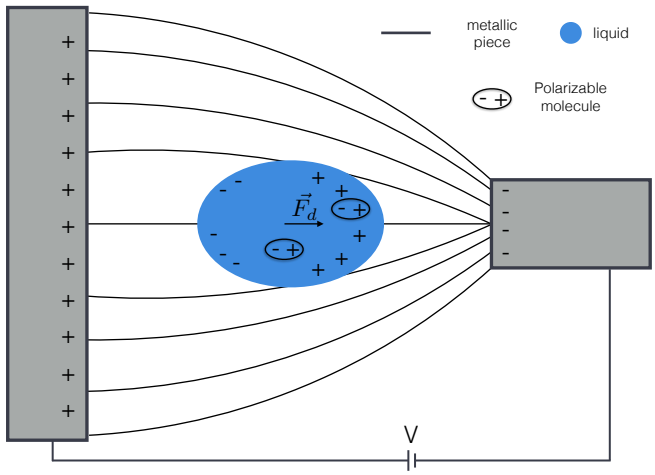

Figure 2.4: Schema of a droplet influenced by a dielectrophoretic force. Free charges in the droplets (or polarized molecules) align with the electric field lines. Because of the non-homogeneity of the electric field, the electric force is more important on one side of the droplet. As a consequence, the free charges and the polarized molecules endure a net force F_d along the electric field. This net force can induce liquid deformation and liquid displacement.

Charged droplet set in motion by an electric field

One of the first scientists to study the interaction between electric fields and charged droplets is Abbé Nollet [25]. Among numerous experiments concerning electricity, he studied the water flow rates from an orifice with both charged and uncharged water streams. His description of the experiment is illustrated in Fig. 2.5. The different setups described as “Fig". 1, “Fig. 2" and “Fig. 3" corresponds to devices emitting droplets. By charging the chain, Abbé Nollet was able the induce charge migration in the ejected droplets. The experimental setup allowed him to demonstrate that the flow rate of charged droplets was more important than the flow rate of neutral droplets. It is explained by the electric repulsion between the emitted droplets. He also indicated that, for significant charges, droplets repels from each other in a conical shape (see Fig. 2.5, “Fig 1 B"). This last observation is now a well known example of the interaction between electrically charged droplets. While charged droplets with the same charge are emitted from the water stream, they endure both the gravity and the electric repulsion between them. The two applied force explain the specific droplet motion that lead to the conical shape of the droplet stream. Of course, the repulsion between charged droplets have been described in more details since the observations of Abbé Nollet [26].

Abbé Nollet publications represent a first qualitative study of electrically charged

Figure 2.5: Schema extracted from Nollet's book "Recherches sur les causes particulières des phénomènes électriques et sur les effets nuisibles ou avantageux qu'on peut en attendre" [25]. Different setups ("Fig". 1, "Fig. 2" and "Fig. 3") emit electrically charged droplets. The part of the schema named Fig 1 B shows the conical repulsion between charged droplets.

droplets. Later, with the evolution of the understanding on electric charges behavior, the charged droplets understanding has also evolved. In particular, the ability to produce precise electric fields allowed studying in detail the interaction between droplets and electric fields. Currently, the simplest way to describe a charged droplet in an external electric field is to model the system by a point charge influenced by an electric field. In this case, the electric force applied on the droplet is expressed by:

$$\vec{F}_{el} = q\vec{E} \tag{2.3}$$

where q is the total droplet charge and $\vec{E}$ the applied electric field. This model was used in the famous Millikan experiment [27]. In his experiment, Millikan studied the motion of a charged droplet between two charged electrodes. The experiment is schematized in Fig. 2.6. The two charged electrodes were vertically aligned. A charged droplet was produced and placed in between both electrodes. Once placed between both electrodes, the droplet endured the force due to its weight $\vec{F}_w$, the electric force due to the electric field produced by the electrodes $\vec{F}_{el}$ and the drag force due to its motion $\vec{F}_d$. By controlling the electric field, it was possible to control the direction and the speed of the droplet. Because of the drag force, the droplet acquired a constant speed after few seconds. This constant speed can be deduced by calculating the equilibrium between the three forces. In doing so, we have:

$$v_{\lim}(E) = \pm \left(\frac{1}{6\pi\eta r}\right)\left[\frac{4}{3}\pi r^3 \mathrm{g}(\rho_h - \rho_a) - qE\right] \tag{2.4}$$

where η is the air viscosity, r the radius of the droplet, g the acceleration of gravity, ρ_h the droplet density and ρ_a the air density. The droplet can move upward or downward, which is expressed by the symbol $\pm$. By measuring the droplet speed, Millikan was able to deduce the droplet charge. By repeating the experiment on several droplets with different charges, he deduced the value of the elementary charge (i.e. q=1.6 10^{-19} C).

Naturally, numerous experiments have been performed since the Millikan experiment [28, 29]. In particular, studies have been focused on the influence of the droplet electric charges on the surrounding electric field [28]. Indeed, the charged droplet produces its own electric field, which can influence the overall electric field landscape of the experiment. However, this phenomenon is a second order effect that can generally be neglected. Experiments and simulations have also been developed to study of the interaction between several charged droplets [3, 30]. In this case, the motion of one droplet in the electric field produced by one or many other charged droplets are studied. Beyond these research, the precise motion of two charged droplets interacting with each other still needs to be experimentally studied. Furthermore, the knowledge deduced from the Millikan experiment (i.e the droplet motion can be modeled as a droplet influenced by its weight, a simple electric force and the drag force) can be used in more complex systems where droplets endures other forces difficult to model.

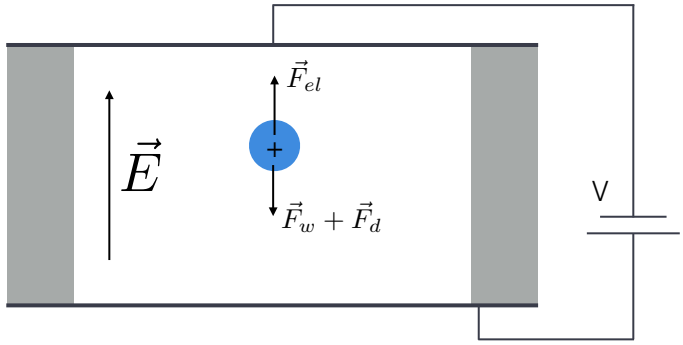

Figure 2.6: The Millikan experiment. The displacement of a charged droplet is controlled by adjusting the external electric field. The electric field $\vec{E}$ can be oriented upward or downward. As a function of the applied electric force $\vec{F}_{el}$, the droplet weight $\vec{F}_w$ and the drag force $\vec{F}_d$, the droplet moves upward or downward.

Charged droplet deformed by an electric field

Beyond generating a displacement of the charged droplet, an external electric field can also influence the droplet surface. Indeed, the electric charges on the droplet surface endure an electric force due to their interaction with the electric field. The pressure endured by the droplet can be expressed as:

$$P = P_{in} + P_{el} = \gamma \left(\frac{1}{R_1} + \frac{1}{R_2} \right) - \frac{\epsilon_r \epsilon_0}{2} E^2 \tag{2.5}$$

where P_{in} is the droplet internal pressure without the influence of an external electric field, P_{el} is the pressure endured by the droplet due to the electric field, R_1 and R_2 are the droplet principal radii of curvature, E is the electric field on the droplet surface and ϵ_r is the droplet relative permittivity. Several studies have been focused on the droplet deformation in an electric field [31,32]. In particular, studies investigated the droplet deformation over time and the droplet instability that can result from this deformation. Indeed, when a charged droplet (or a charged liquid surface in general) is influenced by a significant electric field, it deforms in a conical shape named Taylor cone [33]. For an electric field significant enough, the charged surface is unstable and the Taylor cone emits small droplets.

In this manuscript however, we limit our investigations to electric fields that does not deform droplet. The influence of an external electric field on the droplet shape is

described by the electric capillary number:

$$C_e = \frac{\epsilon_r \epsilon_0 E^2 r}{\gamma} \tag{2.6}$$

The Eq. 2.6 is directly derived from Eq. 2.5. Our experiments studying the interaction between electric fields and charged droplets were limited to $C_e \approx 4\ 10^{-3}$. As a consequence, the influence of the external electric field on the droplet shape was considered negligible.

2.3 Take advantage of the charge in the droplet

The previous Section (see Section 2.2) exhibited the two major properties of droplets with an excess of electric charges. (i) the charges influence the droplet properties (ii) the charges can be influenced by electric fields.

The progress in the charged droplet understanding allowed scientists developing new setups that take advantage of the charged droplet properties. For example, the droplet Coulomb explosion allowed developing sprays of very small droplets and the interaction between charged droplet and electric field allowed controlling the droplet motion. These new setups generated themselves new experimental configurations that required new (or at least more detailed) explanations. In the next lines we examine these new research topics, brought by the industry, which raised up new questions.

2.3.1 The electrospray

Electric fields and electrostatic interactions can be used to give information on more than electrical phenomena. For example, spiderwebs take advantage of the charge accumulated on flying insects to increase their capture probabilities. Indeed, Ortega-Jimenez *et al* [34] have demonstrated that spiderwebs are attracted toward charged insect thanks to their electric conductivity.

In the same way, a significant part of the scientific research on charged droplets is linked to one of their applications: the electrosprays. The phenomenon is schematized in Fig. 2.7. As explained in the previous Section (see Section 2.2), when a liquid surface is subject to a significant electric field, the electric force applied on the surface can overcome forces due to surface tension. If the electric force is significant enough, the liquid surface deforms in a conical shape (i.e. a Taylor cone). When a certain electric field threshold is reached, the Taylor cone emits a jet of small charged droplets. After their emission, the charged droplets quickly endure Coulomb explosions, which produce even smaller droplets. The whole charged jet is called an electrospray [11].

The droplet charge is due to the charge by migration process. When the electric field is applied on the liquid, charges migrate toward the liquid interface. The electric force applied on the charges at the interface explains the conical shape of the liquid.

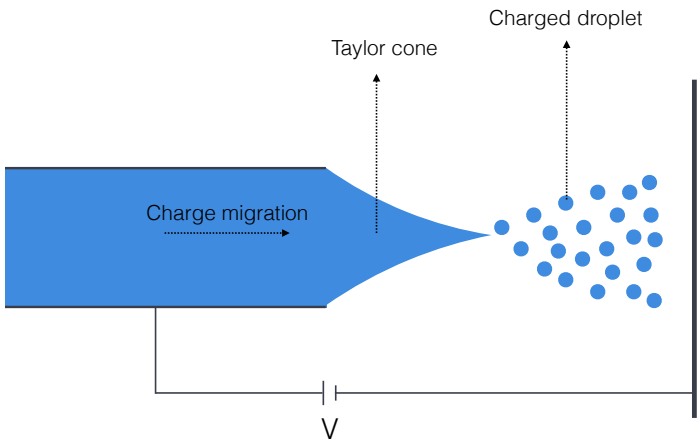

Figure 2.7: Schema of an electrospray. The voltage deforms the surface in a Taylor cone. The Taylor cone ejects charged droplets. These droplets form a spray shaped as a cone.

When a droplet detaches from the Taylor cone, it takes away a part of the electric charges. As a consequence, droplets emitted from the Taylor cone possess an excess of electric charges.

Electrosprays, triggered off only by important electric fields, emit a spray of very small droplets ($r \approx 10$ μm). As a consequence, they are used in numerous applications that need to disperse a liquid via fine aerosols. Because of the electrosprays, electrically charged droplets have been studied in various scientific domains such as agriculture research (pesticide spreading [10]), spectrometry (electrospray ionization technique [11]), microscope development (focused ion beam), satellite research (electric propulsion rocket engine [12]), nanotechnology (deposition of particles for nanostructures [35]),... These side studies improved the understanding of the behavior of small electrically charged droplets. Typically, electrodynamic studies have been able to precisely describe the charge migration process generating charged droplets in electrosprays and the ion evaporation happening at the surface of very small charged droplets.

As explained in the introduction (see Chapter 1), we focus our attention on studying a small number of millimetric droplets rather than generating a droplets spray of thin droplets. However, the progresses made in the domain of electrospray may be useful to understand the behavior of larger droplets. Indeed, notions such as charges

migration or charges interaction with electric fields should not vary with the droplet size. These progresses are discussed throughout this thesis according to their link with particular observations or theoretical developments.

2.3.2 Use a charged droplet to manipulate liquid

One of the last applications developed around electrically charged droplets concerns the micromanipulation of droplets, i.e. doplet-based microfluidics. Generally, microfluidics is associated with the use of closed micro-channels [36]. Studies used electrically charged droplets to control the droplet motion in channels networks [37, 38]. However, closed micro-channels reduce the droplet motion to one dimension. As a consequence, the droplet handling (i.e. the droplet generation, merging, mixing,..) is limited by the droplet flow in the micro-channel. Lately, research have been focused on open microfluidics. Open microfluidics aims to transport and manipulate droplets in two dimensions of space. The transport should be quick, without alteration of the droplet content, and should allow one to perform operations including sorting, mixing, and analyzing the fluids. Open devices were demonstrated to be a more flexible way to perform these different tasks, especially for micro-chemical analysis purposes [39].

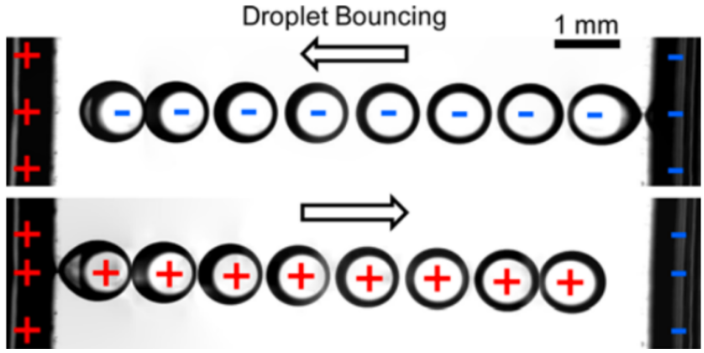

Figure 2.8: Image superposition of a charged droplet micro-manipulation by Im et al [13]. The droplet has a volume of 300 nL and is influenced by an electric field of 3 kV/cm. The time step of time lapse image is 0.06 s.

In this context, research have been performed on the use of electric fields to control the droplet motion. It corresponds to the digital microfluidics. By controlling the voltage between electrodes, it is possible to control electric forces applied on the droplet. The droplet motion may be due to excess of electric charges or to dielectrophoresis forces. The final goal of these setups is to precisely and quickly control the droplet motion and the interaction between droplets. As a consequence, different setup geometries have been developed. For example, droplets can be set in motion at the surface of a grid pattern of electrodes [40]. Droplets can also be set in motion in an insulating liquid by an external electric field. The interest of electrically charged

droplet compare to neutral droplets in digital microfluidics has been recently reviewed by Im [13]. In particular, charged droplets require smaller electric fields.

The Fig. 2.8 shows the microfluidic device developed by Im *et al* [13]. The setup consists in two electrodes facing each other and immersed in silicon oil. A water droplet is set in motion between both electrodes by controlling the voltage between them. On the image superposition in Fig. 2.8, the droplet is influenced by an electric field $E = 3$ kV/cm. Each droplet is separated by 6 ms. The setup takes advantage of electrically charged droplets to perform microfluidics operations. Such a system allows, among other things, to limit the droplet contact with solid surfaces to few seconds. Limiting the droplet contact with solid surfaces is primordial to reduce the droplet contamination.

Recent papers have explored the application of digital microfluidics to biology [40, 41]. They were able to reproduce biological manipulations, such as cell culture, by using digital microfluidics setups. Other studies [42, 43] showed that the use of electric interactions allowed controlling more easily the droplet merging. Indeed, the merge between droplets in microfluidic setups is not always an easy task, especially when the droplets are stabilized with surfactant. The electric interaction between droplets allows reducing this limitation. The development of digital microfluidics is a huge evolution in the world of microfluidics. A last step would be to completely avoid any contact between the droplet and contaminating surfaces. Such progress requires developing particular storage systems, but also to understand the droplet motion in these systems.

2.4 The need and the strategy

In the past Sections we presented briefly the state of the art concerning the research on electrically charged droplets. We showed that charges in excess in a droplet influence the droplet properties and the droplet interaction with electric fields. For example, we showed that a charged droplet could destabilize due to the repulsion of its own charges and that a charged droplet could easily be set in motion by external electric field.

A significant part of the research on charged droplets is focused on the study of a large number of small electrically charged droplets (1 nm to 100 μm) interacting with each other. These research aim to answer to questions about the behavior of systems such as thunderclouds and electrosprays. These experiments are performed with apparatus corresponding to their need. Typically, the Coulomb explosion is studied by trapping micrometric droplets in electrodynamic traps [19] and the charge of electrosprays droplets is studied by using spectrometers [11].

The study of larger charged droplets (around 1 mm) opens the way to questions that are still in suspense. Indeed, little results report the charge loss or the interaction between bigger droplets. Yet, a better understanding of the interaction between

charged raindrops is needed. In the same way, the industry still needs to develop new ways to manipulate such droplets. The study of millimetric charged droplets requires a different approach. Indeed, setups such as electrodynamic traps may only store a small volume of liquid. The droplet theoretical description is also different with, for example, a smaller capillary pressure.

Currently, charged droplets with a size around $l_c = 3$ mm have mainly been studied in contact with solid surfaces. Domains such as electrowetting or digital microfluidics received a lot of interest from industries and scientific research. The lack of studies on the behavior of larger charged droplets without contact with liquid or solid surfaces is explained partially by the difficulty to store these charged droplets.

In this context, we propose to study the intrinsic behavior of millimetric charged droplets as well as their interaction with electric fields. These studies are performed by observing free falling droplets or by developing new storage systems that avoid contact between the charged droplet and solids or liquids.

These storage systems correspond to the microgravity, the vibrating bath experiment and the Leidenfrost effect. Throughout the manuscript, we describe these different environments and show that our approach gives new insights about electrically charged droplets. Furthermore, the interaction between charged droplets and new storage systems give also new understandings on the storage systems themselves, just like the understanding of the Coulomb explosion gave explanations on the production of thin droplets by electrosprays. Beyond the Chapter 1 and 2, the results accumulated throughout this thesis are described in the following Chapters:

- **Chapter 3** - This chapter aims at describing the experimental setups that were developed during this thesis. Throughout the Chapter, we detail the tools used to induce an excess of charges in droplets, measure the droplet charge and store the charged droplet without contact with fluids or solids.

- **Chapter 4** - This chapter presents new progresses made on the understanding of the influence of the electric charge on the droplet. We describe how charges migrate in liquid as a function of the liquid composition and how it affects the droplet charge. We also study the charge loss over time for millimetric droplets. Finally, we give new insights on the influence of the electric charge on the droplet surface energy. In particular, we show that the droplet charge can be simply deduced by looking at the droplet surface energy.

- **Chapter 5** - This chapter is focused on the interaction between two charged droplets. The experiments were performed in microgravity in order to highlight the electric interaction between droplets. During one experiment, two droplets were sent toward each other. Experiments with or without impact between droplets were studied. In particular, we show how electric repulsion may avoid

contact between moving droplets and how electric attraction may, on the contrary, generate contact between charged droplets.

- **Chapter 6** - This chapter is oriented toward the study of charged droplets stored on a vibrating bath. We firstly study a charged droplet set in motion on the vibrating bath by an external electric field. Secondly, we study the interaction between two charged droplets bouncing on the vibrating bath.

- **Chapter 7** - This chapter presents new insights on the influence of electric charges on the Leidenfrost state. We focus our attention on droplets stored in Leidenfrost state on a liquid pool. We first study how the electric charge influences the shape of the liquid bath. Then, We study how electric charges produce early coalescence of the Leidenfrost droplet with the liquid bath.

An organization chart of the Chapters 2, 3, 4, 5, 6 and 7, is shown in Fig. 2.9. After the characterization of the research context (2), we are interested in the experimental setups (3), the influence of the charge on the droplet (4), the charged droplets in microgravity (5), the charged droplets bouncing on a liquid bath (6) and the charged droplets in Leidenfrost state (7). Moreover, a small paragraph at the end of each Section summarizes them. A line in the margin highlights these summaries. This paragraph possesses such a margin.

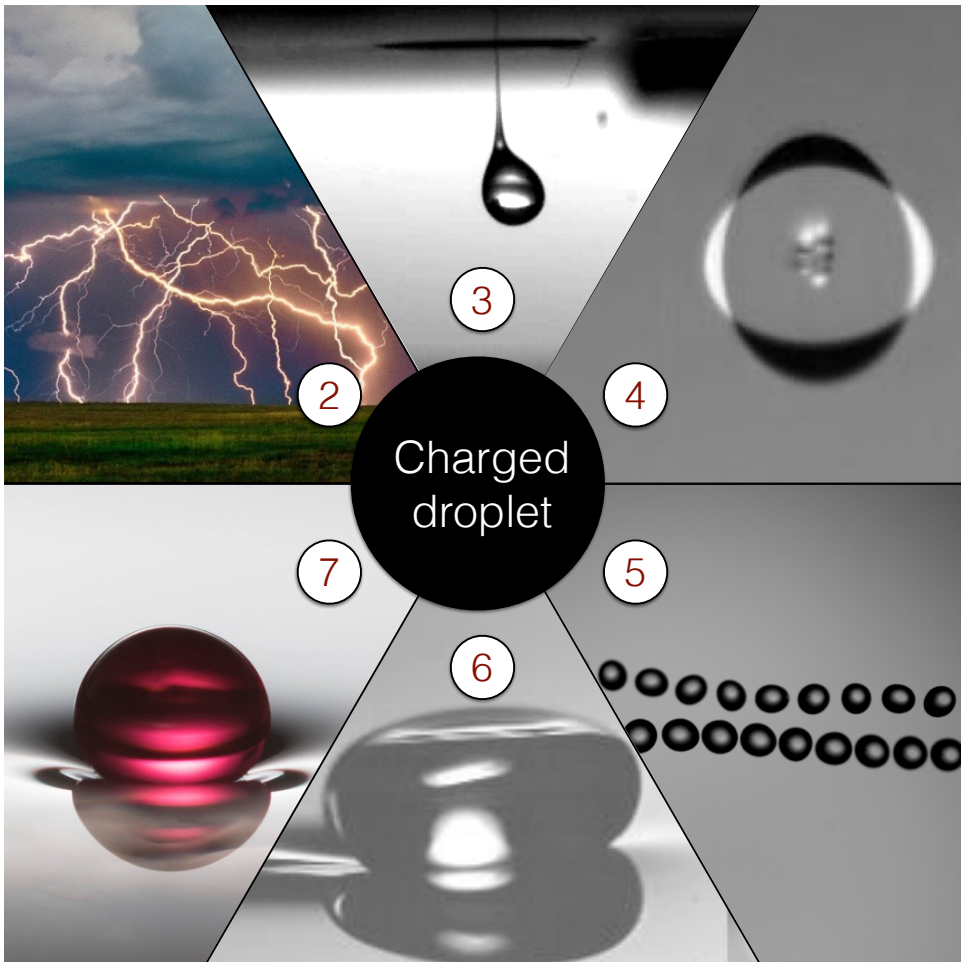

Figure 2.9: Organization chart of the present thesis. Each Chapter number is associated with an image that will gradually take more sense throughout the Chapter that it depicts.

3

Experimental details

Contents

In this Chapter, we describe the various tools that were developed throughout this thesis to create and manage electrically charged droplets. In Section 3.1, we begin by describing the creating process of charged droplets. We show that the charge migration process is a reliable way to charge droplets with a precisely known amount of charges. Then, we detail the ins and outs of the charged droplet generation. In Section 3.2, we explain how the droplet charge was measured. Finally, the Section 3.3 is dedicated to the description of storage methods. Three setups are considered: the bouncing droplet, the microgravity and the Leidenfrost effect. Each of these storage systems limits the charge leakage from the droplet. Throughout the three Sections devoted to their description, we detail the advantages and disadvantages of each method.

3.1 Creating Charged droplets

As described in the introduction, there are four different methods to produce an excess of electric charges in droplets, namely via ionizing radiation, triboelectricity, chemical reactions and charges migration. The charge by ionizing radiation and the charge by friction are commonly used in Millikan famous experiment [27]. By charging a droplet and observing its motion in a homogeneous electric field, Millikan was able to measure the charge quantification. However, both charging mechanisms are difficult to control. Indeed, there are no reliable laws that describe the amount of charges transferred to a droplet by friction. In the same manner, the electron loss induced by ionizing radiations requires to precisely control the kinetic energy of the ionizing particles and the droplet exposure time. The charge by chemical reaction has also some drawbacks. Typically, the process requires the degradation of a chemical component, which limits in time the droplet charge. On the contrary, the charge migration process generates reliable and predictable charge excesses. Indeed, as its name indicates, electric charges migrate (thanks to the influence of an external electric field) into the droplet. Knowing the electric field generating the charge migration, the amount of charges in excess in the droplet can be deduced. In the next lines, we depict the experimental tools necessary to complete the charge migration mechanism and we describe the current state of understanding of such a process.

Basically, the charge migration, also named electrostatic induction, requires a liquid container (such as a needle), an electric field and a liquid containing free charges. The Fig. 3.1 shows the essential procedure of the experiment. A droplet hangs at the edge of the needle. Without any electric field, the droplet and the liquid contained in the needle are overall neutral. Once the system is immersed in an electric field, charges migrate from the liquid contained in the needle to the hanging droplet. As a consequence, it induces an excess of charges in the droplet. At this point, when the droplet detaches from the needle, it carries away an excess of electric charges.

Charged droplet generators using the charge migration process can have different geometries, according to their use. One of the first ways to generate charged droplets via charges migration is called the Kelvin drop generator (or Kelvin water dropper) [44]. This charged droplet generator corresponds to the simplest way to induce charge migration in droplets. Indeed, it only consists in water falling in well connected cups. A schema of such a generator is shown in Fig. 3.2.

The setup is composed of two charged droplet generators and two droplet receptors interconnected. One charged droplet generator is composed of a droplet emitter and an electrode. When the electrode is charged, it generates an electric field near the droplet emitter. This electric field induces charge migration in the droplet emitter. Once charged, the emitted droplets falls trough the electrode in the droplet receptor. The charge of the electrode is due to an avalanche process induced by the interconnection between both charged droplet generators and droplet receptors. On each side,

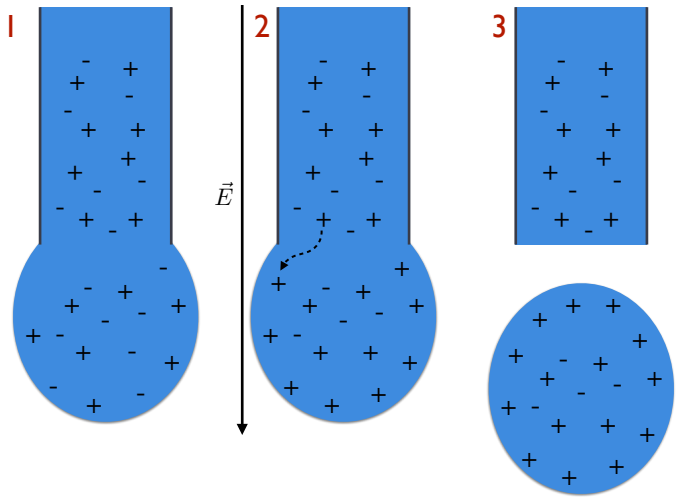

Figure 3.1: Basic description of the charge migration process. The electric field generates charges migration from the liquid container to the droplet. When the droplet detaches, it takes away the excess of electric charges.

the droplet receptor is connected to the opposite electrode. Because of this interconnection, the electric charges accumulated in one droplet receptor induce an excess of electric charges in the opposed electrode. Therefore, the charged droplet generated by the first generator induces charges migration in the second charged droplet generator and *vice versa*. This avalanche process results in an important voltage between both generators. Such a voltage can be put in evidence by inducing electric arcs between both charged droplet generators. The drawback of the setup is that it is difficult to control the charge of each electrode and, as a consequence, the charge induced in the droplet. Nevertheless, the Kelvin drop generator is a beautiful experiment that easily demonstrates the influence of the charge on the droplets. For example, we easily observe the electric repulsion between droplets when the experiment runs. This repulsion between droplets falling from the charged droplet emitter generates a conical shape, exactly like the one observed by Abbé Nollet in his first experiments and the one observed on electrosprays.

Later, scientists developed systems for which the electric field applied on the hanging droplet was adjustable via a voltage generator. For example, Jones and Thong [45] have developed charged droplet generator composed of one needle and one plate. A voltage between the needle and the plate allowed generating an electric field and, as a consequence, emitting charged droplets from the needle. Today, this geometry is commonly used in electrospray devices [46]. More recently, new systems have been developed to create charged droplets in microfluidic devices [37, 47, 48]. In the same

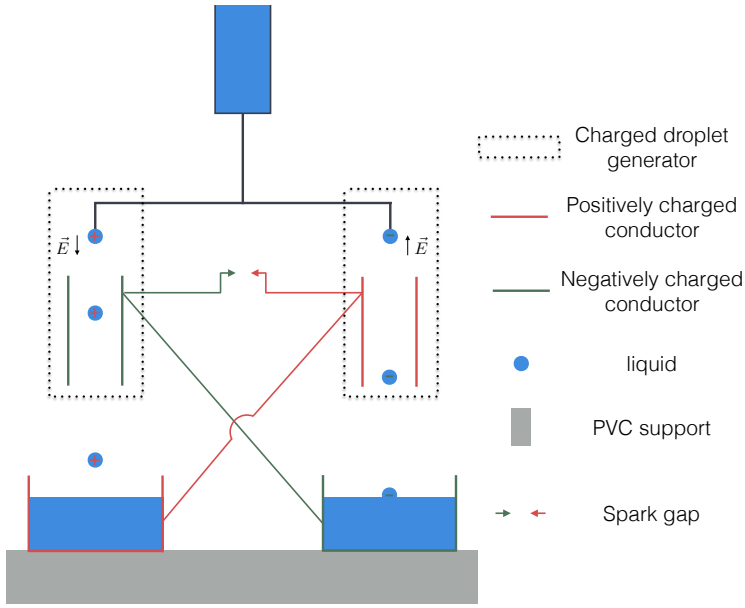

Figure 3.2: Kelvin drop generator. The system is composed of two charged droplet generators interconnected. The avalanche process allows generating high voltage between the electrodes.

way, the method remains the same but the geometry is adapted in order to respect the requirements of small closed-channels generating the droplets.

3.1.1 Charged droplet generators

From the study of previous models, we developed our own generator geometries. The three geometries developed during the thesis are presented in Fig. 3.3. They are named model A, B and C in the rest of this thesis. In each case, the basic components of the charge migration process are present.

- The model A was designed to easily generate charged droplets with various liquids (i.e. a large range of liquid surface tension, viscosity,...). We focused its development on two specific aspects: (i) to be able to deal with low surface tension fluids (ii) to be able to induce an electric field easy to model in order to quantify the charge migration process. In order to tackle these constraints, the charged droplet generator was made of two metal disks, parallel and positioned along a vertical axis. The top plate was pierced by a needle from which droplets was formed. The bottom plate was drilled in its center to allow the droplet falling away from the charged droplet generator. Both metallic plates were tied together by an insulating plastic piece. The model A allowed to handily charge

droplets by connecting a syringe or a syringe pump to the needle and generating droplets while a voltage was applied between the electrodes.

- The model B was designed to produce charged droplets in microgravity conditions. In absence of gravity, droplets cannot detach from the needle because of their weight. To overpass this limitation, the charged droplet generator model B was coupled with a system based on air coaxial entrainment flow. As shown in Fig. 3.3, laminar airflow was produced around the needle. In order to generate droplets, liquid was brought at the edge of the needle. The airflow around the needle then detached the hanging liquid from the needle and entrained it away from the charged droplet generator. By adjusting the airflow, we controlled the droplet generation rate and the droplet size. The absence of the top plane electrode changed the electric field geometry. Despite this variation, the droplet charge process stays the same as the model A.

- The Model C was developed to produce sub-millimetric droplets. The electrode geometry and the charge mechanism was the same as the Model A. The difference lies in the droplet generation process. The bottom of the liquid container was composed of a metallic electrode. A hole of 200 μm in radius was drilled in the center of the electrode. The top of the liquid container was composed of a piezoelectric crystal. A voltage peak could deform the piezoelectric. In doing so, the container deformation ejected liquid by the hole pierced in the electrode, generating a small electrically charged droplet. The mechanism has already been described in the past by Terwagne *et all* [49].

Despite the different geometries, the underlying physics remains the same. The electric field, induced by the voltage between two metallic pieces, generates the charge migration in the droplet. The total charge induced in the droplet depends on the value of the electric field. In order to quantitatively explain the phenomenon, we focus our attention on the model A in Fig. 3.3. In this particular case, the electric field can be approximated by a homogeneous electric field between two charged plates (i.e. a planar capacitor). The electric field generated by a planar capacitor is expressed by:

$$E = \frac{V\epsilon_0}{d} \tag{3.1}$$

where E is the electric field, V the applied voltage on the capacitor, ϵ_0 the vacuum permittivity and d is the distance between the plates. As a consequence, at the equilibrium, the charge on one plate of the capacitor q_p is equal to:

$$q_p = \frac{V\epsilon_0 S_p}{d} \tag{3.2}$$

where S_p is the surface of the plate. If we make the hypothesis that the droplet does not influence the electric field, the total charge induced in the droplet by the electric

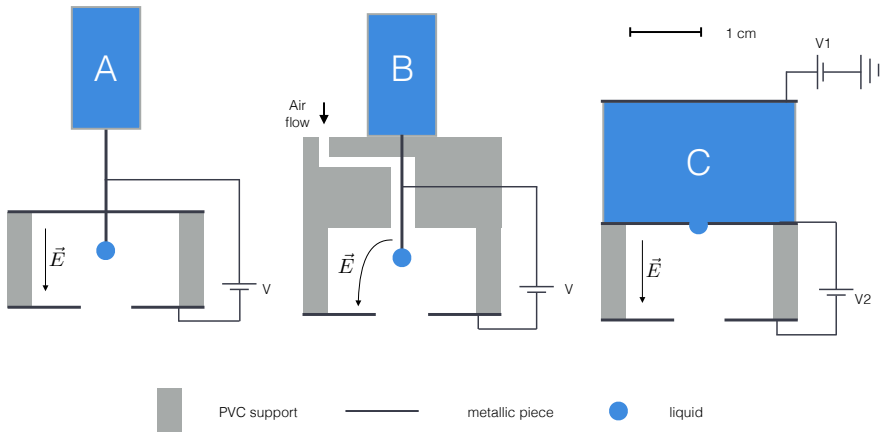

Figure 3.3: Sketch of the three different geometries of charged droplet generators. The voltage between metallic parts generate an electric field ($\vec{E}$) and charge by influence the pendant droplet.

field is:

$$q = \frac{V \epsilon_0 4\pi r^2}{d} \tag{3.3}$$

where r is the droplet radius. Obviously, the reasoning is the same for more complex geometries, such as model B. Once the value of the electric field applied on the droplet is known, the charge induced in the droplet can be deduced. The Eq. 3.3 implies that, for a known voltage, droplet radius and generator geometry, we can deduce the charge induced in a droplet via charge migration. The Eq. 3.3 has been validated experimentally by measuring the droplet charge as a function of the voltage V and the distance between both metallic plates d. The measurement technique is explained in the next Section (see Section 3.2). The Fig. 3.4 (top) shows the excess of charge in a droplet, normalized by the droplet surface $S = 4\pi r^2$, as a function of the voltage V. The Fig. 3.4 (bottom) shows the excess of charges in the droplet as a function of the distance d between the metallic plates. The Eq. 3.3 is in great agreement with the measurements. The hypothesis of a homogeneous electric field only shows its limitation for small distances d. The Fig. 3.4 (bottom) demonstrates that for $d < 5$ mm the predictive law is no more valid.

The present measurements enhance the simple theory explaining how the charge by migration allows to reliably generate electrically charged droplets. However, two questions are still unanswered. The Eq. 3.3 corresponds to the charge induced in the droplet at the equilibrium. Of course, the charge migration from the liquid bulk to the droplet takes a certain amount of time. This migration time may eventually be more important than the droplet generation time. Furthermore, the Eq. 3.3 does not

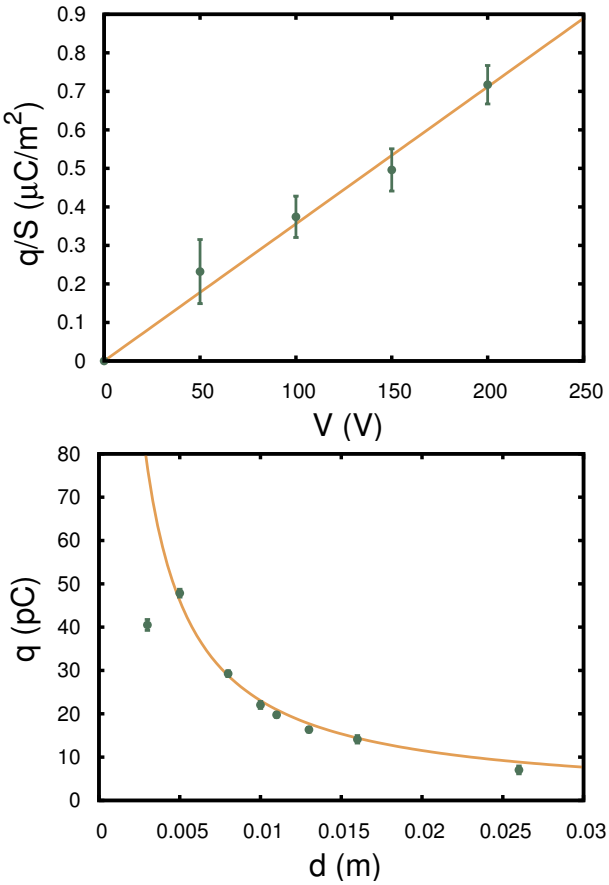

Figure 3.4: Measurements of the electric charges induced in droplets via the charged droplet generator model A. (top) The charge density (q/S) as a function of the applied voltage (V). One triangle corresponds to 10 measures. The error bars show the standard deviation of the measures. (bottom) The electric charge as a function of the distance between the planar electrodes. One green point corresponds to 10 measures. Errors bars are typically of the symbol size. The fit on the two graphs are deduced from Eq. 3.3.

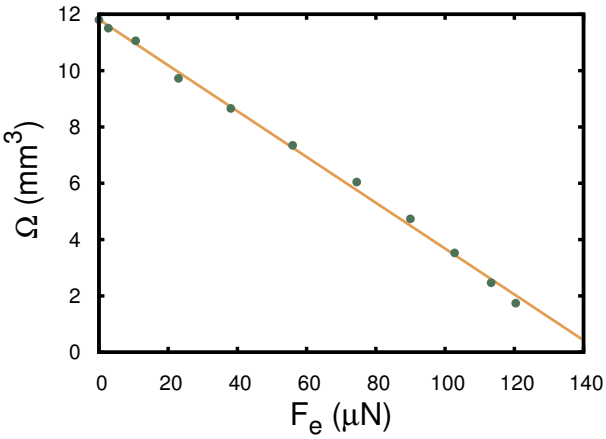

Figure 3.5: Droplet volume Ω as a function of the electric force $F_e = qE$ applied on the hanging droplet. The droplet volume decrease with the applied electric field (i.e. with the applied voltage between the electrodes). One green disks corresponds to 10 measures. Error bars are typically of the symbol size. The orange line corresponds to Eq. 3.4.

indicate the nature of the electric charge induced in the droplet. Such problematics, which require to perform experiments on several kinds of liquids, are tackled in Section 4.1.

3.1.2 Influence of the electric field on the droplet generation

Beyond the droplet charge itself, the electric field induced between both electrodes also influences how the droplet detaches from the needles and the droplet motion after its separation from the needle.

The droplet surface was measured by image analysis. We observed that the droplet surface decreases when the electric field increases. To explain this behavior, we computed the volume Ω of the pendant droplet on the needle of the generator. It can be achieved by expressing the equilibrium between gravity, electrical force between both plates and droplet surface tension:

$$\Omega = \frac{2\pi\gamma r_n - qE}{\rho g} \tag{3.4}$$

with r_n the radius of the needle, γ the surface tension of the liquid, ρ the liquid density and g the acceleration of gravity. The electric field E is supposed homogeneous, which means $E = V/d$. The Eq. 3.4 explains the decreasing of the droplet surface observed experimentally. The comparison between the theory and the experiment is shown in Fig. 3.5. The green disks correspond to the mean on ten measurements. Error bars are hidden by the symbol sizes. When the electric field increases, the electric

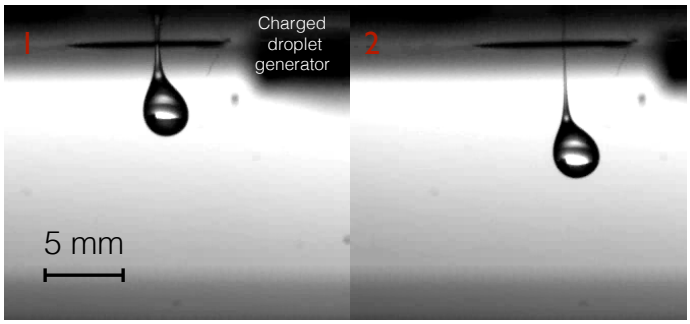

Figure 3.6: The charged droplet generator ejects a viscous droplet. The voltage applied between electrodes is $V = 5000V$. The liquid is composed of silicone oil 50 cSt. Because of the liquid high viscosity, the droplet separates from the liquid outside of the charged droplet generator, which limits the droplet charge.

force tends to pull the droplet away from the needle. As a consequence, the droplet volume decreases with the applied electric force. The Eq. 3.4 is found to be in good agreement with the observations.

It should be noted that the experiments performed during this thesis were always carried out with liquids that are considered Newtonian liquids with a low viscosity (around 1 cSt). The charged droplet generator may be difficult to use with complex or viscous liquids. The present statement is illustrated in Fig. 3.6. The image corresponds the droplet generator model A working with a voltage $V = 5000$ V and a liquid composed of silicone oil 50 cSt. Because of the high viscosity of the silicone oil, the droplet drags away liquid when falling from the charged droplet generator. As a consequence, the droplet is formed outside of the charged droplet generator, meaning that the droplet does not charge as expected.

The electric field induced between both electrodes does not only influence the volume of the charged droplet. It also influences its ejection speed. In order to measure this influence, the droplet instantaneous speed u_0 at 3 mm from the charged droplet generator was measured by high-speed imaging. The experiment is schematized in Fig. 3.7. The measured droplet speed is shown in Fig. 3.8 as a function of the voltage V applied on the charged droplet generator multiplied by the charge q of the droplet and divided by the droplet radius. We deduce from the experiment that the droplet speed increases with the voltage V and the charge q of the droplet.

When the charged droplet detaches from the generator, it still endures the electric

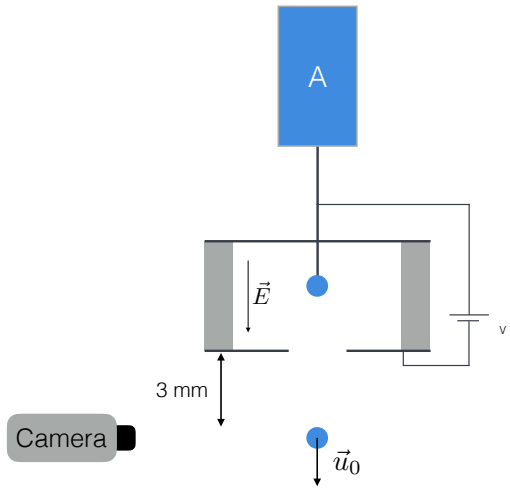

Figure 3.7: Sketch of the droplet speed measurement at the exit of the charged droplet generator.

field induced by the charged droplet generator. As a consequence, the charged droplet is accelerated by both the gravity and the electric force, which explains the increase of its speed. The Fig. 3.8 shows that a charged droplet can be ejected twice as fast as a neutral droplet. The increased droplet speed due to the electric field may be critical when it is question of droplet management and storage. This point is discussed in Section 3.3.

In conclusion, we developed three geometries of charged droplet generators. The model A is the mainly used model, the model B is used in microgravity and the model C is used to generate small charged droplets. The three models use the charge migration process to induce an excess of charges in droplets. The amount of charges induced in the droplet can be predicted by knowing the droplet surface and the electric field produced by the charged droplet generator. Moreover, the charged droplet is influenced by the electric field of the charged droplet generator. Indeed, we measured that the charged droplet volume decreases when the electric field increases. At the exit of the charged droplet generator, we measured an increase of the charged droplet speed with the electric field.

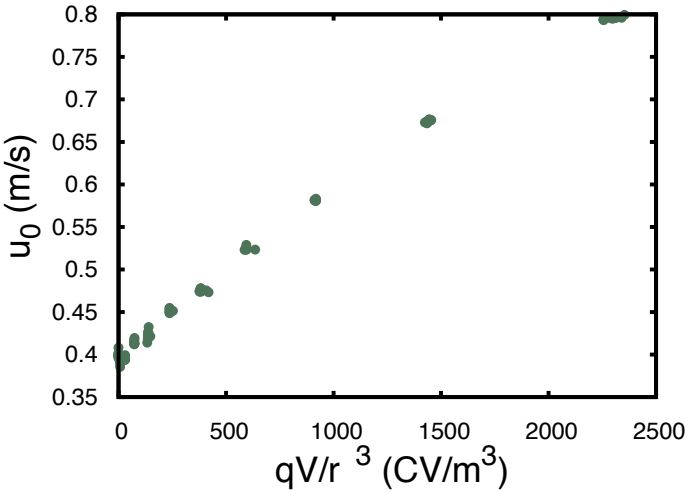

Figure 3.8: The speed, u_0, as a function of qV/r^3. The droplet speed increases with its charge and with the voltage applied on the charged droplet generator. One green point corresponds to 10 measures. Errors bars are typically of the symbol size.

3.2 Measuring the charge of droplets

In the previous Section, we developed the theory necessary to understand the underlying physics of the droplet charge by migration. We showed that by knowing the electric field acting on the droplet and the droplet radius, it is possible to deduce the droplet charge. However, the modeling of the electric field is not always necessary. Indeed, for a given setup configuration, the charge induced in the droplet is always roughly the same. As a consequence, a calibration, via a charge measurement, is enough to know precisely the charge of the droplet. Therefore, the next step is to develop a system able to measure the electric charge of a droplet.

Measurements of the charge induced in thousands of droplet conceived during this thesis were performed by using a Faraday cup. This kind of device is commonly used in ions beam experiments [50]. In practice, the Faraday cup gathers an ion beam and measures its charge over time. We developed a Faraday cup based on the same principles but designed to measure the charge of mesoscopic objects, i.e. millimetric charged droplets. A schema of the setup is presented in Fig. 3.9. Such a setup can also be used to measure the charge of other mesoscopic objects such as granular materials [51].

The Faraday cup in Fig. 3.9 is composed of two concentric cups, which plays the role of electrodes. The sides of both cups, the electrodes, face each other and form a capacitor. The air between the electrodes plays the roles of insulator in the capacitor. The top of the cup was covered with an insulated cap to protect the device from

objects that could fall between electrodes. A BNC connector was hooked up to the Faraday cup as the following: the shield connection of the BNC was connected to the outside electrode while the inner conductor of the BNC was connected to the inside electrode. On the other side, the BNC connector was connected to the triax input of an electrometer thanks to an adapter. Once the electrometer is set in Coulomb measurement function, the charge of any object in contact with the inner cup can be pumped up and measured. The cylindrical shape of the Faraday cup was chosen to minimize the influence of external charges [52].

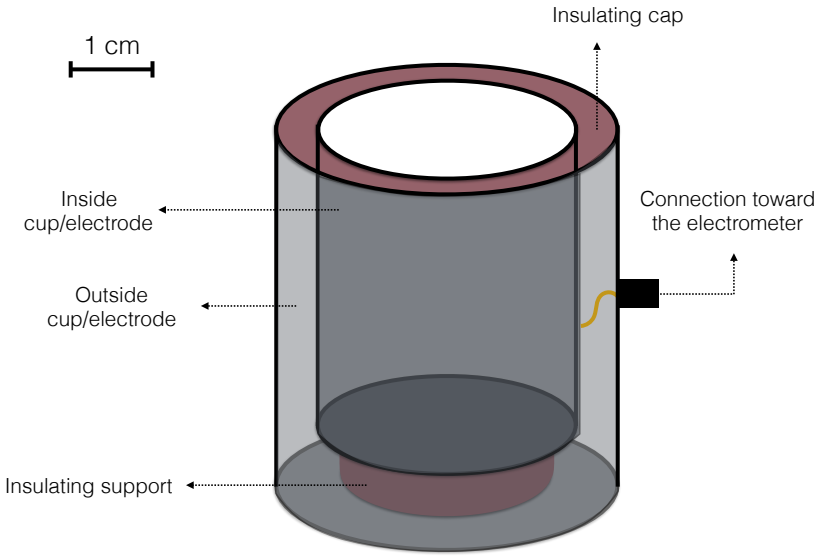

Figure 3.9: Sketch of the Faraday cup. Any charged object falling in the inside cup transmits its charge to the electrometer. The electrometer is then able to measure the charge over time.

In practice, when a charged object contacts the inside of the Faraday cup, it transfers its charge to the capacitor formed by the two electrodes. The charge is then precisely measured by a reference capacitor inside the electrometer. A function ZERO CHECK allows resetting the charge measurement to zero whenever it is necessary. The electrometer used in all the experiments (Keithley 6514) can perform coulomb measurements from $\pm$ 10 fC to $\pm$ 2.1 C. Two different Faraday cups were developed during this thesis, allowing to measure the charge of free falling droplets and bouncing droplets. Both Faraday cups differ by their size but give the same charge measurements, confirming the descriptions above. The Fig. 3.10 shows typical charge measurements. The charged droplets were generated by the charged droplet generator model A. Several droplets were dropped inside the Faraday cup. The Fig.

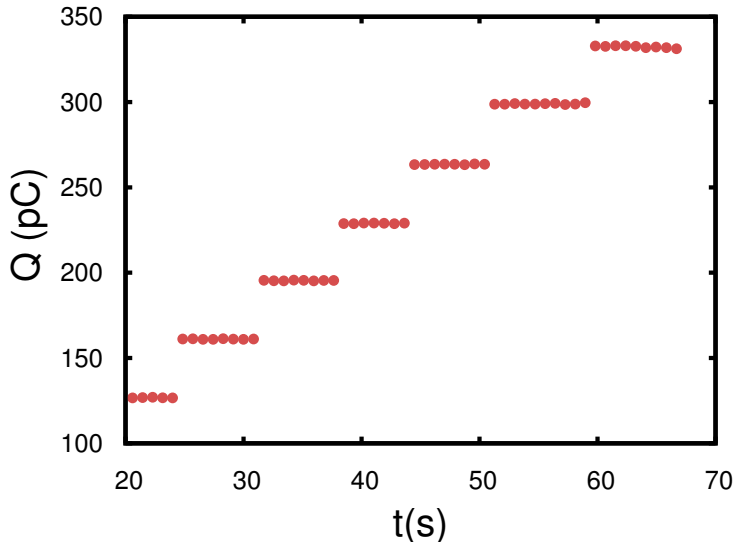

Figure 3.10: Typical measurement of droplet charges via the Faraday Cup. The charge of 6 droplets was measured in 35 s. Half the points were plotted for the clarity of the graph.

3.10 shows the measurement on six of these charged droplets. During each contact between a charged droplet and the Faraday cup, we observe a leap in the charge measured by the electrometer. The leap is the same for all the six charge measurements. This charge measurement confirms that the charged droplet generator induces the same charge in each droplet generated.

Lastly, we have to mention the existence of a “dynamic" Faraday cup. Such a Faraday cup looks exactly the same as the “classic" Faraday cup except that its bottom is hollowed (i.e. the electrodes are composed of two concentric cylinders instead of cups). Instead of measuring the charge by transferring directly the charge from the droplet to the Faraday cup, the droplet falls trough the “dynamic" Faraday cup and induces charges to the electrodes. Such a model is less accurate than the “classic" Faraday cup but can be useful in certain experiments where the charge of the droplet have to be conserved over time. More information about this particular method can be found in [53] or [54].

In conclusion, the Faraday cup, similar to a cup-shaped capacitor, is found to be a good way to measure precisely the charge of electrically charged droplets.

3.3 Droplet storage methods

As explained in the first description of the thesis (Section 2.4), we developed new tools that allow storing a droplet while limiting charge leakage. These new tools are

based on three well known phenomena: The microgravity, the bouncing droplet and the Leidenfrost effect. The three storage methods are described in this Section. Their advantages and disadvantages are detailed.

3.3.1 The microgravity

The first idea that comes in mind when thinking about storing a charged droplet is to avoid the gravity. Indeed, without any attraction toward the Earth, the charged droplet should simply float in the air. Thanks to The European Space Agency, we had the opportunity to achieve these conditions by means of parabolic flights.

An airplane, with good pilots, may perform parabola during a flight. While performing parabola, the airplane passengers endure various accelerations due to the plane motion. The airplane displacement during one parabola is schematized in Fig. 3.11. The airplane altitude is plotted as a function of the time. At the beginning of the parabola, the airplane goes up with an acceleration of 0.8 g (g being the earth gravity). As a consequence, airplane passengers endure an acceleration equals to 1.8 g. Near the top of the parabola, the airplane decelerates as precisely as possible to attain an acceleration of -1 g. After the top of the parabola, the pilot maintain the declaration of -1 g by stepping on the gas in order to compensate the air friction. During all the top part of the parabola, the airplane passengers are in microgravity condition (i.e. at 0 g) in their frame of reference. Finally, the plane re-accelerates at the end of the parabola to come back to its initial horizontal trajectory.

One parabola corresponds to 22 s of microgravity. The microgravity conditions are obtained with a precision of $\pm$ 0.05 g. During this period, a charged droplet can freely move in the airplane. This last point is the best advantage of the microgravity. Indeed, no external forces are applied on the droplet, meaning that the droplet is free to interact with its environnement. On the contrary, the storage via electrodynamic [19], diamagnetical [18] or acoustic [55] traps uses external forces to maintain the droplet in one specific position. In practice, we used the microgravity conditions to measure the interaction between two charged droplets sent toward each other. The study is described in details in Chap 5.

Naturally, the microgravity conditions imply specific adaptations. For example, the absence of gravity makes more difficult the droplet detachment from a needle. As a consequence, during microgravity sessions, charged droplets were generated with the charged droplet generator model B (see Fig. 3.3). A detailed schema of the charged droplet generator is shown in Fig. 3.12. A cylindrical plastic piece (in grey) encircled a metallic needle. A metallic plate was fixed at the edge of the plastic piece. A hole pierced in the plastic piece allowed air to flow around the needle. Two support screws were screwed up in the plastic piece in order to maintain the metallic needle location. A voltage generator allowed controlling the voltage between the support screw (itself connected to the metallic needle) and the metallic plate. The charged droplet generator was coupled with an air pump. As shown in Fig. 3.12, laminar

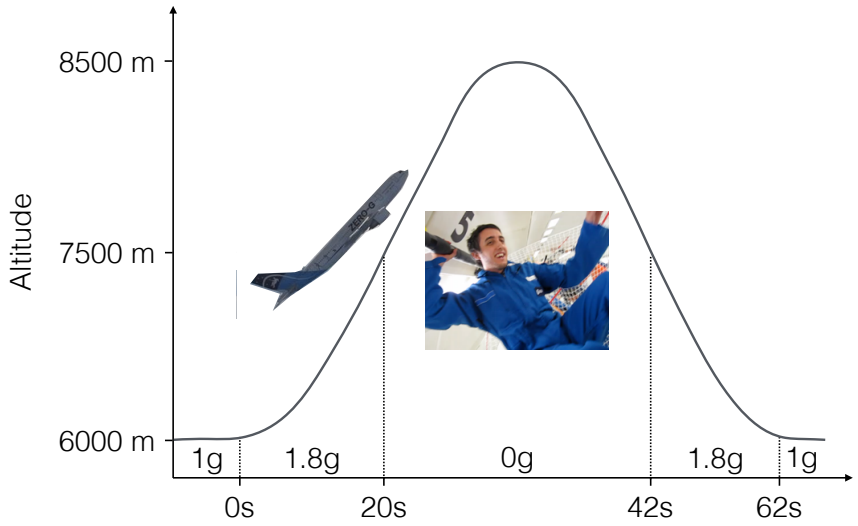

Figure 3.11: Description of the airplane motion during the parabola. The airplane altitude is plotted as a function of the time. At the beginning of the parabola, the airplane goes up, passengers endures a hyper gravity of 1.8 g. At the top of the parabola the airplane decreases its acceleration to -1 g, generating microgravity condition for passengers. At the end of the parabola, the airplane re-accelerates to recover its initial horizontal motion.

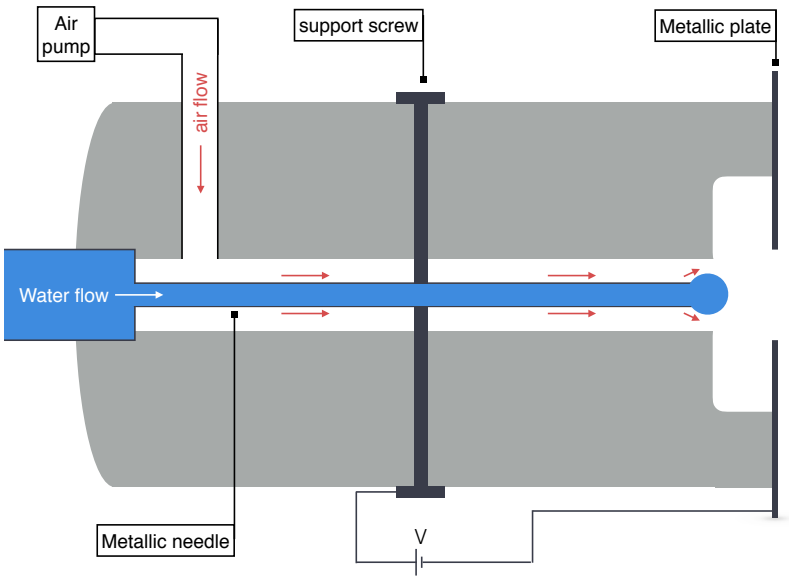

Figure 3.12: Schema of the charged droplet generator model B used during microgravity sessions. By comparaison to the model A, the air pump generates an air flow that allow detaching the droplet in microgravity conditions.

airflow was generated around the needle. In order to generate a charged droplet, we firstly accumulated liquid at the edge of the metallic needle. It was done by controlling the water flow injected in the metallic needle. Then, the airflow detached and blew away the charged droplet. By controlling the airflow, it was possible to control the droplet generation rate and the droplet size.

Finally, experiments carried out during parabolic flights had to respect specific security requirements. Firstly, the experiment had to be developed in a metallic rack of a specific dimension (100 cm x 106 cm x 80 cm). Secondly, any liquids had to be manipulated in a confined space. A typical experiment setup dedicated to parabolic flight is shown in Fig. 3.13. Beyond all the mess, we can observe from the left to the right the high-speed camera, the confined space (the droplet generation chamber) and the lighting setup.

The microgravity conditions were used to study the interaction between two charged droplets moving toward each other. It allowed us highlighting the influence of electric charges on the droplet trajectories and on the impact between droplets. This subject is addressed in Chapter 5.

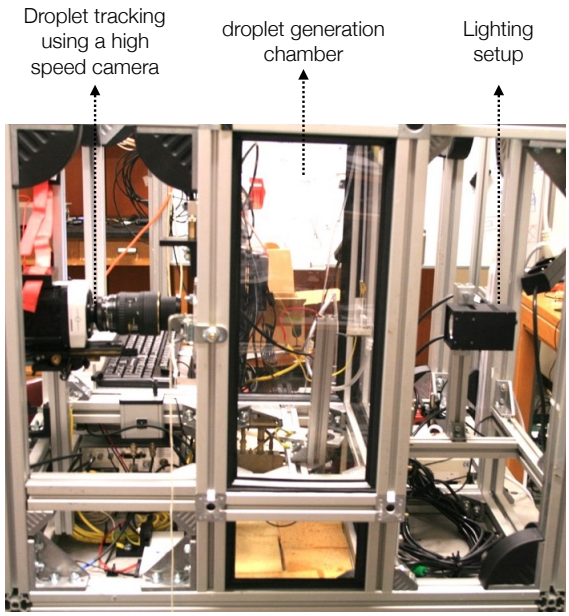

Figure 3.13: Image of the entire microgravity setup. The experiment were performed in the droplet generation chamber.

3.3.2 The vibrating bath

The microgravity session during one parabola is limited to 22 s. However, certain studies require to observe the charged droplet behavior during longer times. The vibrating bath answers to this requirement.

It is known since the work of Lord Rayleigh [56] that the collision between two droplets may lead to a bounce. From this observation, other studies have been focused on the delayed coalescence of a droplet falling on a liquid surface [57–59]. These observations can be basically described by the following statement: when the falling droplet approaches the liquid surface, a thin air layer remains between both liquids. It takes a certain amount of time for the air between the droplet and the liquid surface to drain out. The drainage of the air layer is due to the pressure applied by the droplet on the air trapped between the liquid interface and the droplet. During the time needed for the air to drain out (generally about 1 s), the droplet stays on the liquid surface.

The delayed coalescence can be maintained by various methods. For example, generating a flow in the liquid bath can regenerate the air layer between the droplet and the liquid bath [59,60]. A second approach, developed by Couder *et al* [61] consists in vibrating the liquid bath. Because of the bath oscillation, the droplet bounces on the air layer between the droplet and the liquid bath. If the frequency and amplitude of the oscillation are well chosen, the air layer between the bouncing droplet and the oscillating liquid may be regenerated at each bounce. The phenomenon is schematized in Fig. 3.14 (top). An image of a silicone oil droplet (1 cSt) bouncing on a silicone oil bath (1000 cSt) is shown in Fig. 3.14 (bottom).

The droplet bouncing on a liquid, seemingly simple, led to tremendous numbers of research. Studies have been interested in the conditions for the bouncing to happen [62], but also to other phenomena that come out from this experiment. Indeed, according to the experiment configuration, the bouncing droplet can have different bouncing modes [49] and can also propel itself [63, 64].

The bouncing droplet method is a good candidate for charged droplet storage. Indeed, it allows storing a droplet for a long time (several hours) while the droplet being only in contact with ambient air. The absence of contact with a conductor avoids the rapid charge leakage over time. Moreover, the setup answers to limitations of other storage methods such as the use of diamagnetic or electrodynamic traps [18, 19], droplet storage in silicone oil pool [65] or acoustic traps [66, 67]. Indeed, the bouncing drop method allows keeping millimetric droplets on a relative horizontal plane. Charged droplet may be easily displaced on this horizontal plane and several droplets may be stored on the vibrating bath. The bouncing method also avoids using an external electric field that could influence the charges behavior. Moreover, the study may be performed in ambient air, allowing studying the droplet evaporation.

To perform our experiments, we used an electromagnetic shaker (model GW-V55 or GW-V2). The bath was filed with high viscosity silicone oil (1000 cSt). The defor-

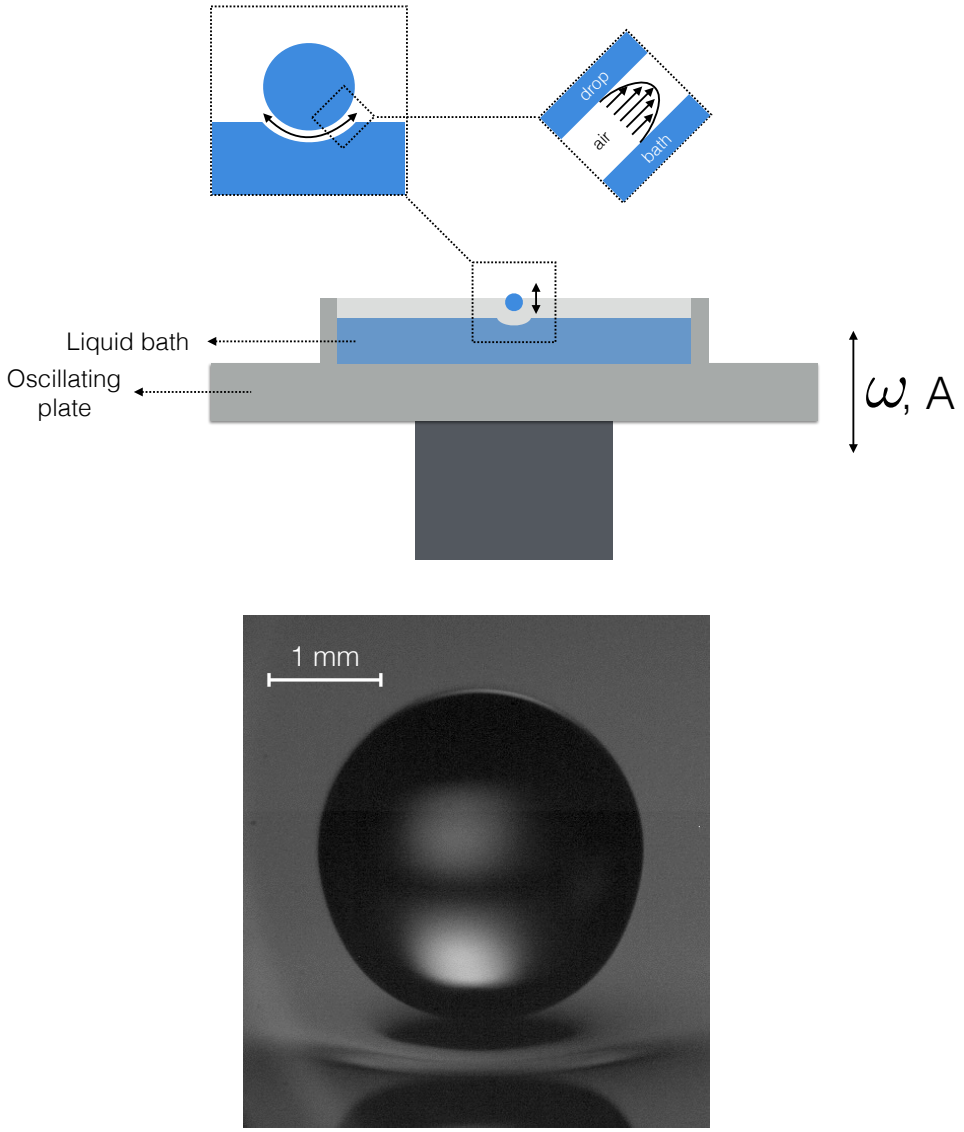

Figure 3.14: (top) Schema of the bouncing drop method. Because of the plate oscillation, the air layer between the droplet and the bath is regenerated. It allows storing the droplet for a long time (more than one day). (bottom) Image of a silicone oil droplet (1 cSt) bouncing on a silicone oil bath (1000 cSt).

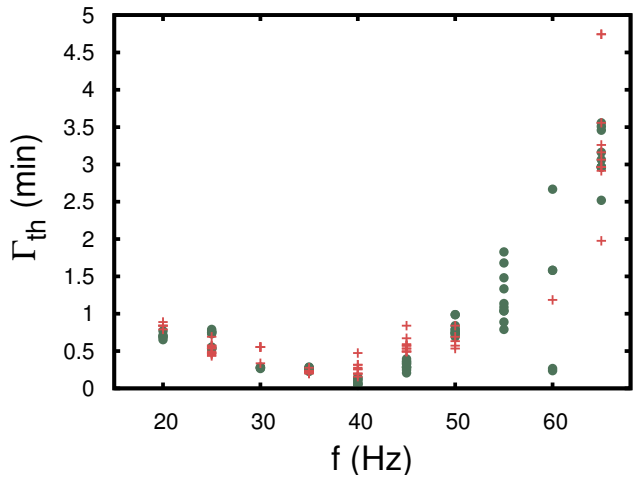

Figure 3.15: Graph of the bouncing threshold of drops with a radius r =0.7 mm and a charge q = 0 pC or q =15 pC. Green disks correspond to neutral drops while red crosses correspond to charged drops.

mation of the liquid bath is greatly damped by the high viscosity. Therefore, without any external perturbation, the droplet only moves vertically due to its bouncing. The bath oscillation is described by the dimensionless number $\Gamma = A\omega^2/g$, where A is the oscillation amplitude of the vibrating bath, ω is the angular frequency of the vibrating bath and g is the acceleration of the gravity. The droplet bouncing is possible only above a given threshold Γ_{th} which depends on the size and the viscosity of the droplet and on the frequency f of the oscillation [68].

In order to study the influence of the charge on the droplet bounce, we looked at the oscillating bath acceleration and frequency needed to store a charged droplet. The common approach is to study the critical acceleration needed to produce bouncing droplets as a function of the oscillation frequency f. Experiments were performed with charged and neutral droplets. Both charged and neutral droplets were composed of silicone oil 1.5 cSt with an addition of 1 percent of ethanol. Such a liquid composition allows to combine the surface tension and viscosity needed for the droplet to easily bounce on the liquid bath and the conductivity needed to charge the droplet. The droplet radius and charge was respectively $r = 0.7$ mm and q =0 pC or q =15 pC. In Fig. 3.15, the red crosses correspond the acceleration threshold for charged droplets while the green disks correspond to the acceleration threshold for neutral drops. The experiment does not evidence any difference between the charged and the neutral droplets. We conclude that the bouncing threshold Γ_{th} is not affected by the charge carried by the droplet.

Because the present experiments, we make the assumption that charged droplets bounce in the same way as neutral droplets. In Section 4.2, the bouncing droplet

method is used to measure the droplet charge over time, while in Chapter 6 we study both the interaction between charged bouncing droplets and electric fields and the interaction between two charged droplets on the vibrating bath.

3.3.3 The Leidenfrost effect

When a droplet is dropped on a surface hotter than the droplet boiling point, it produces a vapor flux. If the vapor flux is important enough, an insulating vapor layer is produced between the droplet and the heated surface. Droplets levitating on their own vapor are defined as being in Leidenfrost state. The phenomenon is named according to one of the first scientists to discover the phenomenon [69].

The Leidenfrost effect is commonly studied with droplets levitating at the surface of a solid. Typically, a water droplet dropped on a surface heated to 250 °C levitates on its own vapor [70–72]. The experiment is easily reproducible while cooking. For example, droplets moving quickly on the surface of a hot frying pan are in Leidenfrost state. However, we had difficulties to keep charges inside droplets in Leidenfrost state above a solid surface. It is explained by small contacts that can occur when the droplet is dropped on the heated surface. The droplet contact does not influence the Leidenfrost state itself. Indeed, liquid in contact with the solid interface quickly evaporates, the majority of the droplet staying in Leidenfrost state. However, electric charges have time to migrate from the liquid to the solid surface during these brief contacts. In Section 4.1, we show that a contact of few milliseconds is sufficient for all the charges to migrate. As a consequence, the droplet is not able to keep its excess of charges while being in Leidenfrost state on a solid surface. Moreover, the electric charges can affect the stability of the Leidenfrost droplet. The destabilization of a charged droplet in Leidenfrost state at the surface of a solid has been studied by Celestini *et al* [71]. They induced a voltage between a needle inserted in the Leidenfrost droplet and the solid substrate. They observed the decrease of the vapor layer when increasing the voltage between the droplet and the liquid substrate. For voltages above 40 V, they observed a destabilization of the droplet leading to the annihilation of the Leidenfrost effect.

The Leidenfrost effect may also occur for droplets levitating above a liquid bath. In this case, the evaporation of the droplet or the evaporation of the liquid bath is important enough to maintain the air layer between the droplet and the liquid bath. Droplets levitating on the liquid bath vapor are defined as being in inverse-Leidenfrost state [73, 74]. On the contrary of the solid substrate, the liquid pool does not allow small contacts between the levitating droplet and the liquid surface. Indeed, one small contact would induce the coalescence between both liquids. As a consequence, electrically charged droplets can be stored via this setup. In the past, inverse-Leidenfrost experiments were performed with water droplets at the surface of liquid nitrogen [74]. However, the experimental setup associated with the experiment (thermostat limiting the nitrogen heating, droplet freezing,...) limits the usage of the

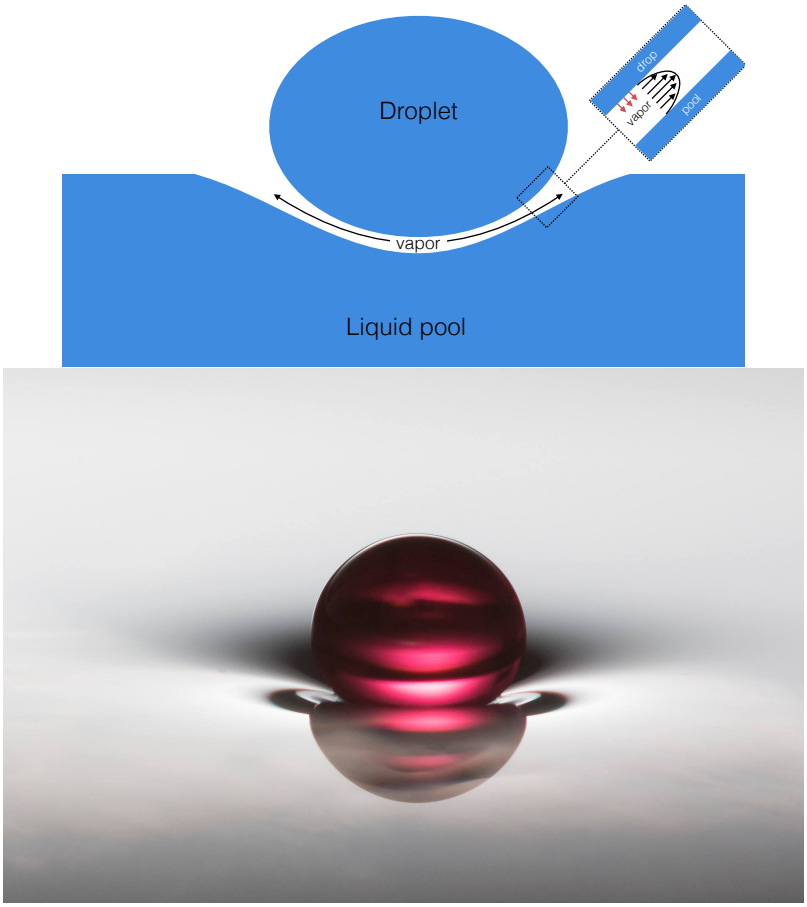

Figure 3.16: (top) Schema of a Leidenfrost droplet levitating on a liquid pool. The liquid pool is heated above the droplet boiling temperature. Because of the droplet evaporation, the vapor layer between the droplet and the bath is regenerated. (bottom) An ethanol drop with red dye levitates in the Leidenfrost state over a pool of silicone oil V20. The drop radius is $R = 1.2$ *mm and the pool is at* $T_p = 80\,^\circ C$ *while the boiling point of ethanol is* $T_{\rm sat} = 78\,^\circ C$*. (Image credit: Florence Cavagnon).*

setup as a storage system.

Recently, it has been shown that droplets can be set in Leidenfrost state at the surface of heated silicone bath [75, 76]. During this thesis we used this particular experimental setup to store electrically charged droplets. The Fig. 3.16 shows a droplet in Leidenfrost state at the surface of a heated silicone pool. In Fig. 3.16 (top), we schematized the Leidenfrost droplet levitation. A thin vapor layer is present between the droplet and the liquid pool. This vapor layer tends to drain out because of the droplet pressure. By evaporating, the droplet regenerates the vapor layer. In Fig. 3.16 (bottom), the droplet was composed of ethanol while the liquid pool was composed of silicone oil 20 cSt. During the experiment, the liquid pool was heated at $T_p = 80$ °C (i.e. above the ethanol boiling temperature $T_{\text{sat}} = 78$ °C). The setup was chosen for the experimental comfort. Indeed, the system is easy to set up and works for a large range of temperature (starting at the droplet boiling temperature, which is exceptional for the Leidenfrost effect). Experiments were performed with two sorts of liquid: ethanol and HFE-7100. The thermal properties of both liquids make them ideal for the study of the Leidenfrost effect.

The detail of the droplet in Leidenfrost state on a silicone bath is described in [76]. The article is focused on the droplet evaporation rate and on both the shape of the droplet and the deformation induced by the levitating drop on the liquid pool. For the purpose of the study of charged droplets, the Leidenfrost effect on a liquid bath possess the following advantages compare: (i) the droplet is not deformed over time (ii) droplets with radii beyond the capillary length may be stored (iii) liquids with various chemical compositions may be stored. Naturally, the setup has also some drawbacks: (i) The droplet freely moves on the liquid pool, which may complicate its imaging over time (ii) The Leidenfrost droplet does not have a spherical shape. Its shape depends on its own properties but also on the properties of the liquid pool. (iii) The quick evaporation of the droplet limits its study time. Beyond the advantages and disadvantages of the storage method, the influence of electric charges on the Leidenfrost state are interesting to study. Indeed, the Leidenfrost state on a liquid pool corresponds to two liquid surfaces separated by a thin vapor layer (with a thickness about 1 μm). At his scale, the electric interaction should be important enough to influence the shape and the thickness of this vapor layer.

In this thesis we focus our attention on the influence of the electric charge on the Leidenfrost state. The Leidenfrost effect is studied in Chapter 7. We investigate how electric charges influence the droplet shape and the droplet stability while stored on a heated liquid bath.

In conclusion, we used three storage methods to study electrically charged droplets. The microgravity conditions allow storing charged droplet without influencing their behavior. However, the experimental requirements and the duration of the storage limit the use of this method. The vibrating bath method allows storing charged droplets during several hours. The charged droplet is free to move

on the two dimensions of the liquid bath, but is deformed over time by its vertical bouncing. The Leidenfrost effect allows storing a charged droplet on its own vapor. We are interested in the influence of electric charges on the Leidenfrost droplets levitating above a heated liquid pool.

4

Influence of the charge on the droplet

Contents

In this Chapter, we focus our attention on the physical behavior of a charged droplet. The first questions arising from this subject concern the relationship between the charge and the droplet. In other words, “how do the electric charges influence the droplet?". But also, “how do the droplet properties influence the charge migration in the droplet?". The Chapter 2 described previous research that attempted to answer to these questions. In this Chapter, we continue these investigations through different experiments.

The first Section (4.1) is dedicated to the influence of the liquid composition on the charge migration in the droplet. In particular, we put in evidence the parameters governing the phenomenon (i.e. the liquid conductivity and relative permittivity). The Section 4.2 questions the charge loss of a droplet. By storing the droplet via the vibrating bath method, we measure and model the droplet charge loss over time. Finally, the Section 4.3 is directed toward the study of the influence of the electric charges on the droplet surface energy.

4.1 Influence of the liquid composition

The Section 3.1 explained the basic process by which an electric field generates charges migration to produce electrically charged droplets. By examining the charge equilibrium, we deduced the charge induced in the droplet as being:

$$q = \epsilon_0 E S \tag{4.1}$$

where E is the value of the electric field applied on the generated droplet and S is the droplet surface. However, numerous questions are left open. Indeed, the Eq. 4.1, does not indicate the characteristic time for the charges to migrate in the droplet neither the origin of these charges. In order to answer to these questions, electrically charged droplets were produced with different kinds of liquids and their charges were measured. Note that in this study, we only examine the physical characteristics of the liquids and not their chemical composition.

The charge deduced from Eq. 4.1 corresponds to the charge equilibrium with the applied external electric field. However, the transition from a neutral droplet to this particular charge density is not instantaneous. Once the external electric field influences the system, charges have to migrate in the droplet until reaching the charge density corresponding to the scalar value of the electric field. In practice, the Eq. 4.1 implies that the characteristic time to generate a charged droplet τ is more important than the charge migration time τ_c. In the next lines, we examine the experimental conditions needed to reach this requirement. The experiments described in this Section were performed with the charged droplet generator model A. The characteristic time τ to generate a droplet was kept constant for each experiment $\tau =$ 1 s.

The first parameter to look at, when talking about charge migration, is the electric conductivity σ. Indeed, the characteristic time for charges to migrate τ_c should vary with the charge ability to move in the liquid. In order to vary the liquid conductivity, we measured the charge of droplets made of HCl solutions with concentrations from 0 to 1 M. We report in Fig. 4.1 the measured charge density as a function of the conductivity of each solution. The conductivity of each solution was deduced from literature [77, 78]. We see on the graph that despite an increase of 10^6 times the conductivity, the droplet charge does not significantly change. Moreover, the charge density is in agreement with the one deduced from Eq. 3.1. In other words, the Fig. 4.1 indicates that the low conductivity of pure water (i.e. HCl mixture of 0M) is important enough to allow the charges to migrate in less than $\tau = 1$ s. Moreover, as stated by Eq. 4.1, once the equilibrium is reached, the charge induced in the droplet does not depend on the liquid conductivity. The addition of ions to increase the charge migration in water was employed in previous publications [65, 79]. We observe in Fig. 4.1 that an addition of ions is does not influence the charge of a water droplet.

From this first observation, we extended our study to other liquids in order to check both the influence of lower conductivities and other properties such as the

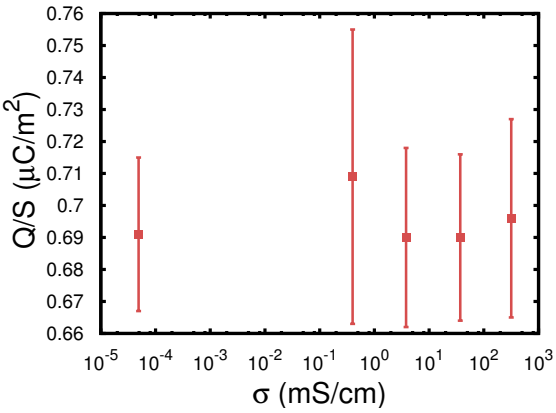

Figure 4.1: Charge induced in HCl droplets with different molarities, normalized by the droplet surface, as a function of the liquid conductivity. The highest conductivity corresponds to a droplet of HCL 1M. One red point corresponds to 10 measures. The error bars show the standard deviation of the measures. Errors bars are typically of the symbol size.

surface tension or the relative permittivity of the liquid. In addition to the HCl solution, we generated electrically charged droplets composed of acetone, ethanol, n-octane, silicone oil and TritonX-100 solutions. The characteristics of all the liquids tested are shown in Tab. 4.1.

The Triton X-100 mixture corresponds to bidistilled water with an addition of 1 CMC (critical micelle concentration, which correspond to 0.23 mM) of the non-ionic surfactant Triton X-100. This solution was used to check the influence of the surface tension on the charge induced in the droplet. Acetone does not possess ions in solutions, it is then possible to check whether the charge in the droplet is due to ion (which compose the liquid) migration. Acetone and ethanol are also polar. On the contrary, n-octane does not possess ions in solution and is apolar. Thus, it is possible to inspect the influence of the molecule polarity. Finally, silicone oil at 1.5 cSt is a liquid with viscosity near water but with a smaller electrical conductivity than any other liquids tested.

	bidistilled water	HCl (1M)	Triton X-100	Acetone	Ethanol	n-octane	Silicone oil
σ (mS/cm)	$5.5\ 10^{-5}$	330	$5.5\ 10^{-5}$	$2.1\ 10^{-4}$	$1.1\ 10^{-6}$	10^{-6}	10^{-11}
r (mm)	1.63	1.56	1.25	1.21	1.19	1.24	1.11
γ (mN/m)	70.8	63.6	32.0	23.7	21.7	21.8	19.0
Polarity	polar	polar	polar	polar	polar	non-polar	non-polar
Ions in solution	yes	yes	yes	no	yes	no	no
ϵ_r	80.1	4.6	80.1	20.7	24.3	2	2.9
τ_c (s)	$1.3\ 10^{-4}$	$1.1\ 10^{-12}$	$1.3\ 10^{-4}$	$8.7\ 10^{-6}$	$1.9\ 10^{-3}$	$1.8\ 10^{-4}$	25.5

Table 4.1: Properties of the considered liquids: the conductivity (σ), the surface tension (γ), the polarity, the presence (or not) of ions in solution, the relative permittivity (ϵ_r) and the relaxation time (τ). All these measurements were reported at room temperature. The conductivity and relative permittivity values are drawn from [77] and [78] while the surface tension was deduced from pendant droplet measurements on a CAM 200 (KSV Ltd).

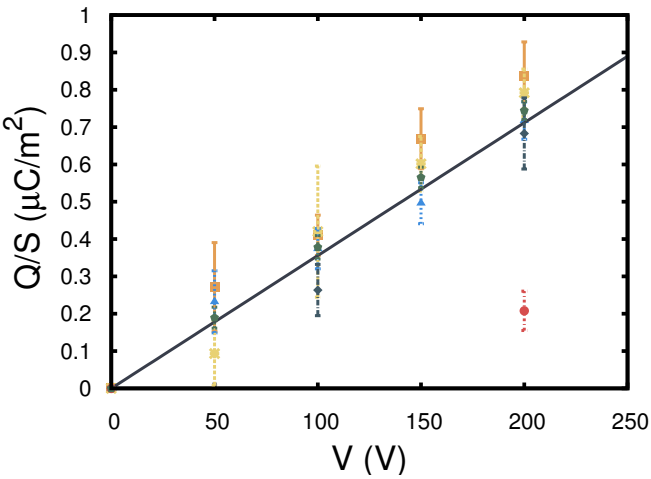

Figure 4.2: Charge induced in a droplet, normalized by the droplet surface, as a function of the voltage applied on the charged droplet generator. Red triangles, purple pentagons, black squares, blue stars, green diamonds and yellow circles represent respectively measurements made on bidistilled water, Triton-x-100, acetone, ethanol, n-octane and silicon oil. Each point corresponds to 10 measures. The error bars show the standard deviation of the measures. The red continuous line is a linear fit on these measurements.

The charge density induced in droplets composed of the various liquid tested is shown in Fig. 4.2 as a function of the voltage applied between the electrodes. In most of the cases, no distinctions can be made between the charge induced in the different liquids. The silicone oil is the only tested liquid that does not charge as well as the others. Indeed, the silicone oil droplets do not charge significantly below 200V.

It seems that it is not surfactant, ions in solution or molecules polarity that cause the droplet to charge. No variation in the droplet charge density is observed for each liquid tested except for the silicone oil, which possess a significantly low electric conductivity. In other words, the time to produce a charged droplet τ is smaller than the charge migration time τ only in the case of silicone oil.

In order to explain these observations, the link has to be made with another system involving electrically charged droplets: electrosprays. As explained in Section 2.3, the literature about electrosprays has grown tremendously in the past years, especially because of the applications that derive from the phenomenon (mass spectrometry [80], colloid propulsion systems [12],...). In particular, scientists have used electrohydrodynamics to model the charges flow in electrosprays. A common model used to describe the droplet charge in electrosprays is the Hendricks model [12]. In their work, Pfeifer and Hendricks used simplified assumptions in order to model the charge migration in a low conductive liquid. In the next lines, we will see that this theoretical approach can be applied to the charged droplet generator.

When an imperfectly conducting liquid is subject to an external electric field E_0, a residual electric field, assumed to be $\epsilon_0 E_0/\epsilon$, is present within the liquid (ϵ_0 corresponds to the vacuum permittivity and $\epsilon = \epsilon_0\epsilon_r$ corresponds to the liquid permittivity). Such an electric field induces a charge/ion migration through the liquid contained in the needle, accumulating charges in the hanging droplet. The time evolution of the surface charge density of the droplet $q_\sigma(t)$ can be expressed as:

$$q_\sigma(t) = \int_0^t \sigma E(t')\,\mathrm{d}t'. \tag{4.2}$$

If we suppose that there is no charge excess at $t = 0$ in the droplet (i.e. $q_\sigma(0) = 0$), the electric field $E(t')$ can be expressed as:

$$E(t') = (\epsilon_0 E_0/\epsilon_r - q_\sigma(t')/\epsilon) \tag{4.3}$$

Indeed, at $t = 0$, there is no charge in the hanging droplet and the electric field inside the droplet is $\epsilon_0 E_0/\epsilon$. Then, charges migrate due to this electric field. Because of the charge migration, the electric field inside the liquid gradually decreases with the factor $q_\sigma(t')/\epsilon$. If the electric conductivity σ is assumed to be constant over time, we deduce from Eq. 4.2 and Eq. 4.3:

$$q_\sigma(t) = \epsilon_0 E_0(1 - \exp(-\sigma t/\epsilon)) \tag{4.4}$$

From Eq. 4.4, we can deduce a characteristic time under which charges have enough time to migrate in the droplet:

$$\tau_c = \epsilon/\sigma \tag{4.5}$$

If the time to generate droplets τ is larger than the migration time τ_c, the equilibrium charge is reached and we have, as predicted by Eq. 4.1:

$$q(\tau \gg \tau_c) = \epsilon_0 E_0 S \tag{4.6}$$

On the other side, if $\tau < \tau_c$, a lesser charge migrates in the droplet before its ejection. As a consequence, the droplet created by the charged droplet generator is less charged than expected. Such a reasoning explains the observation of a low charge induced in the silicone oil droplet.

The Eq. 4.5 indicates that the time τ_c only depends on the electric conductivity σ and the liquid permittivity $\epsilon = \epsilon_0\epsilon_r$. As a consequence, only these two parameters should influence the charge of the droplet. If we take a look back at Fig. 4.2, the theory is endorsed by the experiments. The charge time τ_c has been calculated for each liquid in Tab. 4.1. As expected, only the silicone oil as an ejection time τ smaller than the charge migration time τ_c. Indeed, the small conductivity of the silicone oil lead to a charge time τ_c of several seconds, which is larger than the droplet ejection time.

One last question, which has not already been addressed, is the origin of the charge carrier. Indeed, the description of the charge migration by Eq. 4.4 involves that the liquid contains charge carriers with a certain conductivity σ. In the case of electrolytes, which contains ions in solutions, the conductivity is defined by:

$$\sigma = n_+ q_+ \mu_+ + n_- q_- \mu_- \tag{4.7}$$

where n_+ and n_- are the number of carriers, q_+ and q_- are the charge of the carriers and μ_+ and μ_- are the mobility of the carriers. However, the experimental results from Fig. 4.2 indicate that even non-electrolyte liquids can accumulate charges via charges migration. The explanation that is commonly accepted nowadays [80] is that free charges are present in any liquids, electrolytes or not. The charge presence can be explained by different factors. Firstly, the liquids used during experiments are never perfectly pure. As a consequence, ions in solutions could be present in liquid due to impurities. Secondly, electric charges may appear at the interface between the liquid and the metallic needle due to redox reactions. Finally, charge exchange with gas around the droplet may also occur. All these phenomena, even if they are limited, can explain the presence of sufficient free charges to charge droplets. Indeed, a droplet created by the charged droplet generator possesses a typical charge of $q = 100$ pC. It means that 10^9 molecules with one extra electron or one electron deficit have to migrate in the droplet to charge it. By taking into account that there is 6.022 10^{23} molecules in one mole, a very small amount of charged molecules are required to charge the droplet. As a consequence, the previous factors, even if limited, are adequate to explain the possibility of charge migration in any liquid.

The precise study of the ion composition of each liquid tested comes under the chemical study rather than the physical study. Previous publications, mainly in the domain of electrosprays and mass spectrometry, have studied the origin of charge carriers for numerous kinds of liquids and electrosprays configurations [11, 81].

In conclusion, we studied in detail the influence of the liquid composition on the droplet charge. We showed that the time for the charges to migrate in the droplet τ_c have to be smaller than the droplet generation time τ in order to charge a droplet to its maximum. We demonstrated that the charge migration time increases with the conductivity and decreases with the liquid relative permittivity. Finally, we showed that even non-electrolyte liquids could be charged by charge migration.

4.2 Charge loss over time

At this point, we understand how charges migrate in a droplet and what is the excess of charges induced in a droplet in any configuration whatsoever. However, nothing has been said on the retention of this charge within the droplet. Once the charged droplet

has been created, does the charges, after few seconds, escape from the droplet? Or on the contrary, does the charges remain in the droplet until its complete evaporation?

Once again, the majority of the research answering these questions are focused on electrospray droplets. In particular, the electrospray mass spectrometry requires understanding how electric charges in electrospray droplets behave over time. As a consequence, articles have been focused, with more and more precision, on the charge behavior of micro droplets [11]. The absence of data on the charge loss of millimetric droplets is explained by the lack of experimental setup allowing to store large droplets on a long period of time and measure their electric charge.

4.2.1 Charge loss of a bouncing droplet

Using the bouncing droplet method (see Section 3.3.2), a charged droplet can be stored over a very long period of time. In order to study the evolution of the droplet charge for millimetric droplets, we developed a specific experiment that measures the charge of droplets after their storage on a vibrating bath. The method is schematized in Fig. 4.3. A bath was attached on the topside of a Faraday cup. The whole system was shacked by being attached on an oscillating plate. The oscillation of the plate was controlled via an electromagnetic shaker (GW-V55). Charged droplets were stored on the liquid bath. Their charge were measured by dropping them in the Faraday cup. The droplet charge over time was deduced by measuring the charge of droplet with different storing times.

The liquid bath was composed of 1000 cSt silicone oil while the oscillation frequency was fixed at 40 Hz. Such a configuration maximizes the droplet stability on the vibrating bath, as explained in Section. 3.3.2. Experiments were performed at the room temperature (20-22° C) and with a relative humidity between 20 % and 30 %. During each experiment, a charged droplet was dropped on the vibrating bath. After a certain amount of time, the charged droplet was pushed toward the edge of the vibrating bath. The droplet was move without contact by creating a meniscus on the bath thanks to a needle. Because of the meniscus, the droplet bounced on a non-horizontal surface, which generated a horizontal displacement. The phenomenon is showed in Fig. 4.4. At the edge of the vibrating bath, a spout allowed the droplet to fall into the Faraday cup. As the droplet moved trough the spout, the high viscosity oil allowed the droplet to bounce on the liquid until falling in the Faraday cup.

Measurements have been performed with droplets composed of soapy water and silicone oil (1.5 cSt) mixed with 1 percent of ethanol. Both liquids have been chosen because of their bouncing stability on the vibrating bath. As stated by the Section 4.1, silicone oil is supposed to be difficult to charge. However, the addition of 1 percent of ethanol sufficiently increases the liquid conductivity to reduce the charge migration time. For each droplet composition, the experiment was repeated with different delays between the droplet creation and the droplet charge measurement.

The Fig. 4.5 presents the droplet charge over time. The green disks correspond

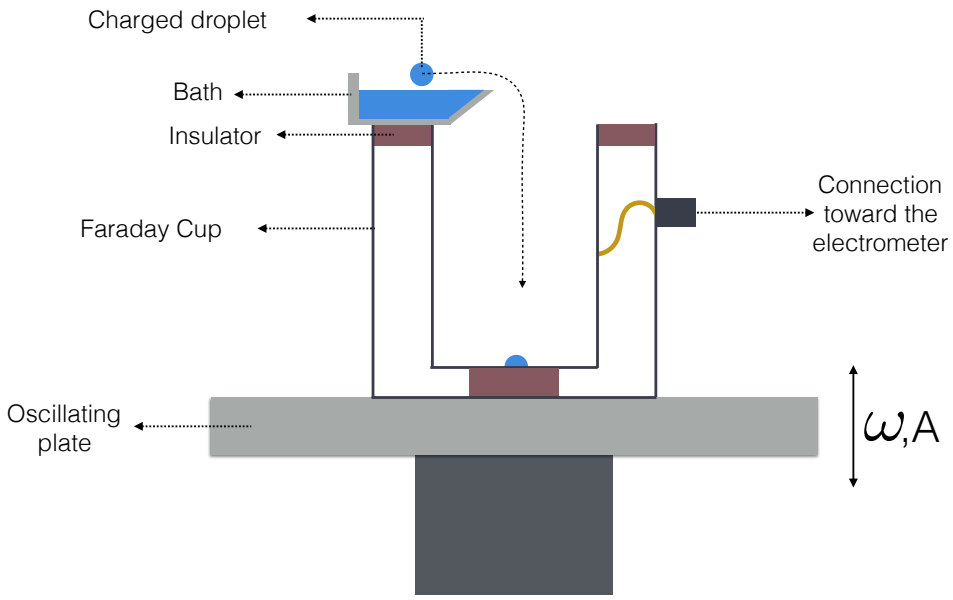

Figure 4.3: Schema of the setup used to measure the droplet charge over time. A bath, attached on the top of the Faraday cup allows bringing the charged droplet down the Faraday cup. The Device is attached to a vibrating plate, allowing storing the droplet via the bouncing phenomenon. For each measurement, a droplet is placed on the vibrating bath, evaporates during a time between few seconds to several minutes and is then brought down the Faraday cup.

to droplets made of soapy water while the red crosses correspond to droplets made of silicone oil 1.5 cSt with an addition of 1 % of ethanol. We observe from both graphs that the charge loss is relatively low. A droplet made of soapy water loses 50 % of its charge in about 1800 s. In the same way, a droplet made of silicone oil loses 30 % of its charge in about 1400 s. Moreover, even if there is a certain variation in the measurements, the charge loss appears to be continuous. In order to explain those two observations, we now have to look at the previous studies made on the charge loss of charged droplets.

4.2.2 Model the charge loss of bouncing droplets

In the present Section, we investigate the different mechanisms that could produce charge leakage from the droplet. We firstly examine models describing the droplet

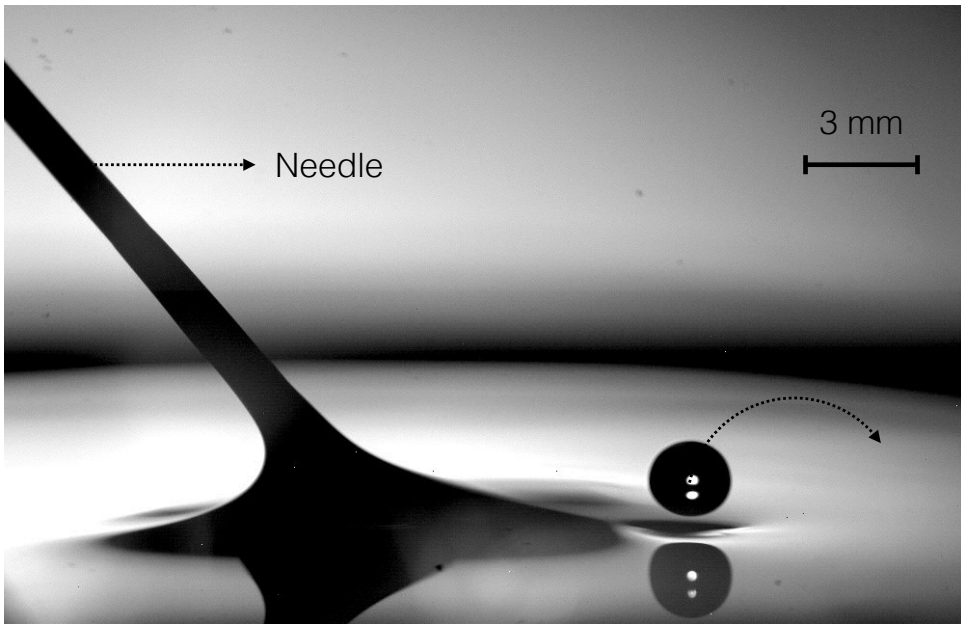

Figure 4.4: Image of a bouncing droplet set in motion by means of a meniscus. The meniscus is created by a needle dived in the silicone oil.

charges loss by Coulomb explosion and ion evaporation. Then, we focus our attention on the interaction between the droplet and the liquid bath. We investigate eventual charge transfers between both liquids via short time contact or charge migration in surrounding air.

In the Section 2.2.1, we described a charge loss mechanism without naming it. Indeed, when the repulsion between electric charges overcomes the droplet surface energy, the droplet destabilizes and ejects small droplets highly charged. The phenomenon, named Coulomb instability or Coulomb explosion, can occur during the droplet evaporation. When the droplet evaporates, electric charges get closer to each other. As a consequence, the electric repulsion increases. For a critical radius, the electric repulsion between the charges overcomes the droplet surface energy, resulting in the droplet instability. The critical radius for the Coulomb instability to occur is expressed by:

$$r_c = \left(\frac{q^2}{64\pi^2 \gamma \epsilon_0} \right)^{1/3} \tag{4.8}$$

The measurements in Fig. 4.5 shows an initial droplet charge of respectively 45.7

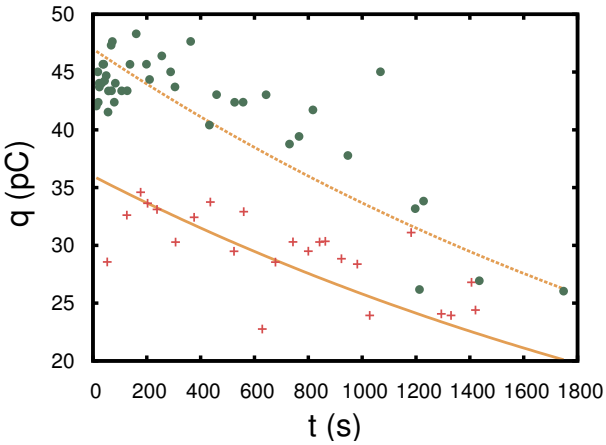

Figure 4.5: Charge of a bouncing droplet over time. The green disks correspond to droplets made of soapy water. The red crosses correspond to silicone oil 1.5 cSt with an addition of 1 percent of ethanol.

and 34.1 pC for the soapy water and the silicone oil. These charges correspond to a critical radius for the Rayleigh instability to occur of respectively 0.19 and 0.22 mm. The droplet radius of bouncing droplets composed of soapy water or silicone oil have been measured over time. In Fig. 4.6, we plotted the droplet radius as a function of time. The top graph corresponds to droplet composed of soapy water. The graph bottom graph corresponds to droplet composed of silicone oil. Both measurements have been fitted by a linear function.

Measurements indicate that the critical radius for a Coulomb instability to occur is attained after a charge loss was already observed. As a consequence, the Coulomb instability seems to be the wrong explanation to the charge loss observed in Fig. 4.5. Moreover, we observe that the electric charge and the radius decrease continuously over time, which means that the charge loss mechanism is a continuous phenomenon rather than an instability occurring at different critical radii.

If the charge loss is not due to Coulomb instabilities, it could be explained by charge evaporation. Indeed, if molecules evaporates from the droplet, reducing its volume over time, it seems reasonable to assume that electric charges / ions could also evaporate from the droplet.

Such a mechanism have already been suggested by Law [82] in his studies on the charge loss of millimetric droplets. Law used a Faraday cup to measure the droplet charge loss of a hanging droplet. He deduced from his measurements that droplets do not lose their charge over time. However, this study raise a number of questions regarding the influence of the contact between the metallic needle (at a fixed potential) and the hanging droplet and regarding the measurement via the Faraday cup itself. Indeed, as explained earlier, the Faraday cup measures charged droplets in contact

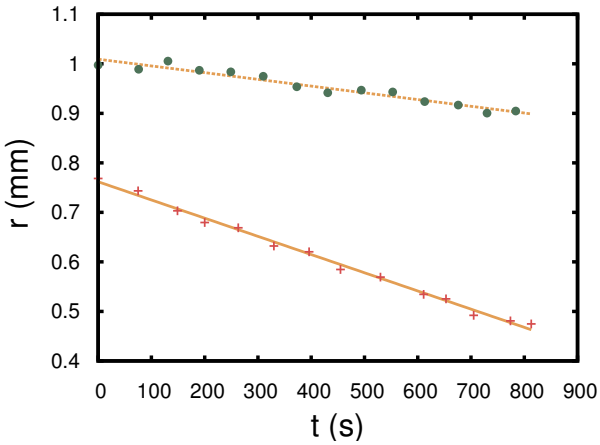

Figure 4.6: Radius of a bouncing droplet over time. The green disks correspond to droplets made of soapy water. The red crosses correspond to silicone oil 1.5 cSt with an addition of 1 percent of ethanol.

but is also influenced by charges at distance. Thus, a variation in charge may be impossible to measure via this method.

Despite the results of his experiments, Law cleverly described the charge evaporation process with few physical variables. He was able to link the charge evaporation rate to the molecule evaporation rate. The number of vapor molecules N leaving the charged droplet can be expressed as :

$$\frac{dN}{dt} = \frac{N_a}{M}\frac{dm}{dt} = \frac{N_A \rho 4\pi r^2}{M}\frac{dr}{dt} \tag{4.9}$$

where N_a is the Avogadro number, M is the molar mass of the ion leaving the droplet and r is the droplet radius. The volume occupied by one molecule can be expressed as:

$$V_m = \frac{\text{droplet volume}}{\text{number of molecules in the droplet}} = \frac{M}{\rho N_A} \tag{4.10}$$

As a consequence, the number of molecules at the surface of the droplet can be expressed as:

$$N_S = \frac{\text{droplet surface}}{\text{area of one molecule}} = \frac{4\pi r^2}{(\frac{M}{\rho N_A})^{2/3}} \tag{4.11}$$

By multiplying Eq. 4.9 by the number of charges per molecules, q/N_s, we deduce:

$$\frac{q}{N_s}\frac{dN}{dt} = \left(\frac{N_A \rho}{M}\right)^{1/3}\frac{dr}{dt} = \frac{dq}{dt} \tag{4.12}$$

The Eq. 4.12 allows to easily link the measurements of the radius and the charge

variation over time:

$$\frac{dq/dt}{dr/dt} = \left(\frac{N_A \rho}{M}\right)^{1/3} = \alpha \tag{4.13}$$

The comparison between the experiment and Eq. 4.13 is summarized in Tab. 4.2. We observe an important difference between Eq. 4.13 and the experiment for both liquids tested. The Eq. 4.13 predicts a much faster charge evaporation than observed.

	Silicone oil	Soapy water
α_{exp}	$1.5\ 10^{-8}$	$7.12\ 10^{-8}$
α_{theo}	$1.15\ 10^{9}$	$31.2\ 10^{9}$

Table 4.2: Experimental and theoretical values of the parameter α deduced from Eq. 4.13.

The different between the experimental and the theoretical result could be explained either by the absence of charges evaporation or by the limitation of the model. Since the model developed by Law, other models have been elaborated to describe with more precision the charge evaporation. These model are based on the chemical behavior of ions in excess in droplets produced from electropsrays. With this approach, the charge evaporation corresponds to the displacement of an ion from the liquid droplet to the surrounding gas.

From this point of view, ions may leave the charged droplet if their free enthalpy of solvation becomes greater than zero. Iribarne and Thomson [83] showed that the condition for the evaporation of ions can be expressed by:

$$\Delta G - G(E) > 0 \tag{4.14}$$

where ΔG and $G(E)$ are respectively the standard Gibbs free energy of solvation of an ion and the energy reduction due to the charge interactions at the surface of the droplets. If the process is supposed to be a first-order reaction, we can express the ion evaporation over time with the following equation:

$$\frac{d \ln N}{dt} = -(kT/h) \exp\left(-(\Delta G - G(E))/kT\right) \tag{4.15}$$

where k is the Boltzmann constant, T is the absolute temperature and h is the Planck constant. In other words, the charges/ions evaporation is modeled by the Arrhenius equation.

The Eq. 6.5 requires to know the standard Gibbs free energy of solvation of the evaporating ion, which is the main drawback of this approach. Indeed, as explained in the Section 4.1, we do not know the exact nature of the charge induced in the electrically charged droplet. As a consequence, it is impossible to know the standard Gibbs free energy of solvation ΔG.

However, studies summarized in Ref. [11] shows that the inequality expressed by Eq. 4.14 is only reached for very small droplets. They showed that droplets should only lose their charges via Coulomb explosion until reaching a small radius at which charge evaporation can occur. By calculating the free enthalpy of solvation of evaporating charged droplets, Hogan *et al* [84] have described the frontier between charge loss via Coulomb explosion and charge evaporation. In their study, they examined charged droplets composed of 50 % of methanol and 50 % of water. The Fig. 4.7 shows the study by Hogan *et al* [84] of the frontiers for the Rayleigh instability and the ion evaporation. The droplet charge is plotted as a function of the droplet diameter. The continuous line corresponds to the Coulomb explosion frontier. The dotted line corresponds to the ion evaporation frontier. In practice, two scenarios, A or B, can occur.

The droplet with an amount of charges and a radius corresponding to the case A firstly evaporates without any charge leakage. Then, the droplet reaches a critical radius at which it endures a Coulomb explosion. The droplet instability results in an important charge loss. After the Coulomb explosion, the droplet continues to evaporate. The droplet can eventually reach once again the limit of a Coulomb explosion and destabilize. This process repeats itself until reaching the charge evaporation limit. At this point, the droplet loses continuously its charge over time.

The second scenario possible corresponds to a droplet with an amount of charges and a radius analogous to the case B. In this case, the droplet firstly evaporates without any charge leakage. Then, It directly reaches a critical radius at which it endures charge evaporation. We see in Fig. 4.7 that only droplet smaller than 40 nm may loss their charge via charge evaporation.

As a consequence, even if we were not able to measure the free enthalpy of solvation of our charged droplets, we deduce from both the mismatch between experiments and Eq. 4.13 (highlighted by Tab. 4.2), and the theory on electrospray droplets (highlighted by the Fig. 4.7) that charge evaporation should not occur in millimetric charged droplets.

Another phenomenon to look at is the droplet interaction with the liquid bath. Indeed, as explained in the Section 3.3.2, droplets bounce on a thin air layer located between the liquid bath and the droplet. Such a small distance between the droplet and the liquid bath can eventually lead to charge loss over time. Ristenpart *et al* [65] have studied the interaction between charged droplets and liquid interfaces. They observed that when the charged droplet approaches the liquid interface, the droplet slightly deforms and contacts the liquid interface during few milliseconds. During the contact, the droplet exchanges charges with the liquid interface. Afterwards, the droplet can coalesce or move away from the interface. They captured, with a high-speed camera, the deformation of the water droplet that leads to a contact with the liquid interface. They showed that, for thin deformations, droplets do not coalesce with the liquid interface but bounce on it. Such a mechanism may have appeared

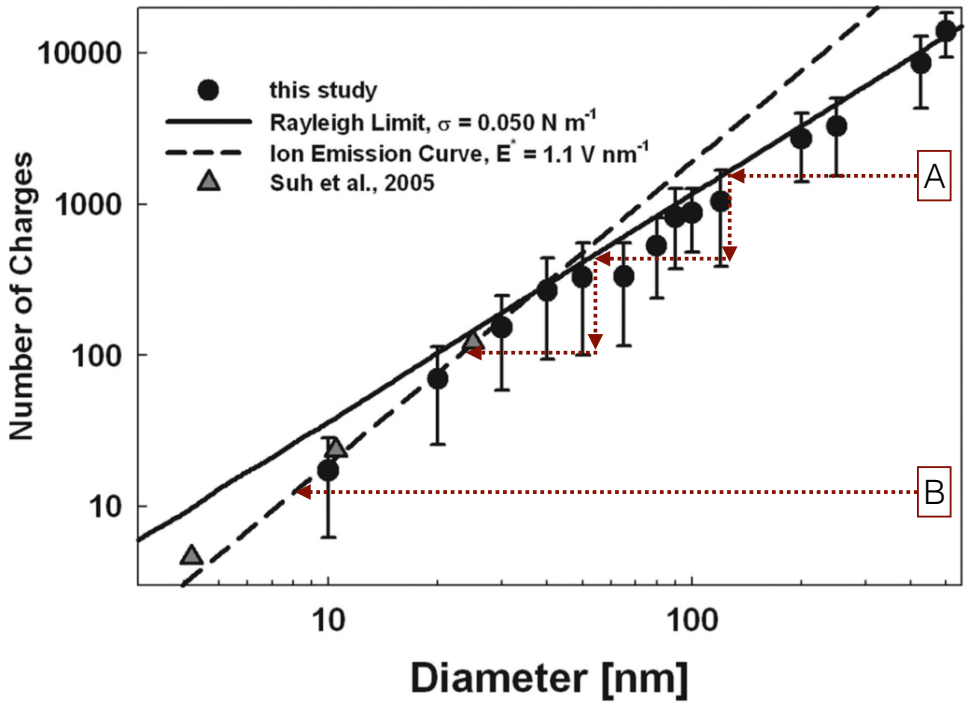

Figure 4.7: Study by C. J. Hogan et al [84] of the limit between charge evaporation and Rayleigh instability. The critical charge is plotted as a function of the critical droplet diameter. The case A and B correspond to two different scenario possible.

during our experiments. Indeed, during the droplet bounce on the liquid bath, a small bridge, similar to the one observed by Ristenpart *et al* [65], could take place between the droplet and the liquid bath. Such a contact between both liquids could lead to charge leakage over time.

In the current system configuration, the charged droplet bounces once at each bath oscillation. As the liquid bath oscillates with a frequency $f = 40$ Hz, the droplet bounces lasts 25 ms. The droplet bouncing is shown in Fig. 4.8. It can be separated in two phases. A first phase during which the droplet actually bounce on the thin air layer (images 2 to 5) and the second phase during which the droplet flies way from the liquid bath (images 6 to 10). Measurements shows that the droplet is in contact with the thin air layer during 10 ms while it is away from the liquid bath during 15 ms.

We know from the Section 4.1 that the characteristic time for charges to migrate depends on the liquid conductivity and relative permittivity: $\tau_c = \epsilon/\sigma$. The migration times for soapy water and pure silicone oil are respectively $\tau_c = 0.13$ ms and $\tau_c = 25.5$ s (see Tab. 4.1). If we take into account that the charged droplet is 40 % of its time

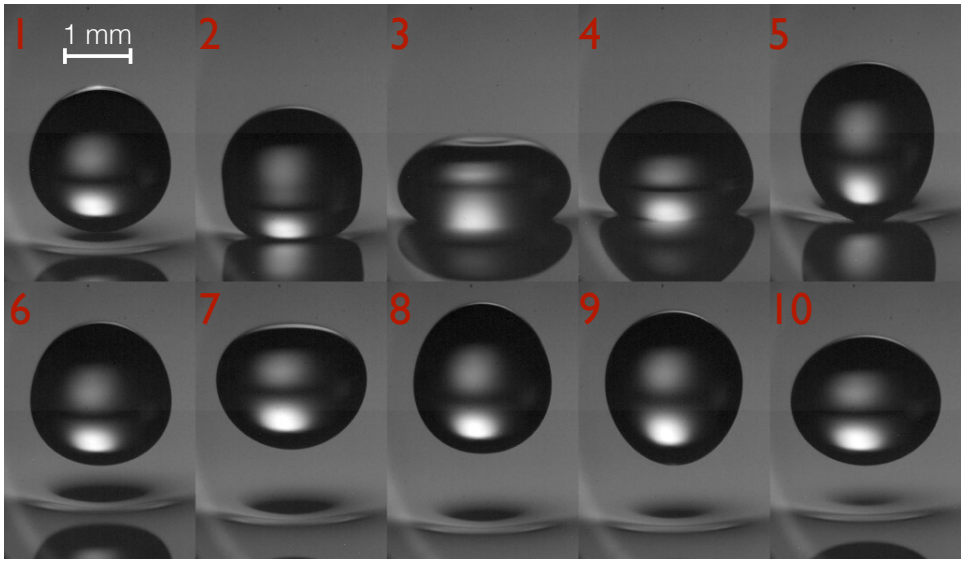

Figure 4.8: Image sequence of a charged droplet bouncing on a vibrating bath. Each image is separated by 3.125 ms. The droplet can be considered near the liquid bath in 4 images over ten.

in contact with the thin air layer, it means that it takes about 64 s for all the charges to migrate from the silicone oil droplet to the liquid bath. The same reasoning can be made with the soapy water. The water droplet should discharge in approximately 0.325 ms.

As a consequence, the theory of the charge loss by thin contacts with the liquid bath is not in agreement with the observation. The charge migration time is too rapid to explain the observations.

However, contacts between the charged droplet and the liquid bath are not necessarily needed to produce charge loss. Charges may leave the droplet simply because of the proximity between the liquid bath and the charged droplet. Indeed, this proximity induces a non-negligible electric field between both interfaces. This electric field may induce charge leakage. In order to describe the phenomenon, we decided to model the charged droplet and the liquid bath as a charged capacitor. The model is schematized in Fig. 4.9. In practice, the dielectric between the plates of a capacitor lets pass a small amount of leakage current, which leads to discharges over time. As a consequence, a capacitor is modeled by a resistance and a capacitance in parallel.

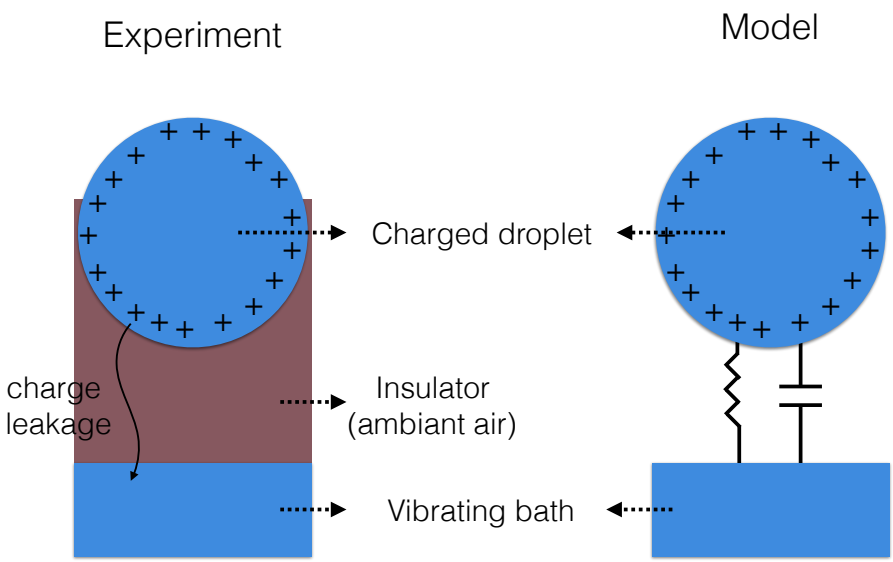

Figure 4.9: On the left, schema describing the charge loss mechanism. Charges displace from the bouncing droplet to the vibrating bath. On the right, schema describing the model. The charge leakage is described as the charge loss from a capacitor.

The charge loss over time of a capacitor is expressed by the following equation:

$$q(t) = q_0 \exp\left(\frac{-t}{RC}\right) \tag{4.16}$$

where q_0 is the initial charge of the capacitor, R is the electrical resistance of the capacitor and C is the electric capacitance of the capacitor.

In order to make the link between the bouncing charged droplet and the capacitor, we have to model the electrical resistance R and capacitance C of our system. Because of the droplet motion, the liquid bath deformation and the droplet deformation, both parameters are difficult to model. From this assessment, two answers can be given. Either R and C are numerically modeled over time or simplifying hypothesis are taken. We chose to take the second approach to describe our measurements. In the present approach, the bouncing charged droplet on the oscillating bath is modeled as a planar capacitor. The resistance R and the capacitance C of a planar capacitor is expressed by:

$$R = \frac{l}{\sigma_{air} S} \tag{4.17}$$

$$C = \frac{\epsilon_0 S}{l} \tag{4.18}$$

where l is the distance between the two plates of the capacitor, σ_{air} is the air conductivity and S is the surface of the plate capacitor. Such a description leads to the following charge leakage from the bouncing droplet over time:

$$q(t) = q_0 \exp\left(\frac{-\sigma_{air} t}{\epsilon_0}\right) = q_0 \exp\left(\frac{-t}{\tau_c}\right) \tag{4.19}$$

where $\tau_c = \epsilon_0/\sigma_{air}$ is the characteristic time of charge motion described in the Section 4.1 (Eq. 6.5). Note that the case of charges leakage outside the droplet, τ_c is calculated in the air and not in the liquid. We obtain $\tau_c \approx 3000$ s. The Eq. 4.19 has been plotted without any fitting parameters, for both the silicone oil and the soapy water, in Fig. 4.5 (orange lines). We observe a good agreement between the measurements and Eq. 4.19.

The Eq. 4.19 corresponds to the best model we found to describe the charge leakage from the bouncing droplet. It correctly describes the charge leakage from the soapy water and silicone oil droplets. The plan capacitor hypothesis allows avoiding measurements of the distance l between the droplet and the liquid bath as well as the surface S of the droplet interacting with the liquid bath. The model indicates that the charge droplet tend to discharge over time because of its proximity with a solid or liquid interface.

4.2.3 Charge loss of droplets in microgravity and Leidenfrost state

The planar capacitor model shows that the charge leakage from droplets does not depend on the distance between the droplet and the second interface. Naturally, this reasoning has to be used carefully, due to the significant assumption of a planar capacitor geometry. For more complex geometries, the charge leakage may depend on the distance between the charged droplet and the second interface or even on the droplet radius. In any case, our results show that the charge leakage due to the droplet interaction with interfaces should be taken into account in any experiments. For example, droplet stored via electrodynamic or acoustics traps should also lose their charges via this process. Of course, this charge leakage process is relatively slow and may be negligible in configurations where the droplet completely evaporates after two or three minutes.

In our case, the model is in good agreement with the measurement on bouncing droplets, but can also be used to describe other storage methods. The charge leakage of droplet stored in microgravity is difficult to describe. Indeed, the droplets are not nearby any interface, which makes the capacitor model difficult to apply. However, if we take into account the low charge migration time in the air ($\tau_c \approx 3000$ s) and

the duration of one parabola (22 s), we can consider that a droplet keeps its charge during one experiment.

In the case of charged droplets stored via the Leidenfrost effect, the capacitor model can be applied more easily. A droplet in Leidenfrost state levitates on a thin layer of its own vapor. The capacitor model can be applied directly on the vapor layer. Because the droplet levitates on its own vapor, the characteristic time τ_c has to be calculated in the liquid vapor and not in dry air. Unfortunately, we do not have access to the conductivity and relative permittivity of Ethanol and HFE-7100 vapor (the two liquids used to store charged droplets in Leidenfrost state). However, we can suppose from data on water [85, 86] that the electric conductivity of the vapor phase only increase by a factor 10 or 100 compared to the electric conductivity of the air. At the same time, the permittivity increases with a factor 10. As a consequence, the characteristic time for the charges to migrate τ_c can decrease to a minimum of 300 s. This characteristic time of charge leakage is important to take into account in experiments involving Leidenfrost state. However, as we will see, experiments on droplet in Leidenfrost state on liquid pool lasted about 30 s, which means that the charge leakage had no influence on our measurements.

In conclusion, we measured the charge loss over time for millimetric charged droplets stored on a vibrating liquid bath. It takes about 1800 s for a soapy water droplet to lose half of its charge. The charge loss measured was not in agreement with previous models such as the Coulomb explosion and the charge evaporation. A new model, inspired by the charge loss of a capacitor, quantitatively explained the observations. The application of the model on the two other storage systems showed that the droplet charge loss should not be taken into account given the time scale involved in both systems.

4.3 Influence of the charges on the droplet surface energy

As introduced in the Section 2.2.1, the excess of electric charges affects the intrinsic behavior of the droplet. Lord Rayleigh showed that electric charges, by repelling each other, influence the droplet surface energy. By looking at small perturbations on the charged droplet, he expressed the influence of the energy decrease on the droplet natural frequency. The charged droplet frequency is:

$$f^2 = \frac{l(l-1)(l+2)}{4\pi^2\rho r^3}\left(\gamma - \frac{q^2}{16\pi^2\epsilon_0 r^3(l+2)}\right) \tag{4.20}$$

where f is the oscillation frequency of the spherical mass of liquid, l determines the oscillating mode of the liquid, ρ is the liquid density, r is the droplet radius, q is the surface charge of the droplet and ϵ_0 is the vacuum permittivity. The droplet natural

frequency corresponds to l =2. As a consequence, we have:

$$f^2 = \frac{2}{\pi^2 \rho r^3}\left(\gamma - \frac{q^2}{64\pi^2 \epsilon_0 r^3}\right) = \frac{2}{\pi^2 \rho r^3}\left(\gamma - \frac{q_\sigma^2 r}{4\epsilon_0}\right) \tag{4.21}$$

where q_σ is the droplet surface charge density. The last term between brackets corresponds to the variation in the surface energy per surface unit due to electric charges. The initial surface energy by unit of surface corresponds to the droplet surface tension, while the second term corresponds to the influence of the electric charge. As explained in the Section 2.2.1, the oscillation frequency of a charged droplet has been verified experimentally several times [18]. It corresponds to one of the most famous experiments demonstrating how electric charges affect the droplet behavior.

The influence of the electric charges on the droplet surface energy can also be deduced by looking at the pressure inside the charged droplet. The Laplace equation indicates the pressure inside a neutral droplet:

$$\Delta P = \frac{2\gamma}{r} \tag{4.22}$$

If the droplet possesses an excess of electric charges, these charges in excess repel each other. The pressure induced by electric charges at the surface of a conducting sphere corresponds to:

$$\Delta P = -\frac{q_\sigma^2}{2\epsilon_0} \tag{4.23}$$

As a consequence, the total pressure inside a charged droplet is expressed by:

$$\Delta P = \frac{2\gamma}{r} - \frac{q_\sigma^2}{2\epsilon_0} \tag{4.24}$$

The Eq. 4.21 and 4.24 show that the influence of electric charges in the droplet can be seen as a variation in the surface energy by unit surface:

$$\gamma^* = \gamma - \frac{q_\sigma^2 r}{4\epsilon_0} \tag{4.25}$$

To summarize, the presence of electric charges in the droplet directly influences its surface energy and, as a consequence, its internal pressure and its oscillation frequency. Note that the electric charge may also influence the evaporation of small droplets, as explained by Law [82]. Moreover, the Eq. 4.25 puts in evidence the three interconnected variables that govern the surface energy of a charged droplet (i.e the surface tension γ, the charge q and the droplet radius r). In other words, once we know these three parameters, we can deduce the charge influence on the droplet surface energy. Of course, the Eq. 4.25 can be turned around. For example, the known variables could be the surface energy by unit surface γ^*, the droplet radius r and the droplet surface tension γ. Knowing these three parameters would allow to deduce the droplet charge q.

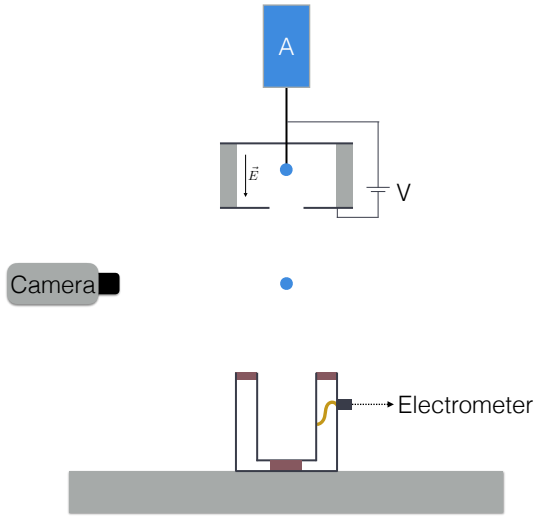

Figure 4.10: Schema of the experiment. The droplet was charged by charge migration using the charged droplet generator model A. Then, it fell from the charged droplet generator. Its oscillation frequency and radius was recorded via the high-speed camera. Finally, the Faraday cup measured the droplet charge.

4.3.1 Surface energy of a charged droplet in free fall

We measured the surface energy by unit surface γ^*, the droplet radius r, the droplet charge q and the droplet surface tension γ of free falling droplets. The experiment is schematized in Fig. 4.10. The electrically charged droplet generator model A was used to produce the charged droplet. When a charged droplet was released from the charged droplet generator, it underwent a small perturbation due to its detachment from the needle. Because of this small perturbation, the droplet oscillated in its natural frequency during its free fall. Once the charged droplet fell away from the droplet generator, we had access to the surface energy by unit surface γ^* via the Eq. A.3 by measuring the droplet oscillation frequency. The droplet oscillation frequency and the droplet radius was measured via a high-speed camera (Phantom MIRO 310). The charged droplet finished its fall in the Faraday cup. It allowed direct measurement of the droplet electric charge q. Note that the electric charge could also have been deduced by calibrating the electrically charged droplet generator. The droplet surface tension γ was deduced from liquids references.

Images of droplet oscillations during their free fall are shown in Fig. 4.11 (a). The image on the left corresponds to a neutral droplet while the image on the right corresponds to a charged droplet ($q = 24$ pC). Both images are a superposition of the droplet horizontal and vertical maximal extension. The charged droplet on the right is smaller than the neutral droplet on the left. It is explained by the electric force

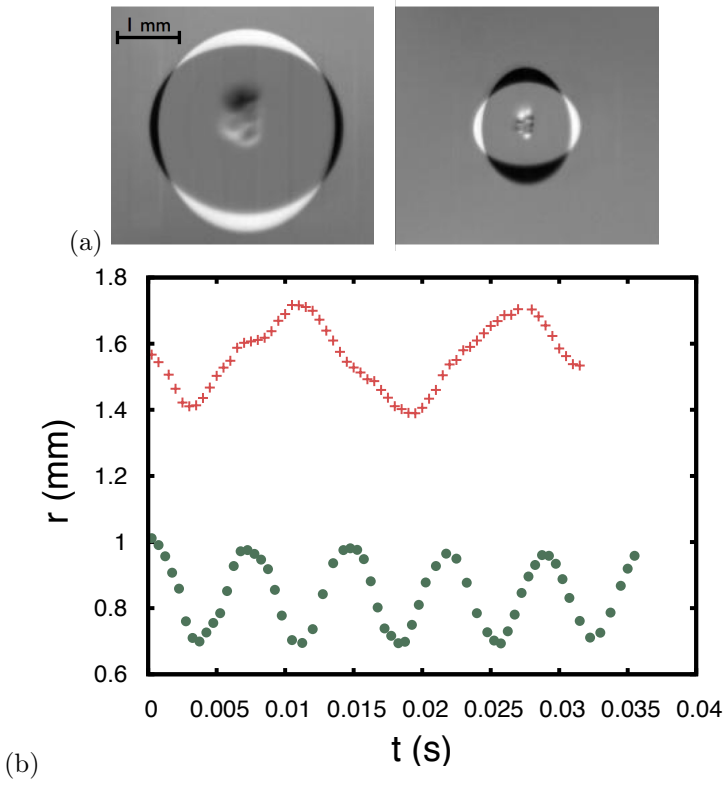

Figure 4.11: (a) Images evidencing the droplet oscillations. Both images results from a subtraction of two snapshots, one on the maximum horizontal deformation (in black) and one on the maximum vertical deformation (in white). The first image, on the left, is the case of a neutral droplet. The second image, on the right, is the case of a charged (24 pC) droplet. (b) Droplet vertical radius variation over time. Red crosses and green disks represent measurements on a neutral droplet and a charged droplet ($q = 24$ pC) respectively. Half the points were plotted for the clarity of the graph.

applied on the droplet by the charged droplet generator model A (see Section 3.1.2). The horizontal radius variation over time is shown in Fig. 4.11 (b). Red crosses and green disks represent measurements on a neutral droplet and 24 pC charged droplet respectively. The graphic shows that the oscillation frequency is increased for the charged droplet, which is explained by its smaller size.

The results of the surface energy, radius and charge measurements are shown in Fig. 4.12. The surface energy variation is plotted as a function of the surface charge density multiplied by the droplet radius. The red crosses are measurements performed on acetone droplets while green disks are measurements performed on bidistilled water. The yellow dotted line is not a fit but the direct surface energy variation deduced from Eq. 4.25. The measurements are in very good agreement with the theory.

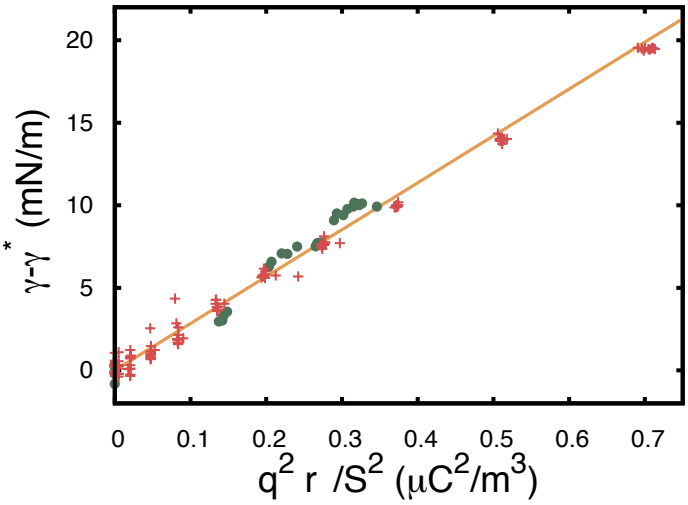

Figure 4.12: Surface energy by unit surface γ^* of falling droplets as a function of the charge q induced in the droplet normalized by the surface S of the droplet. The green disks correspond to bidistillated water droplets while the red crosses correspond to acetone droplets. The minimum measured droplet surface energy by unit surface corresponds to a charge $q = 24pC and to a droplet radius r=0.8mm$.

As claimed earlier, the presented setup gives access to one unknown of the system by knowing the two other variables. Moreover, the measurements on a free falling droplet allow deducing these parameters without any contact with the droplet. Typically, the droplet charge can simply be deduced by looking at the droplet oscillation frequency. Indeed, from Eq. 4.21, we can express the droplet charge as:

$$q^2 = 64\pi^2 r^3 \epsilon_0 \left(\gamma - \frac{f^2 \pi^2 \rho r^3}{2}\right) \tag{4.26}$$

By knowing the droplet oscillation frequency, surface tension and radius, the droplet charge can be deduced. Contrary to the measurement performed via a Faraday cup, the charged droplet can still be used after this charge measurement. Furthermore, the droplet charge can be measured over time while the droplet is stored in systems such as an oscillating liquid bath or in microgravity.

However, the deduction of the droplet charge by measuring the droplet oscillation frequency requires knowing with precision the droplet surface tension, radius and oscillation frequency. In order to illustrate this limitation, we can take the example of an ethanol droplet with a charge $q = 10$ pC and a radius $r = 1$ mm. These characteristics lead to:

$$q^2/64\pi^2 r^3 \epsilon_0 = \left(\gamma - \frac{f^2\pi^2\rho r^3}{2}\right) = 0.0018 \text{ N/m} \tag{4.27}$$

The Eq. 4.27 shows that the term in between brackets is about 1 mN/m. The surface tension of ethanol corresponds to $\gamma = 22$ mN/m. As a consequence, each term in between parentheses should be known with high precision. Furthermore, the term in between parentheses depends on the frequency squared and the radius cubed, which highly increase the error propagation.

We can deduce from this example that small measurement errors on the droplet oscillation frequency, surface tension or radius can lead to a significant error on the droplet charge. Moreover, this error decreases with the increase of the droplet charge. As a consequence, this method should be limited to high precision measurements performed on highly charged droplet. This reasoning explains why we chose to directly measure the droplet charge when we studied the droplet charge leakage over time in Section 4.2.

In conclusion, the electric charge affects the surface energy density of droplets. The influence of the electric charge can be observed by the variation in the droplet oscillation frequency or the droplet internal pressure. We measured the decrease in surface energy density for free falling droplets. Our measurements were in agreement with the theory. We deduced that the measurement of the surface energy density could give information on the droplet charge.

5

Interaction between charged droplets in microgravity

Contents

In this Chapter, we examine the behavior of charged droplets in microgravity. As explained in the Section devoted to the description of the microgravity storage method (see Section 3.3.1), the microgravity allows generating free floating charged droplets. We chose this experimental configuration to highlight the electric interaction between two charged droplets.

The majority of the studies focused on the interaction between charged droplets have been interested in thunderclouds or electrosprays. These systems correspond to several micro droplets interacting with each other. As explained in Section 2.4, this thesis aims to study millimetric droplets in order to bring new insights on the charged droplet understanding. Through this process, we developed tools that allow generating charged droplets one by one. In this Chapter, we take advantage of these tools to study the interaction between only two millimetric and charged droplets. In particular, we study the trajectory of two charged droplets sent towards each other.

Firstly, we introduce the past research performed on the interaction between

droplets and we describe our approach of the subject. Secondly, we describe in detail our experimental setup. Thirdly, we study the influence of the electric interaction on the trajectories of both charged droplets. Finally, we examine experiments that lead to an impact between both charged droplets. From these experiments, we compare the impact between charged droplets to the impact between neutral droplets.

5.1 Droplet collision: Research context and strategy

The physics of collisions between droplets has raised the interest of several scientists since the early 1950s [87, 88]. In the particular case of water droplets, this interest comes specifically from atmospheric research [89–91]. The main goal of these studies was to understand how several collisions between droplets could affect their radius distributions. These experiments were focused on small droplets (i.e. $r \approx 150$ μm to represent cloud droplets) and big drops (i.e. $r \approx 1$ mm to represent raindrops). Over the years, various setups have been developed in order to accurately observe the different panels of collision behaviors between droplets [92, 93]. Indeed, the result of an impact between two or more droplets depends on their respective radius, speed and angle of impact. Recently, Gotaas et al [94], have developed a new setup able to precisely study the boundary between each of the different sort of collisions.

The collision between two neutral droplets (a and b) of the same volume (i.e. the same radius, $r_a = r_b = r$) and the same composition is commonly described by a phase diagram comparing the collision parameter χ with the Weber number We. These parameters are respectively defined by:

$$\chi = \frac{x}{(r_a + r_b)}, \tag{5.1}$$

$$We = \frac{\rho v_{rel}^2 D_m}{\gamma}, \tag{5.2}$$

where x is the projected separation distance between the centers of the colliding droplets normal to the relative velocity vector $\vec{v}_{rel}$ (see Fig. 5.1), r_a and r_b are the radii of each droplet, ρ is the density of the droplet, D_m and γ are respectively the diameter and the surface tension of the droplets. In the case of neutral droplets, two droplets sent toward each other move straight on until impacting. As a consequence, the direction of the relative speed v_{rel} does not vary over time, which mean that the collision parameter is also constant over time.

According to the parameters χ and We, the collision between neutral droplets leads to different behaviors. The collision diagram, shown in Fig. 5.2 (top), points out each of these behaviors. If $\chi > 1$, the droplets do not contact each other. If $\chi < 1$, both droplets impact each other. Four different impacts can be observed: the bouncing between droplet, the coalescence, the stretching separation and the reflexive separation. The two first results are classics. The two last results are described by

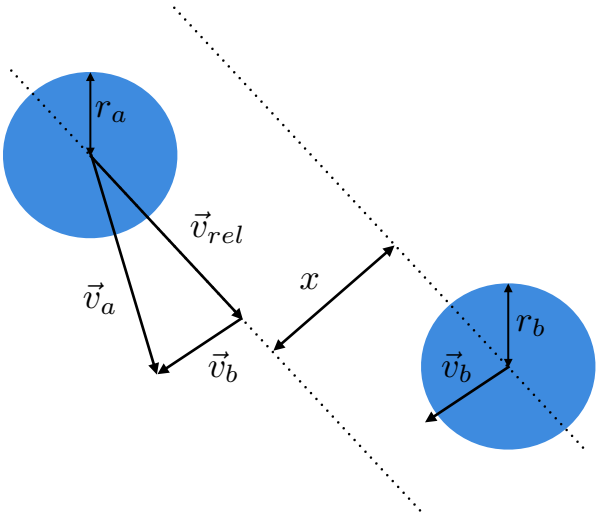

Figure 5.1: Schema of the relative droplet motion. The symbols $\vec{v}_{a/b}$ and $r_{a/b}$ correspond respectively to the speed and the radius of each droplet. The relative speed between both droplets corresponds to the vector $\vec{v}_{rel}$. The collision parameter χ is calculated from the distance x and the radii r_a and r_b.

image sequences in Fig. 5.2 (bottom). Both image sequences are separated by 3.5 ms. In both cases, the droplets contact each other and separate away just after their collision. In the case of stretching separation, both droplets collide on their sides while in the case of reflexive separation both droplets collide on their center. The frontier between each impact behavior was studied experimentally and theoretically. The Fig. 5.2 (top) was built from the results obtained by Ashgriz *et al* [92] and Gotaas *et al* [94].

Studies such as Ashgriz et al [92] and Qian et al [93] led to a better understanding of the collision between two neutral droplets. However, in the case of droplets with an excess of electric charges, the system acquires one more degree of freedom. Indeed, the electric attraction or repulsion between droplets adds an interaction, which influences the collision before and during the impact between droplets. A natural example of the differences existing between the collisions of neutral or charged droplets is the contrast between clouds and thunderclouds.

In order to study the collision between charged droplets, various approaches have been implemented. Studies have been specifically focused on the simulation of several charged droplets interacting with each other [3] while others have been focused on direct measurements (for example by recreating cloud conditions in laboratories [95]). In particular, some researche were focused on the interaction between two droplets. For example, experimental setups were developed in order to study the electrical interaction between free falling droplets [90] or between droplets in contact with a

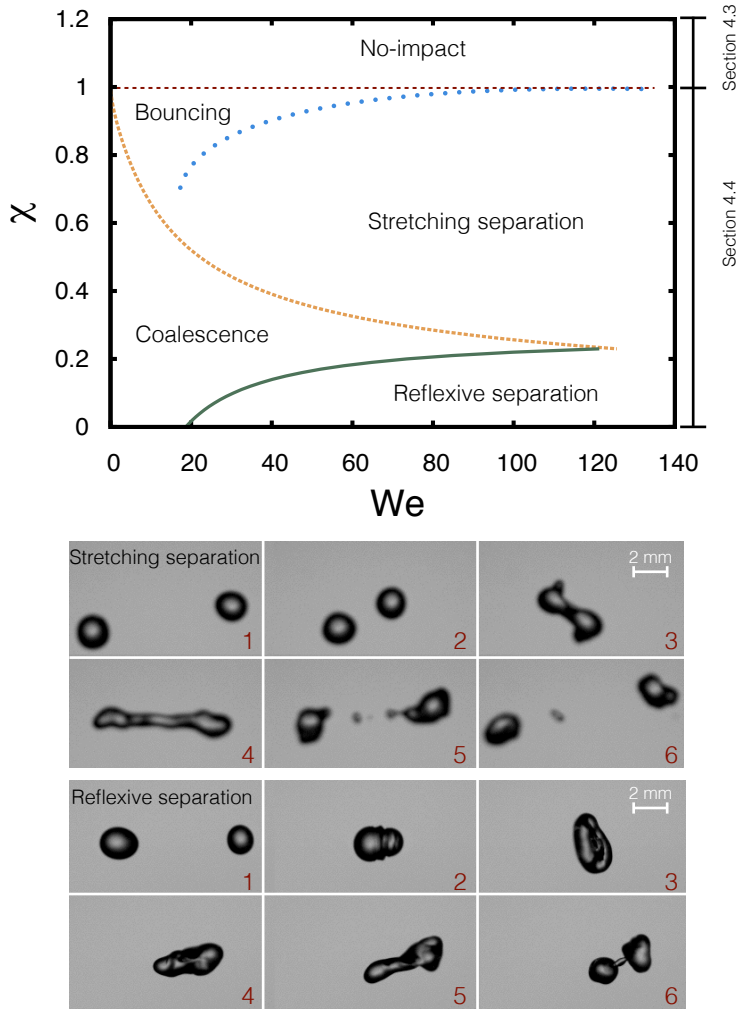

Figure 5.2: (top) Collision diagram. The y axis corresponds to χ (Eq. 5.1). The x axis corresponds to the Weber number We *(Eq. 5.2). The orange dashed line is the theoretical frontier between coalescence and stretching. The green line is the theoretical frontier between coalescence and reflexive separation. Both theoretical predictions come from Ashgriz et al [92]. The blue points are the frontier between stretching and bouncing between droplets (deduced from measurement of C. Gotaas et al [94]). (bottom) Image sequence of a stretching and a reflexive collision. Both image sequences are separated by 3.5 ms.*

charging electrode [96,97]. These studies showed that the electric interaction between two droplets could be modeled has the interaction between two charged spheres a and b. The electric force between two charged spheres is expressed by:

$$\begin{aligned} F_{el} &= F_c + F_{dip} \\ &= \frac{q_a q_b}{4\pi\epsilon_0 d^2} + \frac{1}{4\pi\epsilon_0} q_a^2 r_b \left(\frac{1}{d^3} - \frac{d}{(d^2 - r_b^2)^2} \right) + \frac{1}{4\pi\epsilon_0} q_2^2 r_a \left(\frac{1}{d^3} - \frac{d}{(d^2 - r_a^2)^2} \right) \\ &+ \frac{1}{4\pi\epsilon_0} q_a q_b r_a r_b \left(\frac{1}{d^4} + \frac{1}{(d^2 - r_a^2 - r_b^2)^2} - \frac{1}{(d^2 - r_a^2)^2} - \frac{1}{(d^2 - r_b^2)^2} \right) \end{aligned} \tag{5.3}$$

where $F_c = \frac{q_a q_b}{4\pi\epsilon_0 d^2}$ corresponds to the Coulomb interaction and F_{dip} corresponds to the dipolar forces. The charges q_a and q_b correspond respectively to the electric charge of droplets a and b, d is the distance between the center of the droplets and ϵ_0 corresponds to the vacuum electrical permittivity. This electric force affects the droplet trajectories before they impact each other. As a consequence, two neutral droplets sent toward each other do not impact in the same way as two charged droplets. Even if the droplets initial trajectory is the same, the electric interaction affects the trajectory of a charged droplet while the neutral droplet remains on its initial trajectory. The influence of this electric force on the droplet trajectories and impacts is the exact subject of our study.

Even if the electric interaction between two charged droplets is well known, the majority of the studies investigated the collision between neutral drops. To our knowledge, there is a lack of high speed imaging of the impact between electrically charged droplets. This lack of result is explained by the difficulty to highlight the influence of the electric interaction on the droplet trajectories. Indeed, a rapid calculation of the electric force between two charged droplets shows that the electric force is 40 times smaller than the droplet weight. As a consequence, two charged droplets sent toward each other mainly endure the acceleration of gravity. They quickly acquire an important speed and the electric interaction becomes negligible compare to aerodynamic interactions.

In order to surpass this limitation, we studied the collision between two charged droplets in microgravity. The microgravity was reached via parabolic flights, as explained in Section 3.3.1. The use of microgravity conditions aims to minimize any aerodynamic effect (e.g. a lift force due to air drive) and focus only on the electrostatic interaction between charged droplets. Indeed, the microgravity conditions allow sending two droplets toward each other with a slow speed. In doing so, droplets keep their slow speed throughout their motion and are not accelerated by gravity.

In the following Sections, we propose to compare collisions between charged droplets to measurements and results deduced from the study of neutral droplets. In order to maximize the influence of the electric charges, we focused our study on the interaction between two electrically charged droplets with a radius $r \in [0.41 - 0.97]$ mm interacting in microgravity conditions. The specific range of radius, which is higher

than previous studies, was chosen to maximize the influence of the electric charge. Indeed, while the charge of micrometric droplets is about 0.01 pC [3], our charged droplets had a charge of about 100 pC.

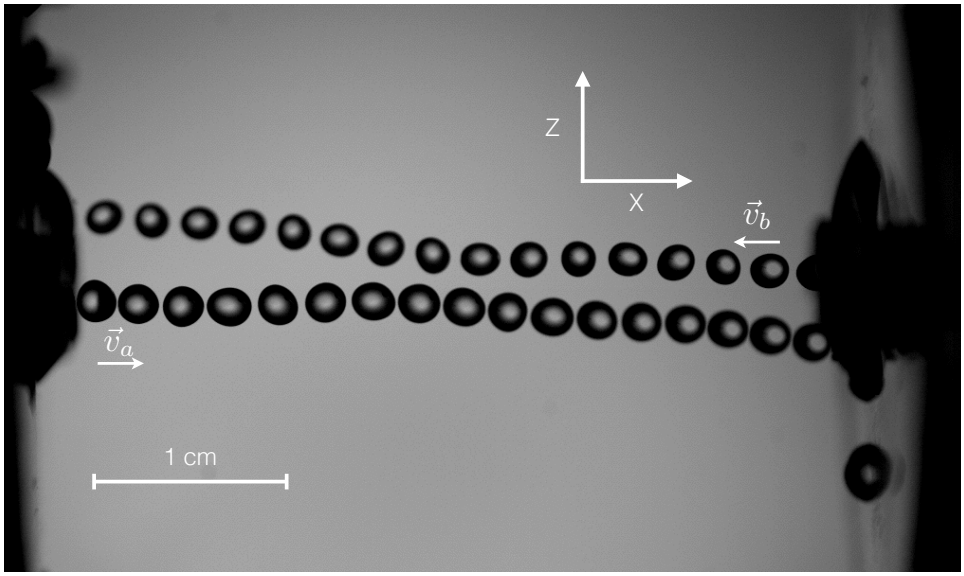

Figure 5.3: Image superposition of a typical experiment. Two droplets were sent toward each other thanks to two charged droplet generators. 4 ms separates each droplet. We observe that the droplet motion is affected by the electric interaction between droplets. The focus plane of the high-speed camera is called XZ.

A typical experiment is shown in Fig. 5.3. On each side of the image, a charged droplet generator ejects a droplet. Images separated by 4 ms have been superposed in order to visualize the droplets motion. Because of the microgravity conditions, the droplets move in the direction indicated by their initial speed. Once they come closer to each other, their displacement is influenced by their electric interaction.

In conclusion, the goal of our approach is to compare the "classic collision diagram" to the collision diagram of charged droplets. Both parameters describing the collision between neutral droplets, χ and We, are used to describe the collision between two charged droplets in the following Sections. In the case of charged droplets, these two parameters are calculated in such a way that the electric interaction between droplets is taken into account.

5.2 Experimental setup

In order to generate the charged droplets in microgravity, we used the charged droplet generator model B. The setup was equipped with a coaxial airflow that allowed detaching the droplet from the needle. The whole experimental setup is shown in Fig. 5.4. Two charged droplet generators faced each other. During one parabola they emitted several droplets toward each other. For all the experiments, the distance between both charged droplet generators was equal to 41 mm. A high-speed camera (Phantom MIRO M310, 2000 fps) recorded the droplets motion between the two charged droplet generators. In Fig. 5.3, the image superposition shows the droplet motion recorded in the XZ plane.

The whole set of experiments performed in microgravity allowed observing the collision between electrically charged droplets for various sets of droplets charges, speeds and radii. From these observations, we discuss the influence of electric interactions on droplet trajectories and droplet contacts.

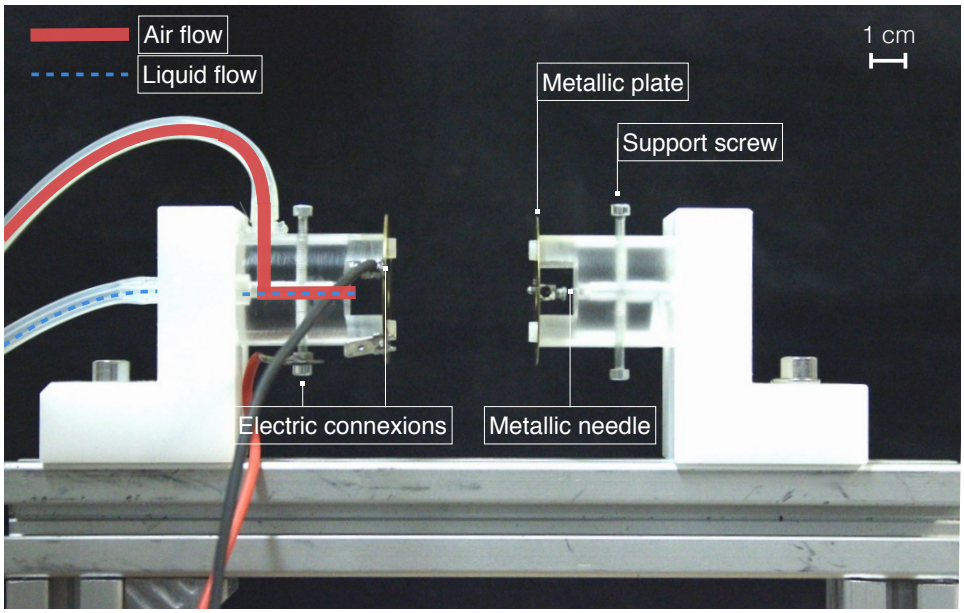

Figure 5.4: Picture of two charged droplet generators facing each other. A voltage was applied between the metallic needle and the metallic plate, generating charges migration. The droplets were then ejected thanks to a coaxial airflow. The droplet motions between both charged droplet generators were recorded with a high-speed camera.

5.3 Influence of the charges on the droplet trajectories

We first investigate the experiments that did not lead to impact between droplets. For neutral droplets, the non-collision corresponds to $\chi > 1$ on the collision diagram (see Fig. 5.2). Naturally, the frontier between collision and non-collision can eventually be changed by the electric interaction. As shown in Fig. 5.3, because of electric interactions, droplets do not move in a straight line. The goal of the present Section is to describe the specific trajectories of these droplets as a function of their relative electric interaction. Such a description allows deducing assumptions on electric interactions between droplets during events that lead to a collision.

	Case 1	Case 2	Case 3	Case 4
$q_a(pC)$	-56.6	125.0	95.7	-91.3
$q_b(pC)$	-56.6	119.0	68.9	63.2
r_a (mm)	0.86	0.91	0.79	0.77
r_b (mm)	0.97	0.88	0.67	0.64
v_{rel} (m/s)	1.08	1.15	1.59	1.64
p_{theo}	0.3206	0.0545	0.0851	0.0821
p_{fit}	0.3386	0.0482	0.0794	0.0824
$p_{err}(\%)$	5.3	13.1	7.2	0.4
e_{theo}	146.18	24.54	33.59	48.94
e_{fit}	156.93	27.38	31.67	50.04
$e_{err}(\%)$	6.84	10.3	6.0	2.2

Table 5.1: Parameter values of each experiment reported in Fig. 5.5. The symbols $q_{a/b}$ and $r_{a/b}$ correspond respectively to the charge and the radius of each droplet. The relative initial speed between two droplets is indicated by the symbol v_{rel}. The symbols $p_{theo/fit}$ and $e_{theo/fit}$ correspond to the parameters from Eq. 5.9 respectively deduced from the droplet parameters or the droplet trajectories. Finally, p_{err} and e_{err} indicates the relative error on p_{fit} and e_{fit} respectively.

The Fig. 5.5 shows a sample of experiments performed in microgravity. The graphs on the left side show the relative position (Δx and Δz, as described in Fig. 5.3) over time of two electrically charged droplets in the XZ plane. We tracked their displacement when they were at a distance $\Delta x \approx 20$ mm. Over time, the droplets get closer to each other until reaching a relative distance $\Delta x = 0$ mm. At this point, the curvature of the trajectories changes, meaning that the droplets influence each other. Then, the droplets continue their relative motion and Δx begin to negatively increase. The charge and the radius of each droplet is indicated in Tab. 5.1.

In Fig. 5.5, the first three graphs correspond to charged droplets with the same sign of charge. On one hand, by comparing the Case 1 and 2, we see that by increasing

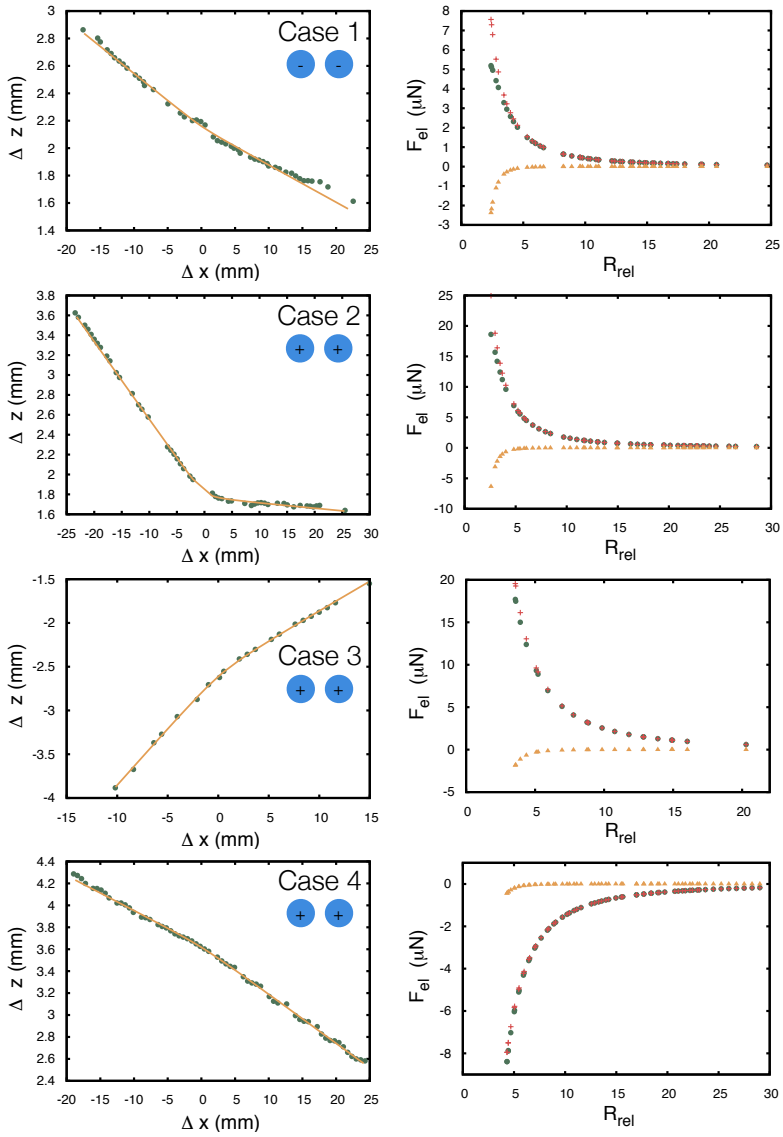

Figure 5.5: The first three couples of graphs show experiments performed with droplets of the same sign of charge corresponding to cases 1,2 and 3 in Tab. 5.1. The last graph shows an experiment performed with droplets of opposite signs of charges corresponding to case 4 in Tab. 5.1. The graphs on the left side exhibits the relative position Δx and Δz of two droplets during their motion in the plane XZ. The orange lines correspond to fits of the trajectory taking into account a Coulomb interaction between droplets. The graphs on the right side compare the value of the Coulomb force F_c (green disks), the dipole forces F_{dip} (orange triangles) and the total electric force F_{el} (red crosses) as a function of the relative distance D_{rel}. Each force was calculated from Eq. 5.4.

the droplet charge, the repulsion between droplets increases. On the other hand, the comparison between case 2 and case 3 indicates that the increase of the relative distance between droplets (or simply an increase in Δz) decreases their repulsion. The last graph on the left corresponds to two droplets with opposite charges (Tab. 5.1, cases 4). Contrarily to the three previous cases, we observe that the relative distance between droplets increases less quickly after their crossing. In other words, the curvature of the function is inverted, indicating an attraction between droplets.

The graphs on the right side of Fig. 5.4 show the calculated electrical force between the droplets as a function of their relative position $D_{rel} = 2d/(r_a + r_b)$, where d is the distance between the center of mass of the droplets and r_a and r_b are the droplet radii. As explained in the previous Section, the force between two charged droplets is modeled as the electric force between two charged conducting spheres. This electric force takes into account the monopole-monopole, monopole-dipole and dipole-dipole interactions:

$$\begin{aligned} F_{el} &= F_c + F_{dip} \\ &= \frac{q_a q_b}{4\pi\epsilon_0 d^2} + \frac{1}{4\pi\epsilon_0} q_a^2 r_b \left(\frac{1}{d^3} - \frac{d}{(d^2 - r_b^2)^2} \right) + \frac{1}{4\pi\epsilon_0} q_2^2 r_a \left(\frac{1}{d^3} - \frac{d}{(d^2 - r_a^2)^2} \right) \\ &+ \frac{1}{4\pi\epsilon_0} q_a q_b r_a r_b \left(\frac{1}{d^4} + \frac{1}{(d^2 - r_a^2 - r_b^2)^2} - \frac{1}{(d^2 - r_a^2)^2} - \frac{1}{(d^2 - r_b^2)^2} \right) \end{aligned} \tag{5.4}$$

where the charges q_a and q_b correspond respectively to the electric charge of droplets a and b, d is the distance between the center of each droplet and ϵ_0 corresponds to the vacuum electrical permittivity. As expected, the first three cases described in Fig. 5.5 correspond to repulsive forces while the last case corresponds to attractive forces between droplets. The absolute value of the force increases with the decrease of the distance between droplets.

In Eq. 5.4, $F_c = \frac{q_a q_b}{4\pi\epsilon_0 d^2}$ corresponds to the Coulomb interaction between two point charges. The second term, F_{dip} corresponds to the dipolar interaction between both droplets. Indeed, the electric field produced by one sphere affects the charge distribution in the second conductive sphere. Note that the electric field affects all the charges inside the sphere, not only the charges in excess. For example, if one sphere is positively charged, the negative charges in the second sphere are attracted toward the first sphere while the positive charges are repelled. In the case of charged droplets, taking into account the dipole interaction means that the time for a charge to move in the droplet is considered non-negligible with respect to the time scale of the droplet motion. The characteristic time for charges to migrate in the droplet (see Section 4.1) is expressed as:

$$\tau = \epsilon_r \epsilon_0 / \sigma \tag{5.5}$$

where ϵ_r and σ are respectively the relative permittivity and the conductivity of the liquid. In the case of bidistillated water, $\tau = 0.13$ ms. The Fig. 3.3 shows that the interaction between both electrically charged droplets becomes non-negligible at

a distance of approximately 3 mm ($d < 3D_{rel}$). If we take a droplet speed of $v = 1$ m/s (which is in agreement with Tab. 5.1), it takes 3 ms for a droplet to cross this distance. We deduce from this reasoning that the time scale of the charge displacement is negligible compared to the droplet motion time scale.

However, even if the charge migration generates dipole interactions, the Fig. 5.5 (right) also shows that, in most of the cases, the dipolar component of the electrical force is mainly negligible until a distance between droplets corresponding to approximately $3D_{rel}$. Indeed, the red crosses and the green disks are superposed during the majority of the experiments. As a consequence, the first step is to describe each droplet trajectory by only taking into account the Coulomb force (i.e. we suppose that $F_{el} = F_c$).

In order to model the trajectories of each droplet, we should solve the equation of motion:

$$m_{a/b}\frac{d^2\vec{s}_{a/b}}{dt^2} = \vec{F}_{el} \tag{5.6}$$

where $m_{a/b}$ and $\vec{s}_{a/b}$ are respectively the mass and the spatial position of the droplet a or b. However, given the complexity of the force $\vec{F}_{el}$, the Eq. 5.6 has no analytical solutions. Hopefully, we showed that the electric force $\vec{F}_{el}$ can be, at the first order, described as a Coulomb force. By doing so, the droplet trajectory can be seen as a two-body problem influenced by a Newtonian force:

$$\vec{F}_N = \frac{k}{d^2}\vec{u}_d \tag{5.7}$$

Where k is a constant (in our case $k = q_a q_b/4\pi\epsilon_0$), d is the relative distance between the droplets and u_d is a unit vector. The classical way to resolve this two-body system is to reduce the problem to a one-body system influenced by a central force:

$$\mu\frac{d^2\vec{d}}{dt^2} = \vec{F}_N \tag{5.8}$$

The reduced mass is $\mu = \frac{m_1 m_2}{m_1+m_2}$ and d is the relative distance between the droplets. This classical problem has a solution in polar coordinates (d,θ). From Eq. 5.8 the distance between the charged droplets as a function of θ is expressed as:

$$d(\theta) = \frac{p}{(\mp)1 + e\cos(\theta - \theta_0)} \tag{5.9}$$

where $p = \frac{(\pm)\mu C^2}{k}$ and $e = (\pm)(\frac{p}{d_0} + 1)$. The sign $(\pm)$ corresponds respectively to droplets with the same sign of charges and droplets with different signs of charges. The constant $C = d^2\dot{\theta}$ is derived from the angular momentum conservation and d_0 is the minimal distance between droplets. The angle θ_0 depends on the initial conditions.

The trajectories in Fig. 5.5 have been fitted by Eq. 5.9. The results of the fits correspond to the orange lines in Fig. 5.5(left). A comparison between the fitting

parameters p_{fit} and e_{fit} and the measured value of p_{theo} and e_{theo} can be seen on Tab. 5.1. The difference between the fits and the experiments are described by the relative errors $p_{err} =\mid p_{theo} - p_{fit} \mid /p_{fit}$ and $e_{err} =\mid e_{theo} - e_{fit} \mid /e_{fit}$.

The fit from Eq. 5.9 in Fig. 5.5(left) are in good agreement with the observations in most of the cases. The parameters p_{err} and e_{err} are relatively low for the majority of the experiments. From these results, we conclude that the Coulomb electric force is adequate to describe the interaction between two electrically charged droplets in this range of droplet charge, radius and speed. However, the measured trajectories and the fit do not match perfectly each other. This discrepancy can be mainly explained by two phenomena: (i) the influence of the dipole force (ii) the droplet going out of the high speed camera focus plane XZ.

Now that the experiments and the Eq. 5.9 have been compared, the assumption of a negligible dipole interaction must be justified. As shown in Fig. 5.5, the influence of the dipole interaction is always attractive. As a consequence, if this part of the electrical force interaction was the main source of error, the fits on each experiment should be deviated toward a smaller repulsion or a larger attraction. In other words, the parameters p_{fit} and e_{fit} should always be smaller than p_{theo} and e_{theo} in the first three experiments and bigger in the last one. In practice, the error on all the experiments is randomly distributed. The main source of error must be found somewhere else.

The discrepancy between the measurements and the theory can be explained by the defocus of the droplets. Indeed, the electrically charged droplet may not remain in the same plane XZ throughout its trajectory. Such a phenomenon can be explained by various experimental limitations. In some circumstances, the droplet does not detach correctly from the needle while in other cases the conditions of zero gravity are not perfectly achieved. These phenomena explain why the trajectory of the droplet may not remain strictly in the XZ plane and derive in the Y direction. Moreover, even if the droplet motion in the Y direction is limited, it is amplified by the repulsion or the attraction between both droplets. Indeed, if the droplets are not exactly on the same Y-axis, their electric interaction leads to a relative motion outside the plane XZ. The droplet defocus influences primarily the data fit and the measurement of the constant C from Eq. 5.9. In order to limit the error on C due to defocus, we chose to measure the constant only on portions where electrically charged droplets were perfectly focused.

In conclusion, the Coulomb interaction is sufficient to describe the relative motion of two electrically charged droplets interacting at distance with each other. In the future, a better setup composed of two high-speed cameras would allow tracking the three dimensional motion of the charged droplets. Such a system would allow detecting the influence of the dipole interaction on the droplet motion.

5.4 Influence of the charges on the impact between droplets

If the electric interaction influences the droplet trajectories of two electrically charged droplets, one can understand that it also influences the impact between electrically charged droplets. In this Section, we focus our attention on experiments where we observed a contact between charged droplets. In the collision diagram between neutral droplets, these experiments correspond to an impact parameter $\chi < 1$. Naturally, the frontier between impact and non-impact between charged droplets can eventually vary. In this Section, we compare the collision diagram for neutral droplets with the collision diagram for charged droplets.

In the case of neutral drops, the respective motion of each droplet before the impact is supposed to be straight. Indeed, neutral droplets do not interact at distance with each other. As a consequence, the collision parameter $\chi = x/(r_a + r_b)$ is the same whichever the distance d between the droplets. Experimentally, χ is generally calculated when droplets are near each other, in order to minimize any measurement errors. In the case of electrically charged droplets, the main goal is to highlight the possible influence of the electric interaction. As a consequence, the collision parameter is calculated at a particular distance at which the electric force is non-negligible. During the analysis of the impacts between two charged droplets, the electrical force F_{el} (Eq. 5.4) was considered non-negligible when it corresponded to 15 percent of its maximal value. The limit is chosen in order to minimize the error on the measurements and maximize the influence of the electric force.

This modification in the calculation of the parameter χ implies that the collision diagram now takes into account the droplet trajectory just before the impact between droplets. In doing this, we highlight any influence of the electric charge just before the impact or during the impact without changing the definition of χ for neutral droplets.

In the case of the parameter We, only a small adjustment on the droplet radius has to be made. Because of the complexity to generate electrically charged droplets in microgravity, the droplet radius may vary from 1 to 15 percent between both interacting droplets. As a consequence, the droplet diameter D_m, needed for the calculation of the Weber number We, is defined as the mean diameter between both droplets (i.e. $D_m = r_a + r_b$).

In Fig. 5.6, the impacts between charged droplets observed in microgravity have been placed on the collision diagram. The parameters χ and We were calculated as described in the preceding paragraph. In order to be consistent, the data in the diagram in Fig. 5.6 are given with an error bar corresponding to the variation in radii between both droplets. During our experiments, we observed collisions between electrically charged droplets within a wide range of radii and charges ($0.41 < r < 0.97$ mm and $57 < |q| < 190$ pC). According to the Weber number, we observed reflexive collisions (red triangles), stretching separations (red circles) or no collisions at all

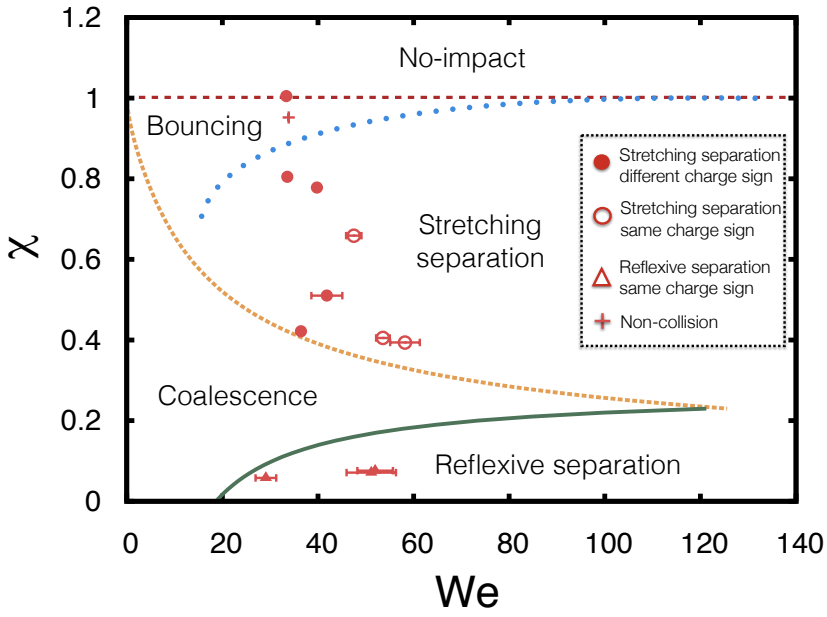

Figure 5.6: Collision diagram. The y axis corresponds to χ (Eq. 5.1). The x axis corresponds to the Weber number We *(Eq. 5.2). The orange dashed line describes the theoretical frontier between coalescence and stretching. The green line describes the theoretical frontier between coalescence and reflexive separation. Both theoretical predictions come from Ashgriz et al [92]. The blue points describe the frontier between stretching and bouncing between droplets (deduced from measurement of Gotaas et al [94]). The red circles, triangles and crosses describe the observed collisions. The red triangles correspond to reflexive separation. The red circles correspond to stretching collisions. The red cross corresponds to a non-collision Experiments performed with the same sign of charges are represented by an empty circles/triangles while the collision between droplets with opposite charges are represented by full circles/triangles. The red cross corresponds to an experiment performed with the same sign of charges. The error bars account for the small difference in radii between both colliding droplets.*

(red crosses). Experiments performed with the same sign of charges are represented by empty circles/triangles while the collision between droplets with opposite sign of charges are represented by full circles/triangles. In order to compare the measurements performed on charged droplets to the collision between neutral droplets, we drew in Fig. 5.6 the frontier between neutral collisions.

In the case of oppositely charged droplets, only stretching collisions were observed. The majority of these collisions is found in the expected zone of the neutral phase diagram. In other words, we observed mainly no differences between neutral droplet impacts and charged droplet impacts. However, at high collision parameter χ, we observed one reflexive collision in the classical bouncing region. Even if more observations are needed to draw conclusions, it seems that the reflexive collision region is extended in the present case. The observation indicates that the bouncing between two electrically charged droplets with opposite charges may be impossible.

In the same way, the majority of the experiments performed with colliding droplets of the same sign of charge are well located in the neutral collision diagram. However, one specific observation, described as the red cross in Fig. 5.6, indicates once again that the presence of electric charges has an effect on the boundary of the classical collision diagram. In this particular case, we observed repulsion between both charged droplets that is sufficient to avoid an impact between them. The present observation indicates that repulsion between droplets may be important enough to avoid the collision between droplets in parts of the diagram where $\chi < 1$.

In summary, we observed two specific experiments where the result of the impact was different from the neutral predictions. Firstly, we observed a stretching separation in the classic bouncing zone. However, the absence of numerous measurements in the present set of experiment does not allow developing a predictive theory on the whole zone corresponding to bouncing between droplets. Indeed, the modeling of the bouncing between two colliding droplets is a difficult problem that was raised several times. Such a phenomenon is linked to several parameters such as the ambient air pressure [93], the droplet surface tension or the droplet viscosity. The observation tends to show that the influence of the electric charge of both droplets can be added to these other variables.

Secondly, we observed a non-collision between two charged droplets with the same sign of charge in the part of the diagram corresponding to $\chi < 1$. In the next lines, we propose a model to answer to this observation. In order to extrapolate the zone of the diagram where collisions may be avoided due to the electric repulsion, we investigate the energy conservation in the reference frame corresponding to the center of mass of both droplets.

Thanks to the previous study of charged drop trajectories, we can take the following assumptions: (i) Droplets can be approximated to point charges (which implies a Coulomb repulsion and no droplet rotation); (ii) there is no dissipating force during the droplet motion. By comparing the energy of the system at an infinite distance

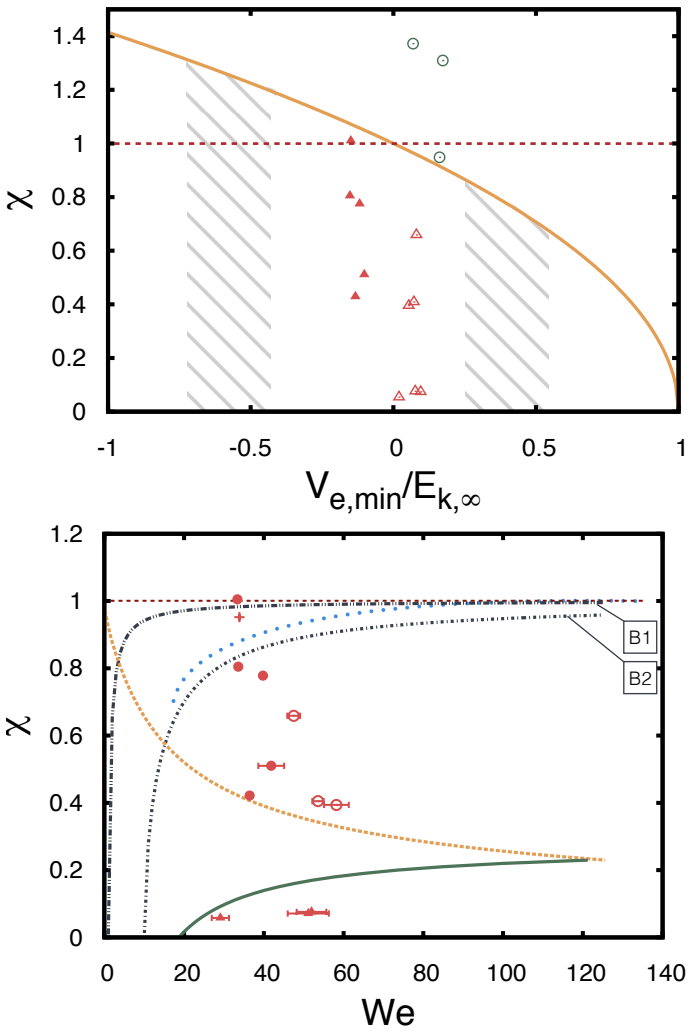

Figure 5.7: (top) Collision parameter χ (Eq. 5.2) as a function of the ratio between the electric energy and the kinetic energy. The red triangles represent interactions between droplets that lead to an impact. The green circles represent interactions between droplets that do not lead to an impact. The orange line corresponds to the limit of a non-impact between droplets (see Eq. 5.13) (bottom) Collision parameter χ as a function of the Weber number We. The black dash-dotted lines describe the frontier of an impossible collision in the case of droplets with the same sign of charge. The curve named b1 corresponds to the configuration of the experiment described by the red cross in Fig. 5.6. The curve named b2 corresponds to the same experiments but with droplets two times more charged.

between droplets to the system energy at the minimum distance between them, we have:

$$\frac{\mu v_{rel}^2}{2} = \frac{k}{d_0} + \frac{\mu C^2}{2d_0^2} \tag{5.10}$$

The left hand side of the equation corresponds to the kinetic energy of the droplets, with v_{rel} corresponding to the droplet relative speed when they are far from each other. The electric energy is considered equal to zero at an infinite distance. On the right hand side of the equation, the first term corresponds to the electrostatic energy of the system. The distance d_0 corresponds to the minimal distance between droplets. The second term corresponds to the rotational energy of the system. At the minimal distance between droplets, the kinetic energy of the system equals to zero. Because of the angular momentum definition, we deduce:

$$C = \chi v_{rel}(r_a + r_b) \tag{5.11}$$

The Eq. 5.10 allows to express d_0 as a function of χ. The limit of an impact can be expressed as the point where the distance between the center of mass of the droplet is smaller than the radius of both droplets:

$$d_0 < (r_a + r_b) \tag{5.12}$$

From Eq. 5.10 and 5.12, we then deduce the following limit for a possible impact between charged droplets:

$$\chi < \sqrt{1 - \frac{V_{e,0}}{E_{k,\mathrm{inf}}}} \tag{5.13}$$

Where $V_{e,0} = \frac{k}{(r_a+r_b)}$ and $E_{k,\mathrm{inf}} = \frac{\mu v_{rel}^2}{2}$. By knowing $V_{e,0}$ and $E_{k,\mathrm{inf}}$, we can deduce the range of χ for which it is impossible to observe any impact between droplets.

In a more general way, the Eq. 5.13 indicates that, for charged droplets, the limit of a possible collision is not anymore $\chi = 1$. In the case of two droplets with opposite sign of charges, $\chi > 1$ can lead to collision between droplets. On the other hand, in the case of two droplets with the same sign of charge, collisions can be impossible for $\chi < 1$.

In Fig. 5.7 (top), the theoretical limitation deduced from Eq. 5.13 is confirmed by experimental measurements. The droplet speeds v_{rel} were calculated at the same distance where the collision parameter χ were calculated. The green circles correspond to the observation of a non-contact between droplets while the red triangles correspond to the observation of a contact between droplets. The green circle on the orange line (i.e. at the edge between a contact and a non-contact between droplets) corresponds to the red cross presented in Fig. 5.6. The Fig. 5.7 (top) not only shows the validity of Eq. 5.13 but demonstrates also that the Weber number and the collision parameter are not anymore sufficient to completely describe the collision between charged droplets.

Indeed, the measurements demonstrate that the electric repulsion/attraction before the impact have to be taken into account.

Now that a first theory is able to describe the behavior of the collision between charged droplets, the future aim is to confirm the diagram in Fig. 5.7 (top) with several measurements. Such a diagram helps to define the collision parameters χ leading to an impact as a function of the range of energy $V_{e,0}/E_{k,\mathrm{inf}}$. Indeed, as shown by the hatched lines in Fig. 5.7 (top), for a defined range of energy ratio, different χ are accessible. For example, we can study several collisions between two droplets. These droplets can have the same charge and the same radii, but different speeds. The range of speed studied (e.g. 0 to 1 m/s) allow deducing the range of energy ratio $V_{e,0}/E_{k,\mathrm{inf}}$ accessible in Fig. 5.7 (top), and as a consequence, the parameter χ necessary to observe impacts.

If the set of droplets studied is composed of both positively and negatively charged droplets, the energy ratio $V_{e,0}/E_{k,\mathrm{inf}}$ can be negative, which means that both hatched regions are accessible. We observe on Fig. 5.7 that for a given range of energy, impacts between oppositely charged droplets can occur on a larger range of collision parameter χ. As a consequence, for a system where collision happens randomly, there is a higher probability of collisions between droplets with different sign of charges. This observation implies that in the case of a system overall neutral composed of oppositely charged droplets, the difference in collision probability leads to a faster neutralization of the charged droplets due to collisions.

Thanks to this simplified theory, it is possible to predict if a collision is possible or not. Unfortunately, the Fig. 5.7 (top) does not indicate the result of the collision between the droplets (a coalescence, a stretching collision,...). However, for a fixed droplet radius and charge, the non-impact boundary can be plotted as a function of We only. Indeed, the Weber number can be introduced in Eq. 5.13:

$$\chi < \sqrt{1 - \frac{k\rho}{We\mu\gamma}} \tag{5.14}$$

In the case of the experiment corresponding to the red cross in Fig. 5.6, the matching frontier has been plotted as a black dash-dotted line (b1) in Fig. 5.7 (bottom). The collisions above the black dash-dotted line are impossible due to charge repulsion. On the contrary, below the black dash-dotted line, the repulsion between droplets is no important enough to avoid collisions.

The frontier shows that, for particular droplet radius and charge, parts of the classic collision diagram are not accessible. Indeed, the Fig. 5.7 (bottom) shows that a part of the bouncing and the coalescence region is not accessible. Of course, in other configurations, with a more important droplet charge or a smaller radius, a more important part of the classical collision diagram may be inaccessible. For example, in the case of droplets with a charge two times more important, the second frontier (b2) shows that a larger part of the classic diagram is inaccessible.

In conclusion, the present Chapter shows that electric charges influence directly the droplets motion and the droplet collision. Throughout our experiments, we observed a soft influence of electric charges on the classic droplet motion and collision. Indeed, we observed slight variation in the droplet trajectories due to electric attraction or repulsion as well as slight variations in the classic collision diagram. However, these small changes can result in significant changes of behavior. Typically, we showed that the electric interaction directly influences the collision parameter between droplets and the collision results. Our approach gives a first insight on the influence of the electric charges on the classic droplet collision diagram. However, more experiments are needed to design the precise charged droplet collision diagram. The natural next step would be to perform experiments with a setup comparable to the one developed by Gotaas et al [94] on earth. Such a set of experiments will need to be compared to experiments performed in microgravity. If the aerodynamic forces are found to not affect the influence of the electric charges, the setup would allow to conclude on the collision between charged droplets.

6

Charged droplets bouncing on a vibrating bath

Contents

The storage via vibrating bath has the great advantage of storing droplets for a long time (more than an hour) on the two dimensions of the oscillating liquid bath. The experimental setup leading to the bouncing of the droplet on the vibrating bath was described in Section 3.3.2. In the Section 4.2, we used the vibrating bath method to measure the droplet charges loss over time. However, we only tackled the complexity of the charged droplet bouncing on a vibrating bath. In particular, a droplet bouncing on a vibrating bath is kept at a relatively constant vertical position (except for the droplet bouncing), but can be displaced along the horizontal plane. Naturally, the droplet displacement on the vibrating bath is complex to describe. Indeed, the droplet, while bouncing, deforms the vibrating bath. In exchange, the

deformed liquid bath influences the droplet bouncing.

This relation between the liquid bath and the bouncing droplet can take several shapes. For example, small droplets bouncing on low viscous vibrating bath can self-propel [64]. In our case, we focus our attention on millimetric droplets bouncing on highly viscous liquid bath (1000 cSt). In this particular configuration, droplets do not displace on the surface of the liquid bath (at the exception of specific range of frequency that are not tackled in this Chapter [63]). Without external perturbations, the droplet indefinitely bounces at the same horizontal place.

This is where the excess of electric charge comes into play. Indeed, we showed in the Chapter describing the experimental setups (see Section 3.3.2) that electric charges do not influence the way the droplet bounces on the vibrating bath. However, as shown during the study of droplets in microgravity (see Chapter 5), an electric field can influence the motion of charged droplets. In this Chapter, we study how a charged droplet is set in motion via external electric fields. In the first Section (see Section 6.1) we investigate the basic case of a charged droplet sets in motion by a homogeneous electric field. In the second Section (see Section 6.2), we study the case of two droplets set in motion by their reciprocal electric interaction. Both Sections give new insights on droplets in motion on a high viscous vibrating bath.

6.1 Influence of a homogeneous electric field on a charged droplet bouncing on a liquid interface

When a high viscous liquid bath is oscillating, the droplet bounces on it vertically while keeping its horizontal position. However, an external horizontal force can be applied on the droplet. If this horizontal force is important enough, the droplet moves on the surface of the liquid bath. For example, blowing air on the system induces the displacement of the droplet. In our case, we can take advantage of the excess of charges to move the droplet by applying an electric force via an external electric field.

The study of two charged droplets in microgravity (see Chapter 5) demonstrates that the electric field generated by one electrically charged droplet can influence the motion of another charged droplet. For two charged droplets ($q = 10$ pC) separated by 5 mm, we have typically $E = \frac{1}{4\pi\epsilon_0}\frac{q}{r^2}$ =3.6 10^3 V/m. Such an electric field can be easily overtaken by experimental setups. For example, two metallic plates separated by 5 cm only need 180 V to produce the same electric field. Such an electric field, applied horizontally on the droplet should be sufficient to generate the horizontal displacement of the droplet on the vibrating bath.

In doing so, the droplet acquires a complex motion composed of its vertical bouncing and its horizontal displacement. The droplet interaction with the liquid bath as a function of the applied electric force determines the adopted motion. In the next lines, we describe the experimental setup and model the observations obtained from the experiments.

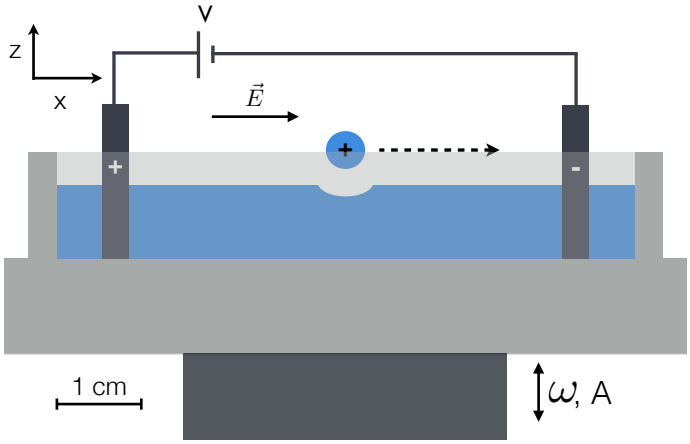

Figure 6.1: Sketch of the vibrating bath device. A charged droplet bounces on a liquid bath composed of silicone oil 1000 cSt. The liquid bath oscillates with an angular frequency ω and an amplitude A thanks to an electromagnetic shaker. The electrodes on each side of the bath allow generating a homogeneous electric field. Once the voltage is switched on, the charged droplet is set in motion.

6.1.1 Experimental setup

The Fig. 6.1 illustrates the experimental setup. The bath (60 x 60 mm) is vertically shacked via an electromagnetic shaker (GW-V2). For specific ranges of oscillating amplitudes A and angular frequencies ω, the charged droplet may bounce on the liquid interface. We define the x and z axis in Fig. 6.1. In the following of this Chapter, the z axis corresponds to the vertical axis while the x and y axes correspond to the horizontal axis. Two plane electrodes were placed on opposite sides of the oscillating bath to apply a horizontal electric field onto the electrically charged droplet. The use of two large (compared to the droplet size) planar electrodes (60 x 45 mm) separated by 53 mm allowed obtaining a homogeneous electric field between the electrodes. The homogeneous electric field prevents the experiment from dielectrophoresis effects. The electric field between the two large metallic plates can be supposed to be:

$$\vec{E} = \frac{V}{L}\vec{u} \tag{6.1}$$

where V is the voltage applied between electrodes, L the distance between electrodes and $\vec{u}$ is a unit vector pointing toward one of the electrodes.

The charged droplet was made of silicone oil 1.5 cSt. In order to ensure a minimum conductivity of the silicone oil, a small amount of ethanol (less than 1%) was added to the liquid used to generate the droplets. Electrically charged droplets were created with the charged droplet generator model A (see Section 3.1). Overall, electrically charged droplets were produced in the same way as the experiment on the charge

leakage (see Section 4.2). The charged droplet generator was calibrated before each experiment by using a Faraday cup. The calibration consisted in measuring the droplet radius and charge for the set of voltage used in each experiment. The typical duration of an experiment was of the order of 1 min. As shown in the Section 4.2, the charge loss during this duration is negligible. Throughout the experiments performed on the setup, the droplet radius r was tuned between 0.35 and 0.9 mm while the measured charge carried by the droplet q was in the range between 11 and 20 pC. Experiments were also performed with negatively charged droplets and gave the same results as the one obtained for positively charged droplets.

The liquid bath was made of silicone oil with a kinematic viscosity of 1000 cSt. The high viscosity limits the liquid bath deformation. Typically, a droplet bouncing on the bath only slightly curves the liquid bath. The oscillation frequency of the vibrating bath was set at $f = 40$ Hz. As shown in Fig. 3.15 in Section 3.3.2, this frequency allows stabilizing the bouncing droplet on a large range of acceleration. The oscillation amplitude of the vibrating bath was varied in order to study the influence of the bath oscillation on the droplet motion. The bath reduced acceleration $\Gamma = A\omega^2/g$ (A being the oscillation amplitude and ω being the angular frequency) was tuned between 0.5 and 1.75. The voltage V between electrodes was tuned between 1000 and 10000 V.

A first camera allowed tracking the charged droplet from the top of the bath. The tracking was made at 25 fps. The top camera was equipped with a wide-angle lens, allowing capturing the droplet motion at the scale of the liquid bath. On the side of the liquid bath, we tracked the droplet motion with a high-speed camera (Phantom Miro M-310) at 2000 fps. The high-speed camera was equipped with a zooming lens, allowing capturing the detail of the droplet motion. In the following, we firstly look at the observations obtained at the scale of the vibrating bath and then focus our attention on the droplet scale observations. The two different approaches (the macroscopic and the microscopic observations) allowed us to obtain a complete understanding of the system.

6.1.2 Observations at the scale of the vibrating bath

The Fig. 6.2 is the image superposition of the droplet motion took from the top of the vibrating bath. One second separates each droplet. The charged droplet is set in motion from the left to the right thanks to the external electric field. On the right side of the liquid bath, the droplet is kept away from the electrode because of the liquid meniscus.

The droplet moves along the x direction when a voltage is applied between both electrodes. The data in Fig. 6.3 (top) correspond to droplet trajectories taken from experiments for which the voltage was varied while the radius and the droplet charge was kept constant (i.e. $r = 0.8$ mm and $q = 15 \pm 5$ pC). The red crosses, green disks and orange triangles correspond to applied voltages V of respectively 2000 V,

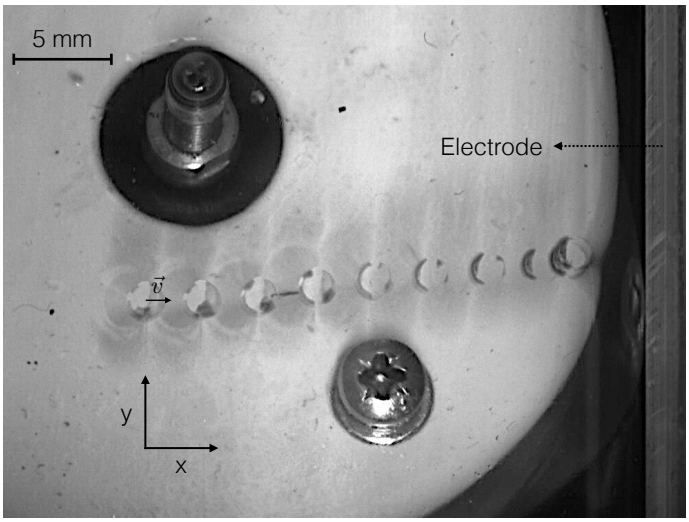

Figure 6.2: Image superposition of the horizontal droplet motion. The droplet moves with a speed $\vec{v}$. On the right side of the liquid bath, the droplet is kept away from the electrode because of the liquid meniscus.

3000 V, 4000 V. The charged droplet position over time is linear, which means that droplets with this set of radius and charge move with a constant speed. Moreover, this constant speed is acquired very quickly after the voltage on the lateral electrodes is switched on. Besides, the higher is the voltage the faster is the droplet.

The data of Fig. 6.3 (bottom) correspond to trajectories taken from experiments for which the droplet size was varied while the voltage between the electrodes $V =$ 1000 V and the charge $q = 14 \pm 3$ pC was kept constant. Open circles, triangles and squares correspond respectively to droplets of 0.56, 0.60 and 0.70 mm in radius. We observed that when the size of the charged droplets decreases, they stop moving with a constant speed. Moreover, the second derivative of the trajectory (i.e. the acceleration) increases when the radius decrease. Note that the variation in the droplet radius was obtained via droplet evaporation on the liquid bath. It took about 300 s to go from a droplet with a radius of 0.70 mm to a droplet with a radius of 0.56 mm. The study on the droplet charge leakage in Section 4.2 (in particular, the Eq. 4.19 modeling the phenomenon) shows that the droplet loose about 1.3 pC during its evaporation. This charge loss over time is enclosed into the errors bars.

To determine the crossover point between the accelerated and the constant speed regimes, the trajectories of electrically charged droplets (14 ± 3 pC) were recorded for several radii during the droplet evaporation. During these experiments, the evaporation time was always lower than 500 s, guarantying a charge loss of the order of the error bar according to Section 4.2. The voltage between the electrodes was

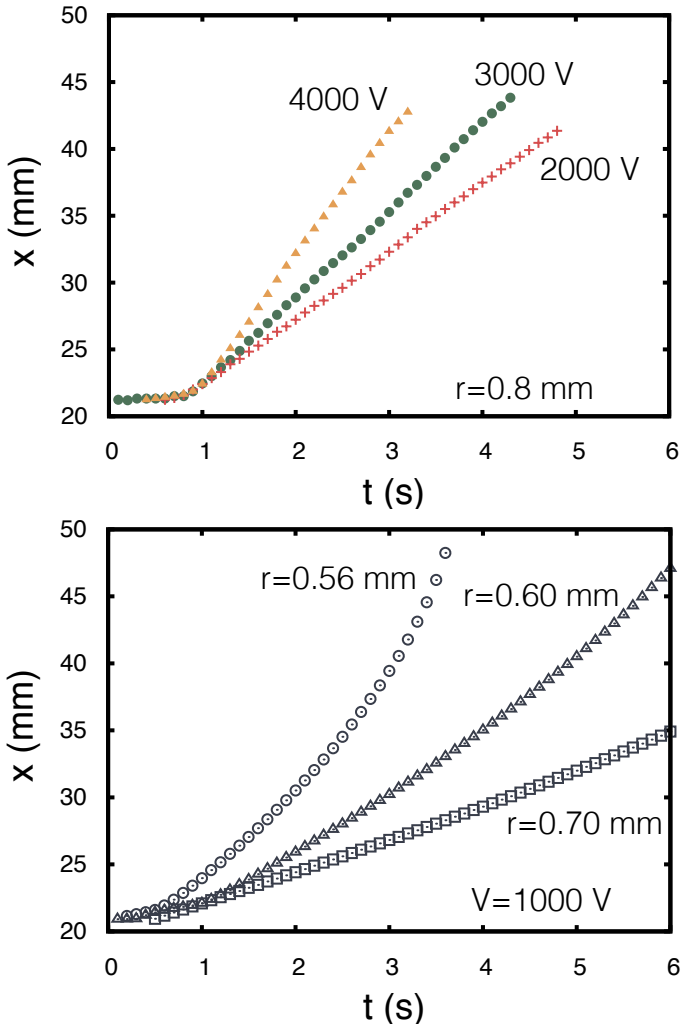

Figure 6.3: (Top) The trajectories $x(t)$ corresponding to charged droplets ($q = 15 \pm 5$ pC and $r = 0.8$ mm) under 2000 V (red crosses), 3000 V (green disks) and 4000 V (orange triangles). (Bottom) Horizontal position x over time for charged droplets ($q = 14 \pm 3$ pC and $V = 1000$ V) of radius 0.70 mm (open squares), 0.60 mm (open triangles), 0.56 mm (open circles).

kept at 1000V. As a first approach, the trajectories were fitted by the parabola $x(t) = at^2 + bt + c$ which can be considered as the first terms of the development of any exact solution. The parameters a (the second derivative) and b (the slope of the trajectories) are reported as a function of the droplet radius in Fig. 6.4. The parameter a (red crosses) increases when the droplet size decreases. The increase is suddenly rapid for $r \approx 0.5$ mm, showing a change of behavior at such a radius.

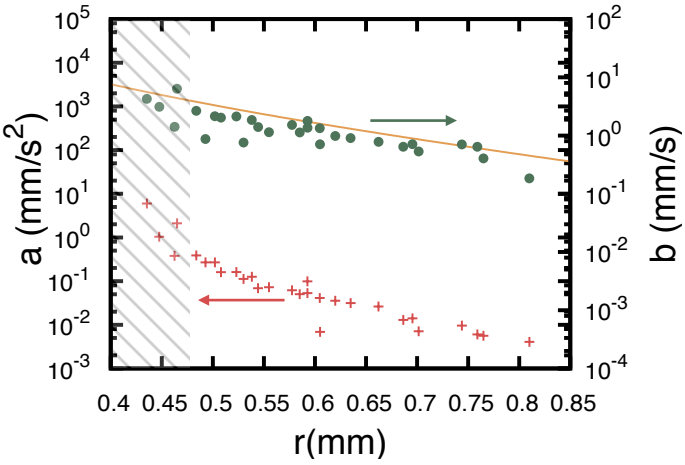

Figure 6.4: Dependence of the fitting parameters a (red crosses) and b (green disks) from the fit $x(t) = at^2 + bt + c$, as a function of the drop radius r. The orange curve is the droplet average speed computed according to Eq. 6.4. The hatching describes the theoretical description of the cross over between the two kinds of drop motion (i.e. when the acceleration is considered negligible or not, see Eq. 6.7). All the experiments were performed at $V = 1000$ V with $q = 14 \pm 3$ pC.

The observation of a movement with a constant speed may seem counter intuitive. Indeed, the charged droplet endures a constant horizontal force during its motion. As a consequence, a constant acceleration is expected. However, the droplet also interacts with the liquid bath. This interaction between the droplet and the liquid bath is the major unknown of the system. Indeed, macroscopic observations do not indicate how the droplet deforms the vibrating bath neither how the bath deformation affects the droplet bouncing. To better understand the droplet motion with a constant speed, we looked at the droplet speed as a function of the voltage applied on the electrodes (see Fig. 6.5 (top)). The dependence on the applied voltage for a large droplet was determined by using a droplet of r =0.8 mm charged with q =11 $\pm$ 2 pC. The Fig. 6.5 (top) shows that the droplet speed depends linearly on the voltage applied between electrodes.

The droplet speed was measured as a function of the oscillation amplitude of the liquid bath A. The Fig. 6.5 (bottom) shows the droplet speed as a function of the reduced acceleration $\Gamma = A\omega^2/g$. The dependence on the reduced acceleration was determined by using a droplet of r =0.8 mm charged with $q = 20 \pm 2$ pC. We see in Fig. 6.5 (bottom) that the droplet speed does not seem to vary with the bath reduced acceleration.

To summarize, small droplets are accelerated while larger droplets move with a

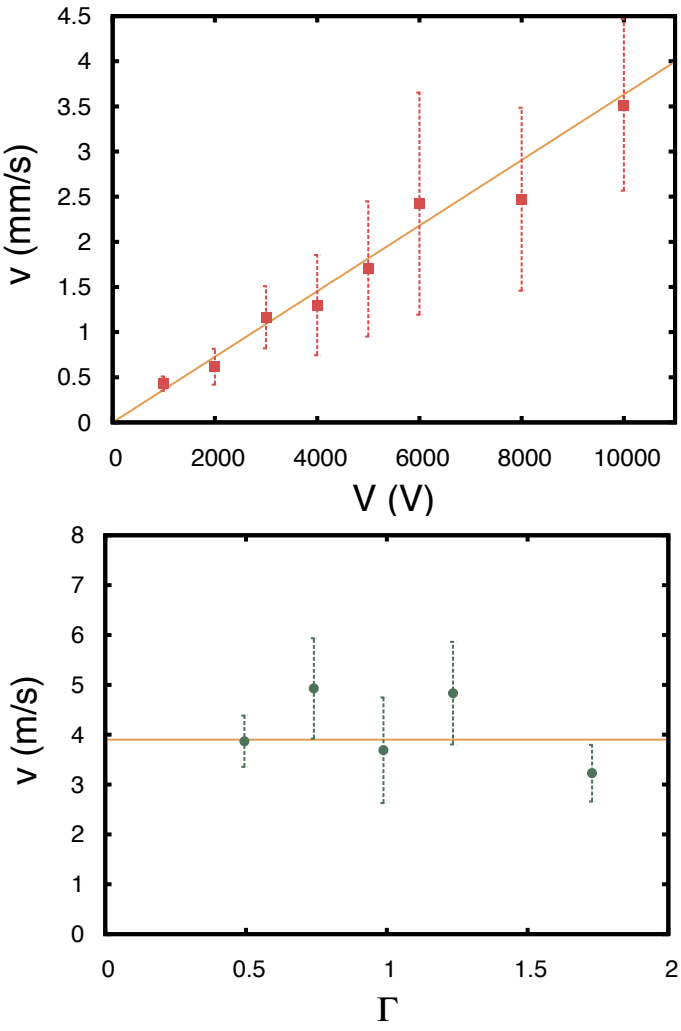

Figure 6.5: (Top) Speed v of a charged droplet (q =11 ± 2 pC and r = 0.8 mm) as a function of the voltage between both electrodes. The error bars are the standard deviation on 10 experiments. The orange line is a fit based on Eq. 6.4. (Bottom) Speed v of a charged droplet (q = 20 ± 2 pC and r = 0.8 mm) as a function of the bath reduced acceleration Γ. The error bars are the standard deviation on 10 experiments.

constant speed. In the case of large droplets, the measurements performed at a time scale of few seconds do not present any transient regime between the droplet at rest and the constant speed regime. As soon as the voltage is switched on, the droplet moves with a constant speed. We deduce that the origin of the constant speed has to be found on the time scale of one bounce.

6.1.3 Observations at the scale of the droplet

We investigated the droplet motion at the scale of one bounce by placing a high-speed camera on the side of the oscillating bath. It allowed capturing the motion of the droplet in the XZ plane.

The details of a charged droplet (r = 0.9 mm and q = 19±5 pC) bounces is shown on the image sequence in Fig. 6.6 (top). Each image is spaced by 3.125 ms. The voltage between both electrodes was V = 5000 V. The displacement of the center of mass of the charged droplet is shown in Fig. 6.6 (bottom). The z position (vertical) and the x position (horizontal) are represented by red disks and green crosses respectively. Along the z axis, the drop bounces with a frequency of 40 Hz, namely the same frequency as the oscillating bath. Between two cushioned impacts with the bath, the droplet center of mass experiences successive parabolic flight in the z direction. The $x(t)$ trajectory reveals a more complex structure than the macroscopic trajectory $x(t)$ presented in Fig 6.3 (top). Indeed, the position over time x(t) reveals that the droplet horizontal motion is the succession of the same pattern.

This periodic pattern is not observed for small droplets (r <0.5 mm) for which the trajectory is more complex. The Fig. 6.7 (top) shows an image sequence of a small droplet in motion. Each image is spaced by 3.125 ms. We observe that the bath is less deformed by the impact of the small droplet. The voltage applied on the droplet was V = 1000 V. The droplet had a radius r = 0.35 mm and a charge q = 14 pC. The tracking of the droplet motion is plotted in Fig. 6.7 (bottom). The z position (vertical) and the x position (horizontal) are represented by red disks and green crosses respectively. The droplet still has a periodic pattern in the vertical direction. However, we do not observe any pattern in the horizontal direction. The absence of horizontal pattern between each bounce is put in evidence at the scale of the liquid bath in Fig. 6.8. The Fig. 6.8 is an image superposition of a small charged droplet (r =0.35 mm q = 14 ± 3 pC) set in motion by an external electric field V = 1000 V.

In the case of the Fig. 6.6 (bottom), the horizontal motion of the bigger droplet seems influenced by its interaction with the oscillating bath. Indeed, when the droplet vertical position is minimum, the droplet is slowed down (i.e. the slope of x(t) decreases). A further look at the Fig. 6.6 (bottom) shows that the droplet interaction with the liquid bath stops its horizontal motion. Indeed, a straight line can be drawn along the green crosses. This straight line corresponds more or less to the diagonal of the graph. Such a line can only be drawn if the droplet endures a horizontal periodic motion with a speed that is periodically reset to zero. The reset to zero of the droplet horizontal speed implies that the droplet moves with a constant average speed. As a consequence, we observe a droplet motion with a constant speed at a macroscopic scale (i.e. a scale much larger than the bouncing droplet scale).

On the contrary, in Fig. 6.7 (bottom), the horizontal motion of smaller droplets is

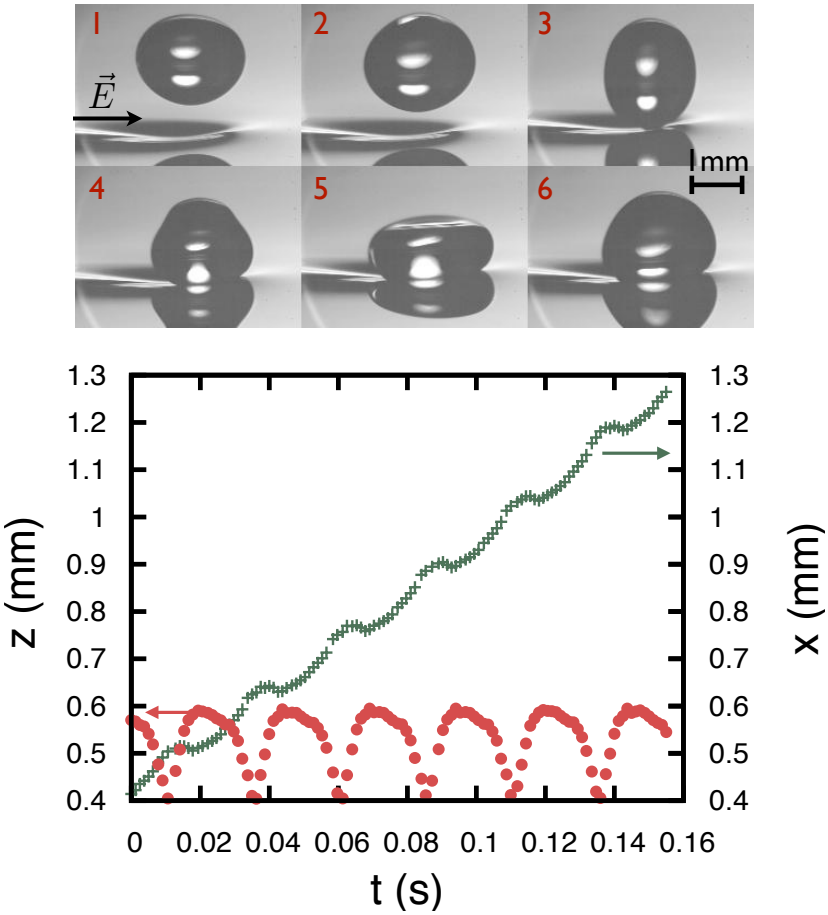

Figure 6.6: (Top) Image sequence of the drop motion during one bounce. Images are spaced by 3.125 ms. The droplet has a radius of 0.9 mm and a charge $q = 19 \pm 5$ pC. the applied voltage is V is 5000V. The electric field is oriented from left to right and the droplet is charged positively. (Bottom) Horizontal and vertical positions of the charged droplet as a function of time. Red disks and green crosses represent the vertical and the horizontal coordinates of the droplet respectively. A quarter of the measured points were plotted for the clarity of the graph.

never influenced by its interaction with the vibrating bath. From the beginning of the droplet tracking until the end, the droplet moves with the same tendency. Moreover, a straight line cannot be drawn along the green crosses, meaning that the droplet accelerates. This observation is confirmed by the image superposition in Fig. 6.8. On the image, the horizontal distance crossed during one bounce increases after each

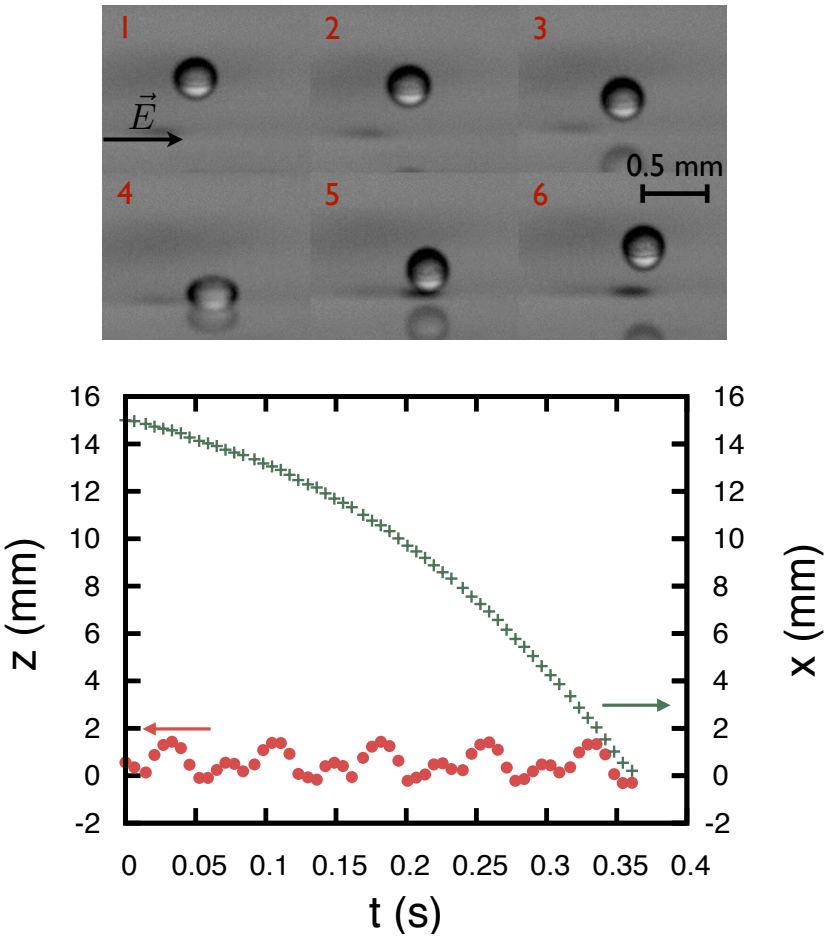

Figure 6.7: (Top) Image sequence of the drop during one bounce. Images are spaced by 3.125 ms. The droplet has a radius $r = 0.35$ mm, a charge $q = 14 \pm 3$ pC and the applied is voltage $V = 1000V$. The electric field is oriented from left to right and the droplet is charged positively. (Bottom) Horizontal and vertical positions of the charged droplet as a function of time. Red disks and green crosses represent the vertical and the horizontal coordinates of the droplet respectively. Twenty percent of the measured points were plotted for the clarity of the graph.

bounce. Such a behavior shows that the droplet horizontal speed is never reset to zero after a bounce. As a consequence, the droplet moves with a certain horizontal acceleration.

Beyond the difference between the horizontal motions, the droplet vertical motion (the z positions over time) in Fig. 6.6 differs from the Fig. 6.6. In the case $r =$

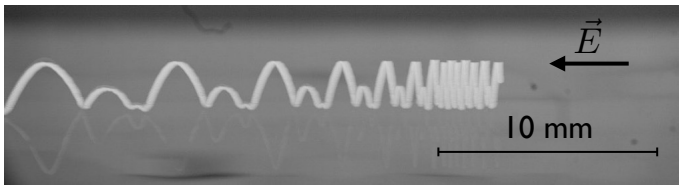

Figure 6.8: Image superposition of a small charged droplet (r =0.35 mm q = 14 pC) set in motion by an external electric field (V = 1000 V). The white line corresponds to the droplet image superposition.

0.9 mm, the droplet follows a simple bouncing mode with a frequency equal to the oscillating bath frequency. On the contrary, the case $r = 0.35$ mm corresponds to a more complex bouncing mode. The bouncing pattern is composed of a small bounce followed by a higher bounce. The frequency, however, is still the same as the oscillating bath.

The vertical bouncing of a droplet on an oscillating liquid bath have already been studied in previous research [68]. The studies modeled the system by a ball bouncing on an oscillating plate or bouncing mass-spring-damper [49]. The droplet bouncing mode depends on the reduced acceleration Γ, but also on the liquid surface tension and the droplet radius. In the present case, it is clear that the variation in radii generates a variation in the bouncing mode. However, we believe that this variation is not at the basis of the two different sorts of horizontal motions observed in Fig. 6.6 (bottom) and 6.7 (bottom). Indeed, the two different bouncing height of the smaller droplet should influence the interaction with the liquid bath but not suppress them.

Following this argument, we chose to focus our attention on the interaction between the droplet and the liquid bath. In the next Section, we attempt to model how the interaction between the droplet and the bath affects the horizontal motion of the charged droplet. In doing so, we find a criterion to differentiate droplets moving with a constant speed from droplets moving with a non-constant speed.

6.1.4 The model

From the observations at a low frame rate, we deduced that a droplet can move with a macroscopic constant speed. The observations at a higher frame rate indicate that the difference between the motion with a constant macroscopic speed and an accelerated motion have to be found in the interaction between the droplet and the liquid bath. In the next lines, we firstly model the horizontal motion of a droplet with a macroscopic constant speed. We then give a criterion for the crossover between the two different motions and describe the ingredients needed to model the droplet motion with a non-constant speed.

First of all, we focus our attention on the droplet horizontal motion with a macroscopic constant speed. This displacement corresponds to the Fig. 6.3 (top) and 6.6

(bottom). We deduced from our measurements that the macroscopic observation of a constant speed corresponds to a periodic horizontal motion with a reset to a zero speed at each period. The Fig. 6.9 shows the droplet horizontal position (x) as a function of the time multiplied by the angular frequency of the vibrating bath (ωt). The graph is a zoom on two horizontal periodic motions of a charged droplet ($r = 0.9$ mm and 19±5 pC). For the clearness of the graph, the green crosses correspond to the average horizontal position of the droplet calculated from ten bounces. The Fig. 6.9 highlights the previous observation performed with the high-speed camera (see Fig. 6.6):

1. The droplet interacts with the bath (step I). During its interaction with the liquid bath, the droplet speed is quickly decreased to zero. The step I is located in the grey area of Fig. 6.9.

2. The droplet is in flight (step II). It is submitted to the electric force and therefore, it is accelerated in the horizontal plane.

As a result of the step I and step II the droplet experiences a go-stop motion. In Fig. 6.9, the times τ_b and τ_f corresponds respectively to the time during which the droplet deforms the liquid bath and the time during which the droplet is away from the liquid bath (i.e. the charged droplet is "in flight"). The total time τ corresponds to the duration of one horizontal periodic motion. Because the droplet bounces with the same frequency as the vibrating bath, we have $\tau = 1/f$.

The characteristic times τ_b and τ_f can be estimated by looking at the bouncing mode of the charged droplet. As a first approximation, a bouncing droplet can be modeled by a linear spring [98,99]. Thanks to this hypothesis, the interaction time τ_b during the impact with the bath is constant and scales with the Rayleigh period [100] of vibration of a droplet, namely $\tau_b = \sqrt{3\pi m/8\gamma_d}$ where m is the mass of the droplet and γ_d the air-oil droplet surface tension. The deduced interaction time is $\tau_b \sim$12 ms. As observed previously, the droplet bounces with a frequency equal to the bath oscillation frequency, i.e 40 Hz. As a consequence, the flying time τ_f can be deduced from the equation $\tau_f = \tau - \tau_b$.

During the interaction time, we observed that the droplet horizontal motion is very quickly annihilated. In other words, the horizontal droplet speed is equal to zero during the contact time. As soon as the droplet takes off, the electric field exerts a force on the droplet due to the excess of charges carried by the droplet. In first approximation, the horizontal motion can be described by considering a point charge submitted to the electric force generated by the homogeneous electric field $E = V/L$. In this case, the point charge follows the simple law:

$$x(t) = \frac{a_c t^2}{2} = \frac{qE}{2m} t^2 = \frac{3qV}{8\rho\pi r^3 L} t^2 \tag{6.2}$$

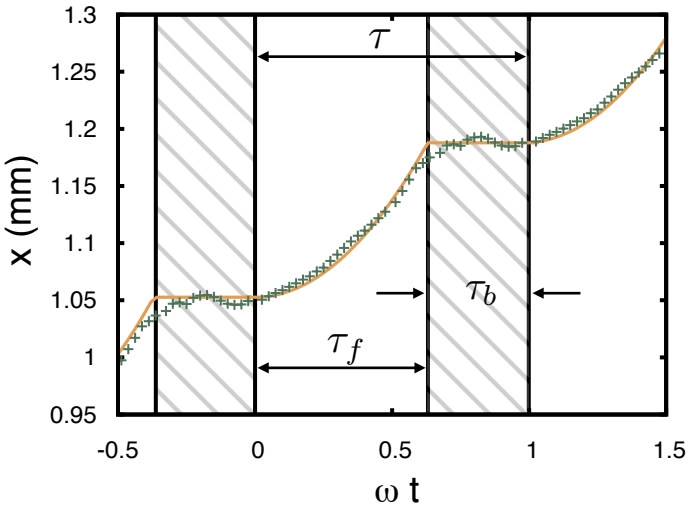

Figure 6.9: The green crosses are the average horizontal position of the droplet over time (during two bounces). The resting period (step I) is located in the shaded area. The orange curve is the fit made from Eq. 6.2 during the accelerated period (step II).

where a_c is the theoretical acceleration due to the electrostatic charge and ρ is the density of the droplet. This equation was applied to the case presented in Fig. 6.9, with L =53 mm, ρ=850 kg/m^3 and r=0.9 mm. The only fitting parameters in Fig. 6.9 are the time of contact τ_b and the value of the constant horizontal position in the "No Flight" zone (i.e. the shaded area). We deduce the acceleration a_c=0.34 m/s^2. The result, plotted in orange in Fig. 6.9, shows the good agreement between the theoretical trajectory and the experimental data. The contact time deduced from the fit, $\tau_b = 10$ ms, is smaller than expected (i.e. 12 ms). This variation is explained by the simplifications of our model. Indeed, in the present model, the droplet deformation, the influence of the bath deformation on the droplet bouncing, the dissipation in the air film and the characteristic time needed for the droplet to stop was not taken into account. However, in the following, we show that this simple description contains the basic and relevant physical ingredients to explain the macroscopic observations reported in Fig. 6.3 (top).

In summary, the model stating that the droplet endures a go-stop motion is in good agreement with the microscopic observations. On a side note, other systems can be described by the go-stop motion of point charges. Indeed, Drude [101, 102] described the motion of electrons in solids (especially metals) by supposing that electrons endured a go-stop motion due to their collisions with relatively immobile positive ions constituting the solid. In this case, the electron corresponds to the charged droplet and the network of immobile positive ions corresponds to the liquid bath. Even if

the discovery of quantum mechanics showed that the Drude model is based on false hypothesis, it provides a very good explanation of DC and AC conductivity in metals.

To confirm the validity of our approach, the model has to be confronted to the macroscopic behavior presented in Fig. 6.3 (bottom), 6.4 and 6.5. Because the drop speed is reset to zero at each bounce, the memory of the previous jump is annihilated. This statement ensures that the horizontal motion is periodic and that the average speed is constant. This later is given by the sum of the distance covered during flight time τ_f and during the interaction time τ_b divided by the period τ, namely:

$$\langle v \rangle = \frac{qV}{2mL} \frac{\tau_f^2}{\tau} \tag{6.3}$$

The flying time τ_f is deduced from the equation $\tau_f = \tau - \tau_b$. As a consequence, the Eq. 6.3 is written as:

$$\langle v \rangle = \frac{3qV}{8\pi\rho r^3 L} \left(\tau - \sqrt{\pi^2 \rho r^3 / (2\gamma_d)} \right)^2 \frac{1}{\tau} \tag{6.4}$$

The radius dependence can now be checked by comparing Eq. 6.4 and the average speed measurements in Fig. 6.4. The Eq. 6.4 was plotted in Fig. 6.4 by taking $q = 14$ pC, $V = 1000$ V, $L = 53$ mm, γ_d=0.017 N/m. The agreement between the experimental data and the model is excellent.

The relation between the average speed $\langle v \rangle$ and the voltage V applied on the electrodes is also captured by Eq. 6.4. Indeed, Eq. 6.4 predicts a linear dependence of $\langle v \rangle$ with V, which is in agreement with the observations. The fit from Fig. 6.5 (top) gives a slope of 0.36±0.02 μm/sV, which is in agreement, given the experimental error bars, with the slope computed from Eq. 6.4 (0.45±0.08 μm/sV).

Finally, we observed in Section 6.1.2 that the constant horizontal speed does not significantly vary with the reduced acceleration Γ. The physical parameter that was varied during the experiments was the oscillation amplitude. The bath oscillation frequency was not varied. The non-dependence of the average speed with the oscillation amplitude in Fig. 6.5 (bottom) is explained by the droplet bouncing mode. The charged droplet bounces with the same frequency as the bath oscillating frequency, independently of the bath oscillating amplitude. As a consequence, the total bouncing time τ does not vary with the bath oscillating amplitude. The flying time being the only parameter linked to the plate oscillation, it is clear that the average velocity (Eq. 6.4) should not depend on the bath oscillating amplitude. In other words, the Eq. 6.4 also captures the horizontal speed non-dependence with the bath oscillating amplitude.

A closer inspection of the Fig. 6.5 (bottom) shows, however, that the horizontal droplet speed measured at $\Gamma = 1.75$ is lower than the other measurements. The disparity can be explained by a variation in the droplet bouncing mode. Indeed, for significant bath accelerations, the bouncing droplet can adopt different bouncing

modes. Different bouncing modes can explain slight variations in the interaction time τ_b and, by deduction, slight variations in the droplet horizontal speed.

As indicated by the variation of the second derivative a in Fig. 6.4, the approximation of a constant speed for the droplet is not valid for small droplets. In other words, small droplets are not stopped during their interaction with the bath. As a consequence, a criterion on the droplet size has to be provided to set the domain of validity of our model. When the droplet falls on the oil bath, the droplet slightly bends the liquid surface. The idea is to estimate the horizontal force (i.e. the electrical force in our case) necessary to extract the droplet out of this dimple. Indeed, if the electrostatic force exceeds the extraction force, the droplet is not stopped when interacting with the bath.

In order to describe the droplet-liquid bath interaction, we have to model the shape adopted by the liquid bath. A basic model is to express the maximum depth of the bend in the liquid bath and suppose a linear growth toward the liquid surface. The maximum depth of the deformation can be approximated by balancing the droplet kinetic energy and the energy necessary to deform the bath with a depth h:

$$\frac{2}{3}\rho\pi r^3 v_i^2 = \gamma_b 2\pi r h \tag{6.5}$$

where v_i is the droplet speed just before interacting with the oil bath, γ_b the surface tension of the oil bath and h is the depth of the deformation. The vertical speed v_i is related to the flight time τ_f, i.e. $v_i = g\tau_f/2$ where $\tau_f = \tau - \tau_b$. This equation leads to a deformation of approximately 200 μm for a millimetric droplet. This order of magnitude is in agreement with the observation in Fig. 6.6 (top). In Fig 6.7 (top), we see that the bath deformation induced by the smaller bouncing droplet is far less significant. The width of the bath deformation can be supposed as being equal to the droplet radius r.

Let us consider that the droplet is on an incline plane when the droplet is at the bottom of the dimple. The problem is schematized in Fig. 6.10. The tangent of the slope $\tan(\alpha)$ of the incline is given by the ratio h/R. The horizontal electric force $F_e = qE$ is not able to extract the droplet when the projection along the parallel direction of the incline of the electric force $\vec{F}_{e,p}$ is smaller than the projection of the weight of the droplet $m\vec{g}_p$, namely:

$$qE\cos(\alpha) < mg\sin(\alpha) \tag{6.6}$$

The inequality leads to the following criterion:

$$\frac{qE}{hr^2} < \frac{4}{3}\pi\rho g \tag{6.7}$$

Equations (6.6) and (6.7) provide the conditions on r, E and q to observe a constant speed motion of the droplet. In the present case, the radius $r^\star$ below which

the electrical force qE exceeds the extraction force can be computed. Taking into account the experimental conditions from Fig. 6.4, namely $q = 14$ pC, $V = 1000$ V, $L = 53$ mm, one obtains $r^\star = 0.46$ mm. A shaded area in Fig. 6.4 materializes the separation between the two kinds of motion. Even if the second derivative of the droplet motion a is not equal to zero beyond this limit, the Eq. 6.7 gives a good criterion for the limit between the two observations (i.e. Fig. 6.3 top and bottom). The Eq. 6.7 also shows that bigger droplets could accelerate if they had a larger electric charge or if they were influenced by a larger electric field.

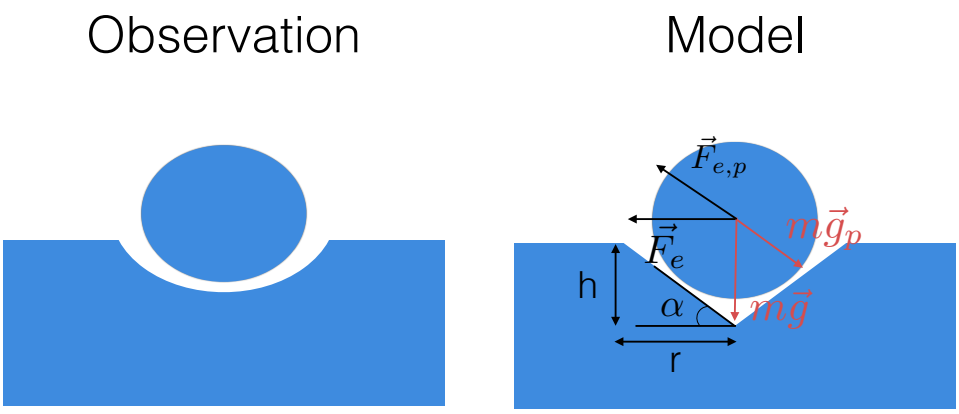

Figure 6.10: Schema of the model described by Eq. 6.6. If the projection of the electric force $\vec{F}_{e,p}$ is smaller than the projection of the droplet weight $m\vec{g}_p$, the droplet does not move during its interaction with the liquid bath.

We are now able to describe the droplet motion with a constant average speed and to predict the limit beyond which acceleration is observed. Beyond the limit described by the Eq. 6.7, the droplet horizontal speed is never reset to zero. As a consequence, the droplet moves with an average acceleration. However, the droplet acceleration does not necessarily mean that the droplet does not endure any friction forces. Indeed, processes such as dissipation in the air layer during the interaction with the liquid bath and air drag during the droplet flight take place during the droplet displacement. The direct result coming out of this reasoning is that the charged droplet does not simply endure the electric force during its accelerated motion. The smallest droplet studied in Fig. 6.4 ($r = 0.35$ mm, $q = 14$ pC, $V = 1000$ V, $d = 53$ mm) possess an acceleration of $a \approx 50$ mm/s^2. The electric acceleration endured by

a point charge in the same electric field would be:

$$a_e = \frac{3qE}{\rho 4\pi r^3} = 1.16 \text{ m/s}^2 \tag{6.8}$$

As a consequence, the droplet interaction with the liquid bath still has to be modeled to be able to fully describe the droplet motion. However, the establishment of a model for the droplet motion faces two major problems. (i) The influence of the air layer on the droplet slow down is difficult to model. Indeed, there is no information on the dynamic thickness of the air layer. (ii) Experiments are more difficult to perform because of the error on the acceleration measurements. Indeed, a larger liquid bath (L >53 mm) is needed in order to precisely measure an acceleration of the order of 100 mm/s^2. This restriction comes with the difficulty to produce a homogeneous electric field in a larger liquid bath.

6.1.5 futures investigations

In this Section, we take a brief look at further investigations that have been started. A first point concerns the use of a known charge and a known electric field to describe an unknown interaction. In this particular case, the known droplet charge and electric field allowed to describe the droplet motion. During the droplet motion, the main unknown is the dynamic interaction between the droplet and the liquid bath. Such an interaction could have been studied by moving the droplet via other applied forces. For example, it is possible to blow air on the droplet to generate the droplet displacement. However, the aerodynamic force is applied on the droplet surface and not on the droplet bulk. Moreover, the aerodynamic force would be far more difficult to model. On the contrary, using a known electric force allows focusing the investigation on the droplet interaction with the liquid bath. In the future, a complete model of the dynamic interaction between the droplet and the liquid bath could allow to deeply understand the behavior of the air layer between the droplet and the liquid bath.

Beyond the fundamental understanding of the droplet/bath interaction, the system studied allows to remotely control the droplet motion on the two dimensions of the liquid bath. The droplet control can be put in evidence via a setup slightly different from the previous experiment. The image sequence in Fig. 6.11 presents the top view of the oscillating liquid bath. The bath is surrounded by four electrodes, meaning that an electric field can be applied on the droplet in both horizontal directions. Red lines indicate which electrode is switched on. Moreover, obstacles were placed in the liquid bath. They correspond to the white plastic pieces visible from the top view.

We were able to guide the electrically charged droplet around the obstacles by controlling the voltage V between electrodes. The Fig. 6.11 shows image sequence of a charged droplet starting its motion on the bottom left of the liquid bath and ending its displacement on the top left of the liquid bath. The ability to precisely control

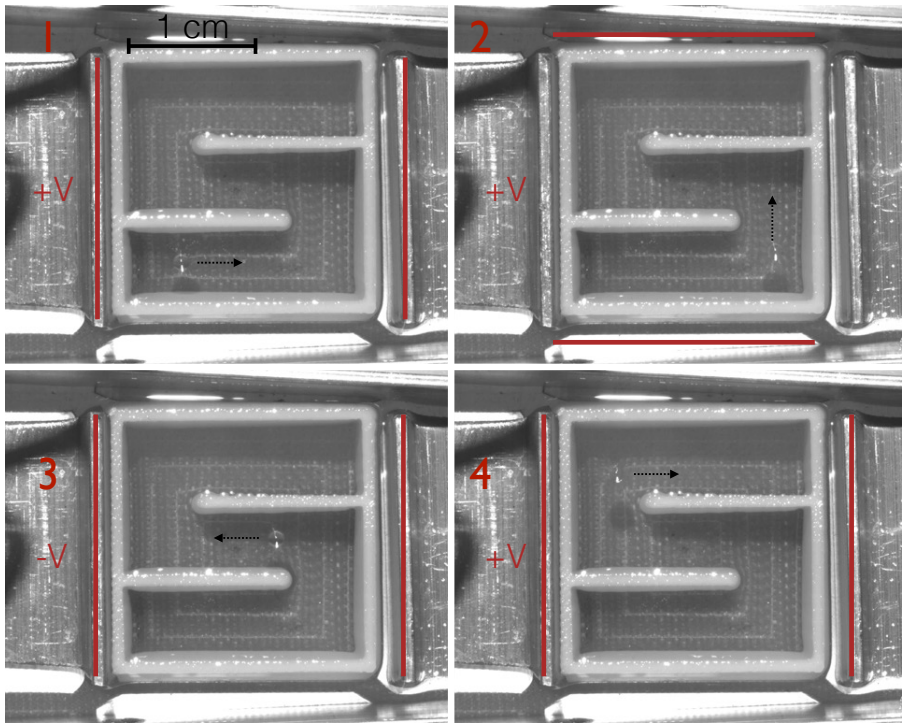

Figure 6.11: Top view of the 2D control of the charged droplet motion on the liquid bath. Red lines indicate which electrode is switched on. The positive or negative voltage is indicated by the symbol ± V.

the charged droplet motion on the liquid bath could allow performing microfluidic manipulations. As explained in the introduction (Section 2.3.2), the open microfluidic is booming. Open devices were demonstrated to be an interesting way to perform these different tasks especially for micro-chemical analysis purposes [39]. However, one of the remaining problems is the liquid alteration due to the contact with dirt on the guiding surface. The bouncing droplet is a good answer to this kind of problem. Indeed, the bouncing droplet is only in contact with ambient air, which means that dirt may only come from polluted surrounding air.

Moreover, the use of side electrodes in the previous experiments was due to the need of a homogeneous electric field. However, such an electric field is not necessarily needed. As a consequence, submarine electrodes may be used to control the droplet motion. Such a configuration is shown in Fig. 6.12. The submarine electrodes are dived in the liquid bath and connected to a voltage generator. An electric field can be produced between them and generate droplet motion. Eventually, the final step would be to be able to tailor any electric potential landscape at the surface of the vibrating bath.

The demonstration of the 2D electric control of the droplet motion on the oscillating bath shows that it is possible to develop microfluidic system based on this technology. The study developed during this thesis showed that the system may be configured to move the droplet with a constant speed. Such a configuration allows a precise manipulation of the electrically charged droplet. Of course, the technology still needs to be developed before being able to perform specific lab-on-a-chip, or in this case lab-on-a-bath, manipulations. We mainly need to study how to control the interaction between two bouncing droplets.

A last restriction to the manipulation of droplets on a vibrating bath could be the nature of the droplet. Indeed, the stability of a droplet bouncing on a vibrating bath depends on the liquid viscosity and surface tension. At this point, we can affirm that liquids such as silicone oil and soapy water can be considered stable on the liquid bath. On the other side, other liquids such as ethanol and water can be considered usable but with a lower stability. However, this limitation in the chemical composition of the droplet could be overcome by encapsulating liquids in silicone oil droplets. Indeed, encapsulated liquids have been stored on vibrating bath with success [103].

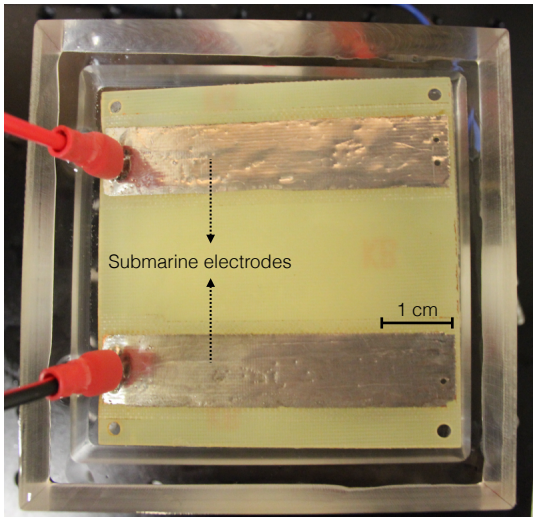

Figure 6.12: Top view of the control of the charged droplet motion via submarine electrodes. Both electrodes are dived in the liquid bath and connected to a voltage generator. By controlling the voltage between electrodes, an electric field can be applied on a bouncing droplet.

Finally, our discovery could play a key role in one of the most prolific studies on bouncing droplets: the walkers. Walkers are small droplets ($r \approx 0.5$ mm) bouncing at half the forcing frequency on low viscous silicone oil ($\mu \approx 20$ cSt) near the Faraday threshold of the oscillating liquid bath [64]. In this configuration, the droplet generates waves when it bounces on the liquid bath. Furthermore, the bouncing droplet interacts

with these waves. This interaction generates the self-propulsion of the droplet. Early measurements have been made on charged walkers. The subject is tackled in the Perspectives (see Chapter 8).

In conclusion, we demonstrated that large droplets influenced by a weak electric force move with a constant speed that is proportional to the charge and the voltage (see Eq. 6.3). The constant speed is due to the reset to zero of the droplet speed during each oscillation. The droplet is accelerated in the air by the electrical forces and stopped during its interaction with the oscillating bath. Small droplets influenced by a large electric force are not stopped during the contact period. As a consequence, their horizontal motion is accelerated. A criterion was proposed to separate both regimes (see Eq. 6.7). Moreover, first investigations showed that the displacement of a charged droplet on a vibrating bath could be useful for further developments in microfluidics or in the study of walkers.

6.2 Interaction between two electrically charged droplets on a vibrating bath

In the Chapter focusing on droplets in microgravity (see Chapter 5), we studied the interaction between two electrically charged droplets. Naturally, the interaction between two charged droplets can also be studied via the vibrating bath setup. The study is different from the experiment in microgravity because of the interaction between the droplets and the vibrating bath. Moreover, in the last Section, we claimed that the displacement generated by the electric field could be used for microfluidics applications. However, microfluidics rarely involves only one droplet. For example, the mixing between two small quantities of liquid requires two droplets. As a consequence, the interaction between two charged droplets bouncing on a vibrating bath should be understood to perform these tasks. Questions about the influence of the attraction or the repulsion between droplets on the droplet displacement or the droplet coalescence need to be addressed.

The interaction between charged droplets is particularly decisive in the case of two droplets with the same sign of charges. Indeed, the repulsion between droplets could prevent any contact between them. In the next lines, we focus our attention on two charged droplets with the same sign of charges interacting with each other while being stored on a vibrating bath.

In order to store the droplet, we used a bath filed with silicone oil 1000 cSt. The bath oscillated with a frequency $f = 40$ Hz and a reduced acceleration $\Gamma = A\omega^2/g = 1$. The charged droplets were created with the charged droplet generator model A. The droplets were composed of silicone oil 1.5 cSt with an addition of 1 % of ethanol. We performed experiments with three different droplet charges: neutral droplets (q=0), weakly charged droplets ($q = 32$ pC) and highly charged droplets ($q = 44$ pC).

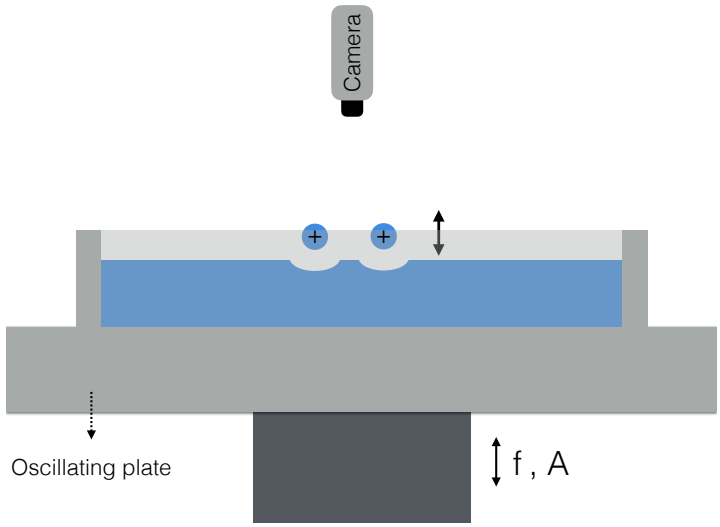

Figure 6.13: Schema of the setup developed for the study of the interaction between two charged droplets bouncing on a vibrating bath. Two droplets are released on the liquid bath. Their relative motion is then recorded over time by a camera located above the vibrating bath.

	case 1	case 2	case 3
q (pC)	0	32	44
r (mm)	1.0	0.8	0.8

Table 6.1: Charges and radii of the three configurations used to study the interaction between charged droplets bouncing on a vibrating bath.

As explained in the Section 3.1.2, the radius of charged droplets decreases with the electric field applied by the charged droplet generator. The droplet charge and radius of the three configurations are presented in Tab. 6.1. The experiment is schematized in Fig.6.13. During one experiment, two droplets were dropped near each other on the vibrating bath. A camera located at the top of the vibrating bath recorded the droplets positions over time.

The motion over time for three typical experiments is reported in Fig. 6.14. The graphs show the x and y horizontal positions over time of both droplets on the vibrating bath. Both droplets were dropped on the vibrating bath at a time t_0. The first graph corresponds to neutral droplets ($q = 0$), the second graph corresponds to weakly charged droplets ($q = 32$ pC) and the third graph corresponds to highly charged droplets ($q = 44$ pC). We observe in Fig. 6.14 that neutral droplets tend to move closer to each other. In the case of charged droplets, the motion is more erratic.

The erratic motion could be due to small external perturbations such as uncontrolled airflows. However, even if droplets seem to move erratically, they tend to stay at a fixed distance from each other.

Beyond the horizontal motion of each droplet, we are interested in the motion of one droplet compared to the other. In Fig. 6.15, we plotted the horizontal distance between droplets d over time. Each curve corresponds to one experiment. The first graph corresponds to neutral droplets (q=0), the second graph corresponds to weakly charged droplets (q = 32 pC) and the third graph corresponds to highly charged droplets (q = 44 pC). As previously observed in Fig. 6.14, the graph displaying the relative distance between neutral droplets shows that droplets tend to move closer to each other over time. Moreover, the droplet displacement over time seems to be suddenly accelerated around $r \approx 6$ mm. The two following graphs show that charged droplets rapidly repel each other before remaining at an equilibrium distance d_e. Even if this equilibrium distance varies slightly over time, it fluctuates around the same value over a very long period of time. The small variation in the relative distance between droplets is the most likely due to the erratic motion of the droplets. By comparing the second and the third graph on the Fig 6.15, we observe that the equilibrium distance between droplets is slightly more important in the case of highly charged droplets. The equilibrium distance d_e is respectively $d_e \approx 7$ mm and $d_e \approx 9$ mm for the weakly and highly charged droplets.

In the following, we first examine the interaction between neutral droplets and then study the interaction between charged droplets. Indeed, the attraction between two neutral droplets observed in Fig. 6.14 and 6.15 should also exist for two charged droplets. As a consequence, charged droplets should repulse each other because of their charges and attract each other because of their bouncing. The attractive force can be isolated and measured by studying neutral droplets. Then, the attractive force can be compared to electric repulsion in the case of charged droplets.

The attractive force between two neutral droplets can be deduced by knowing the droplet mass and calculating the second derivative of the relative distance d between droplets over time. The deduced attractive force is shown in Fig. 6.16. The force is plotted as a function of the relative distance between droplets d. We observe on the graph that the attractive force increases when droplets move closer to each other until a critical distance. At a distance of approximately d =3.5 mm, the attractive force decreases with the distance decrease. For $d < 3.2$ mm, the force becomes repulsive. The maximum of the repulsive force, $F = 40$ nN, is located at $d \approx 2.5$ mm, which corresponds approximately to two times the droplet radius. The maximum of the attractive force, $F = 20$ nN, is located at $d = 3.5$ mm.

The repulsive force between two neutral droplets close to each other can be explained by direct interactions between droplets. Indeed, when droplets are close to each other, we observe that droplets bounce on each other without coalescing. This is equivalent to the mechanism occurring for the droplet bouncing on the vibrating

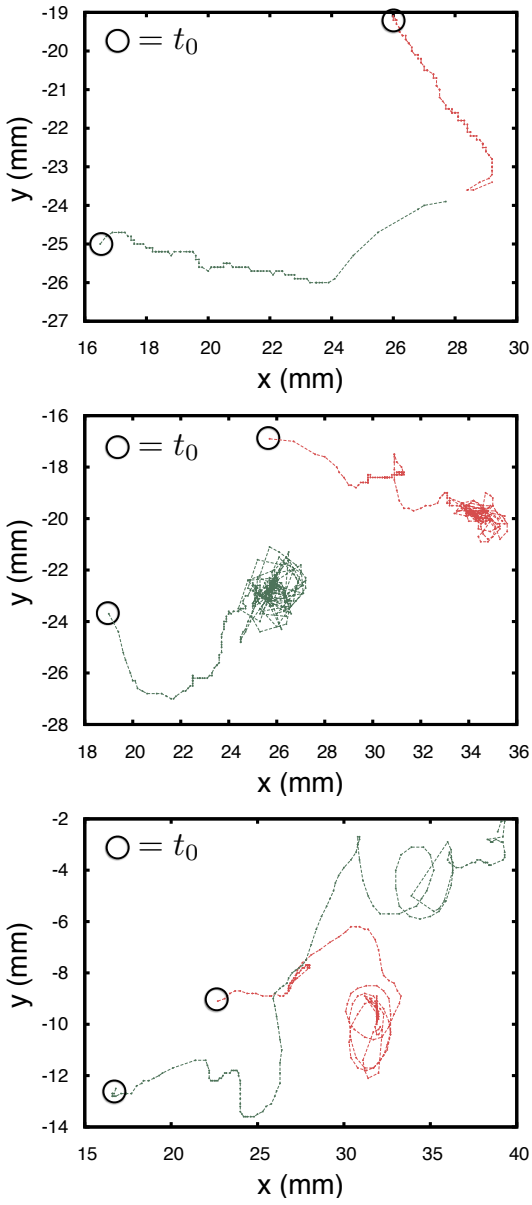

Figure 6.14: Horizontal positions (x-y) over time for two droplets bouncing on the vibrating bath. The circles correspond to the time t_0 at which both droplets were dropped on the bath. Each color corresponds to one droplet. The first graph corresponds to neutral droplets (case 1), the second graph corresponds to weakly charged droplets (case 2) and the third graph corresponds to highly charged droplets (case 3).

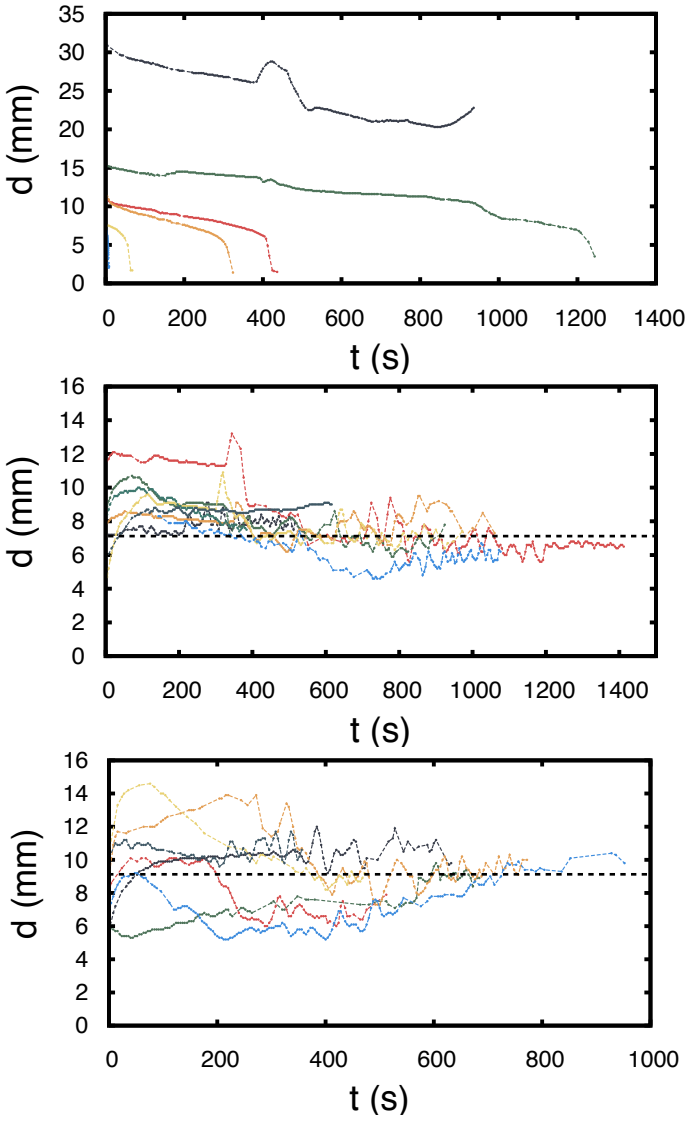

Figure 6.15: Relative distance d between the two droplets bouncing on the vibrating bath over time. The first graph corresponds to neutral droplets (case 1), the second graph corresponds to weakly charged droplets (case 2) and the third graph corresponds to highly charged droplets (case 3). Each color corresponds to one experiment. The black dashed lines correspond to guidelines of the equilibrium distance d_e.

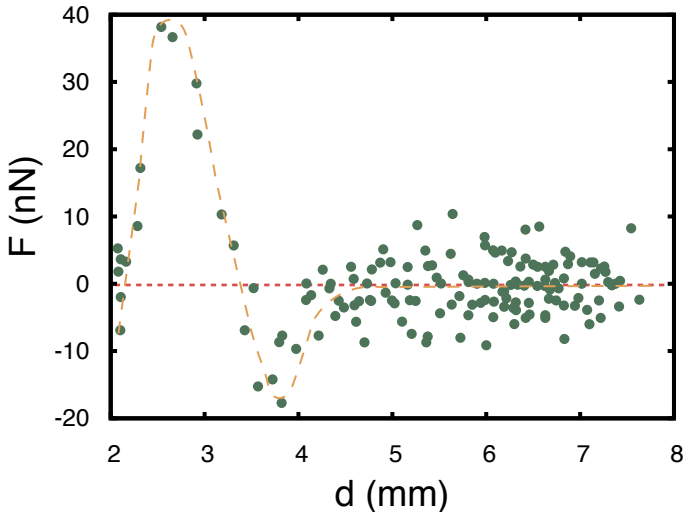

Figure 6.16: Calculated force between two neutral droplets during their bouncing on the vibrating bath. The green disks correspond measurements from four different experiments. The force is deduced by taking the second derivative of the droplet relative displacement. The orange dashed line corresponds to a guideline of the force between droplets.

bath. This bouncing between droplets corresponds to the repulsive force observed in Fig. 6.16 between $d = 2$ mm and $d = 3.2$ mm. Both droplets being deformable, it is understandable that they bounce on each other at a distance larger than twice their radius.

The attractive force between neutral droplets, observed for $d > 3.2$ mm, is more surprising. Indeed, at this distance, droplets do not interact with each other by any way. However, each droplet interacts with the vibrating bath. When the droplet bounces on the liquid bath composed of silicone oil 1000 cSt, the silicone oil is deformed. This bath deformation is highlighted in Fig. 6.17 (top). We know from Nicolson [104] that two deformations at the surface of a liquid interact with each other because of the liquid surface tension. The phenomenon is commonly called Cheerios effect and is schematized in Fig. 6.17 (bottom). A liquid interface always tends to reduce its surface. In order to do so, the two hollows generated by the bouncing droplets attract each other.

Naturally, the mechanism involved in this experiment is a bit more complex. Indeed, the droplet deforms the liquid bath during each bounce, which means that the attraction between both cavities evolves with the droplet motion itself. Furthermore, the droplet is not always interacting with the liquid bath, which means that the capillary attraction should not be applied permanently on the droplet. In order to model this behavior, we suppose that, at each bounce, the droplet resets the deformation of the liquid bath. In other words, when the droplet falls on the liquid bath, the liquid

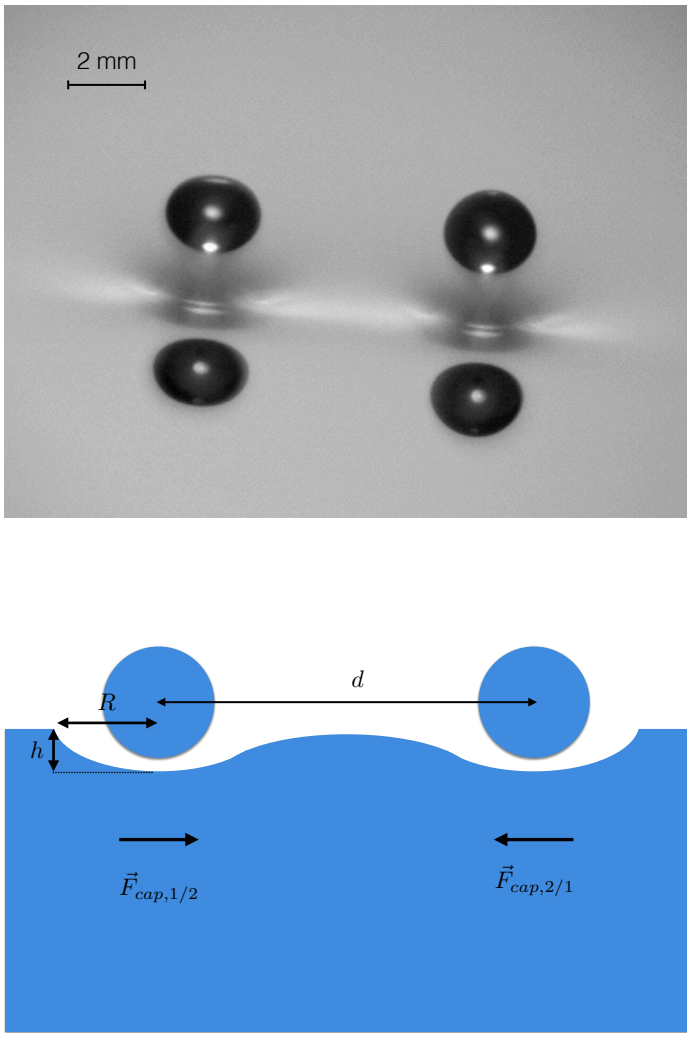

Figure 6.17: (top) Image of two neutral droplets bouncing near each other. In order to highlight the bath deformation, the droplets bounced on an oscillating bath with a reduced acceleration $\Gamma = 3.5$. Both deformations in the liquid bath are attracted to each other due to cheerios effect. (Bottom) Schema of two bath deformations attracted toward each other. The width and the depth of the deformation correspond respectively to R and h.

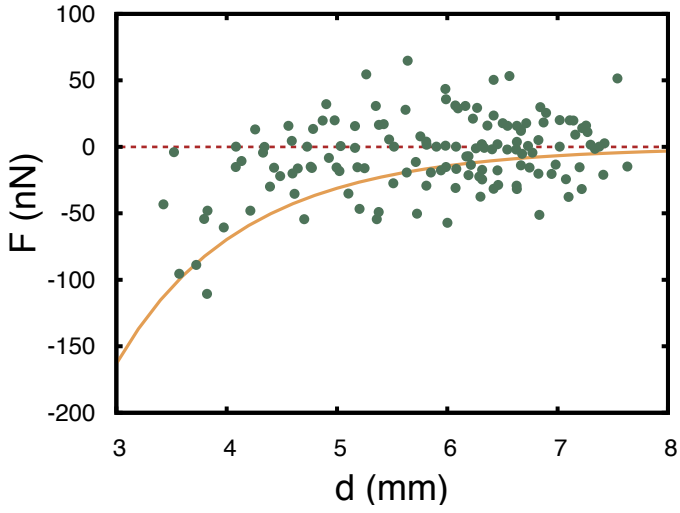

Figure 6.18: Recalculation of the attractive force between two droplets during their bouncing on the vibrating bath. The green disks correspond measurements from four different experiments. The attractive force is deduced by taking into account the time during which the attractive force is applied on the droplet. The maximum of the attractive force ($F \approx 100$ nN) is observed at a distance $d = 3.5$ mm. The yellow curve corresponds to a fit by Eq. 6.9.

surface is deformed. Furthermore, during a time τ_b the bouncing droplet interacts with the liquid bath and both the droplet and the bath deformation endures the capillary force due to the Cheerios effect. Then, the droplet bounces away from the liquid bath and does not interact with the liquid bath during a time τ_f.

The direct consequence of this reasoning is that the attractive force observed in Fig. 6.16 for $d > 3.5$ mm was underestimated. Therefore, it should be recalculated by taking into account the correct time during which the force is applied on the droplet. Indeed, during the time of one bounce $\tau = \tau_b + \tau_f$, the droplet is only subject to the attractive force during a time τ_b. We showed in the previous Section (see Section 6.1.4) that, for the present experimental conditions, $\tau_b = 10$ ms and $\tau_f = 15$ ms. Therefore, the droplet horizontally moves only during 40 % of one bounce. The new calculation of the attractive force applied on the droplet is shown in Fig. 6.18. The maximum of the attractive force (at a distance $d = 3.5$ mm) equals $F \approx 100$ nN. This effective attractive force can be compared to capillary attraction between two deformations in liquid surfaces. According to Kralchevsky *et al* [105], the capillary attraction between two hollows of the same size can be expressed as:

$$F_{cap} = \frac{-2\pi\gamma_b Q^2}{l_c} K_1\left(\frac{d}{l_c}\right) \tag{6.9}$$

where $\gamma_b = 21$ mN/m is the surface tension of the vibrating bath, Q is a geometric

factor describing the hollow, $l_c = \sqrt{\gamma_b/\rho_b g}$ is the capillary length, $\rho_b = 971$ kg/m^3 is the bath density, K_1 is the modified Bessel function of the first order and d is the distance between the center of both hollows. The geometric factor Q can be deduced by knowing the deformation depth h and width R of the hollow (see Fig. 6.17 (top)).

$$Q = \frac{h}{K_0(\frac{R}{l_c})} \tag{6.10}$$

Once the geometry of the hollow in the vibrating bath estimated, the capillary force can be deduced. In the previous section (see Section 6.1.4), we supposed that the width of the deformation was equal to the droplet radius $R = r$. Moreover, we calculated the depth of the deformation by comparing the droplet kinetic energy and the liquid bath surface tension. We deduced that the bath deformation had a depth of approximately $h = 200$ μm. However, this deformation depth was possibly overestimated. Indeed, a smaller depth of $h = 80$ μm is in better agreement with the present observation. The capillary force calculated with $h = 80$ μm and $R = r$, is plotted as an orange line in Fig. 6.18. The Eq. 6.9 correctly reproduces the trend of the measurements in Fig. 6.18. Moreover, we observe in Fig. 6.18 that the attractive force rapidly increase around $d \approx 6$ mm. It corresponds to the distance at which droplets move quickly to each other in Fig. 6.15.

Even if we were not able to measure the depth of the deformation h (see Fig. 6.17), we can suppose that the correct depth is situated between $h = 80$ μm and $h = 200$ μm. Indeed, on one side, the comparison between the kinetic energy and the bath surface tension did not take into account the droplet deformation, which led to an overestimation of the depth h. On the other side, the bath deformation dynamically evolves with the droplet bouncing, which is not taken into account by the present model. However, beyond the exact value of the hollow depth, the agreement between the model and the measurements shows that the Cheerios effect correctly describes the attraction between two neutral droplets bouncing on a liquid bath.

Once the attractive force between bouncing droplets described, we can add the electric interaction between two charged droplets to our study of the phenomenon. As shown in Section 5.3 the electric force between two charged droplets is expressed by:

$$\begin{aligned} F_{el} &= F_c + F_{dip} \\ &= \frac{q_a q_b}{4\pi\epsilon_0 d^2} + \frac{1}{4\pi\epsilon_0} q_a^2 r_b \left(\frac{1}{d^3} - \frac{r}{(d^2 - r_b^2)^2} \right) + \frac{1}{4\pi\epsilon_0} q_b^2 r_a \left(\frac{1}{d^3} - \frac{d}{(d^2 - r_a^2)^2} \right) \\ &+ \frac{1}{4\pi\epsilon_0} q_a q_b r_a r_b \left(\frac{1}{d^4} + \frac{1}{(d^2 - r_a^2 - r_b^2)^2} - \frac{1}{(d^2 - r_a^2)^2} - \frac{1}{(d^2 - r_b^2)^2} \right) \end{aligned} \tag{6.11}$$

where $F_c = \frac{q_a q_b}{4\pi\epsilon_0 d^2}$ corresponds to the Coulomb interaction and F_{dip} corresponds to the dipolar forces. The charges $q_a = q_b = q$ and the radii $r_a = r_b = r$ correspond

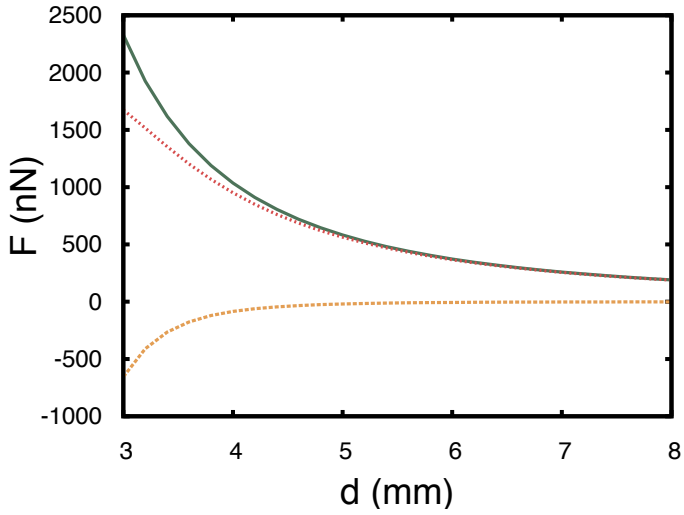

Figure 6.19: Comparison between the total electric force F_{el} (red dotted line), the Coulomb force F_c (green line) and the force due to dipole interactions F_{dip} (orange dashed line). The electric forces are calculated from Eq. 6.11.

to the electric charge and radii of each droplet and ϵ_0 corresponds to the vacuum electrical permittivity.

In the following lines, we focus our attention on the case of droplets weakly charged (i.e. case 2, $q = 32$ pC). The scalar value of F_{el} (red dotted line), F_c (green line) and F_{dip} (orange dotted line) for $q = 32$ pC are plotted in Fig. 6.19. We observe that, even for small distances between droplets d, the influence of the dipolar forces remains low. However, the comparison between the capillary force in Fig. 6.18 and the electric forces in Fig. 6.19 indicates that the electric interaction is about ten times greater than the capillary attraction. As a consequence, we decided to take into account the entire electric force (see Eq. 6.11) in the following reasoning.

Even if the electric repulsion is more important than the capillary attraction, they are not applied in the same way on the charged droplet. During our description of the motion of a neutral droplet, we showed that the droplet motion could be modeled by the following events:

1. The droplet interacts with the liquid bath and moves horizontally due to the capillary attraction.

2. The droplet does not interact with the liquid bath and does not horizontally move.

The motion of a charged droplet on the vibrating bath can be sliced in the same way:

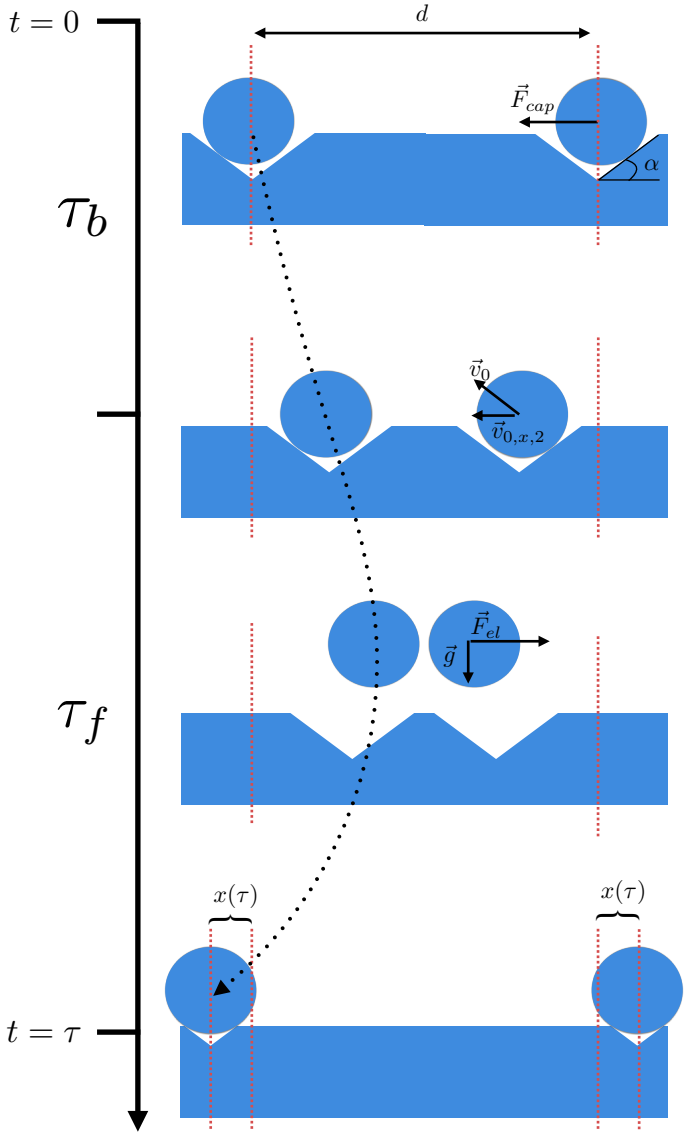

Figure 6.20: Schema of both charged droplets bouncing on the vibrating bath over time. During the time τ_b the droplet interacts with the liquid bath and moves because of the capillary attraction F_{cap} between both bath deformations. Then, the droplet bounces away from the liquid bath during a time τ_f. During this time, the droplets initial speed $v_{0,x,2}$ tends to move closer both droplets, the electric repulsion F_{el} draws them away. If $x(\tau) = 0$, both droplets did not horizontally move during their bounce.

1. The droplet interacts with the liquid bath and moves horizontally due to the capillary attraction.

2. The droplet does not interact with the liquid bath and moves horizontally due to the electric repulsion.

In the same way as the previous Section (see Section 6.1.4), we should be able to explain macroscopic observations by modeling the microscopic displacement of the droplet (i.e. the droplet displacement during one bounce). In particular, the observed equilibrium distance between droplets d_e should correspond to a horizontal displacement equals to zero during one bounce. In other words, if x describes the droplet horizontal displacement and τ the time of one bounce, we should have:

$$x(\tau) = 0 \tag{6.12}$$

If we suppose that the droplet displacement during one bounce is very small compared to the distance between droplets, we can express the droplet motion as:

$$x(\tau) = v_{0,x,1}\tau_b + \frac{F_{cap}}{2m}\tau_b^2 + v_{0,x,2}\tau_f + \frac{F_{el}}{2m}\tau_f^2 \tag{6.13}$$

where m is the droplet mass, $v_{0,x,1}$ is the droplet initial horizontal speed when the droplet interacts with the liquid bath and $v_{0,x,2}$ is the droplet initial horizontal speed when the droplet bounces away from the vibrating bath. The Eq. 6.13 corresponds to the mathematical description of the two steps of the droplet horizontal motion. The displacement of both charged droplets during one bounce is schematized in Fig. 6.20.

During the first step, the droplet interacts with the liquid bath. We showed in Section 6.1.4 that for $F_{el} < \frac{4}{3}\pi\rho ghr^2$, the electric force is not important enough to deform the vibrating bath. Thus, the droplet is subject to a go-stop motion during its displacement. In the present configuration, this criterion is verified for droplets separated with a distance $d \approx 3$ mm. Therefore, we can suppose that the droplet horizontal speed is reset to zero at the beginning of its interaction with the liquid bath. This reasoning leads to $v_{0,x,1} = 0$. As a consequence, when the charged droplet interacts with the vibrating bath, it only endures the capillary attraction between both bath deformations. If the droplet interacts with the vibrating bath during a time τ_b, we have: $x(\tau_b) = \frac{F_{cap}}{2m}\tau_b^2$.

After its interaction with the liquid bath, the droplet bounces away from the liquid bath and does not interact with the liquid bath during a time τ_f. During this time the droplet displacement is also governed by its initial speed and the forces applied on the droplet. The only horizontal force applied on the droplet being the electric interaction between both droplets, we have $x(\tau_f) = v_{0,x,2}\tau_f + \frac{F_{el}}{2m}\tau_f^2$.

Combining both motions leads to a total displacement $x(\tau)$. If $x(\tau) = 0$, the droplet does not move during one bounce, which means that both droplets remain at an equilibrium distance. The key factor in the Eq. 6.13 is the droplet initial horizontal

speed $v_{0,x,2}$. This initial speed is composed of two terms, $v_{0,x,2} = v_{0,x,2,a} + v_{0,x,2,b}$. The first term $v_{0,x,2,a}$ corresponds to the horizontal speed acquired by the droplet during its interaction with the liquid bath:

$$v_{0,x,2,a} = \frac{F_c}{m}\tau_b \tag{6.14}$$

The second term $v_{0,x,2,b}$ corresponds to the influence of the vibrating bath on the droplet initial speed. Indeed, because the droplet is influenced by the electric force, it bounces on the side of the bath deformation. As a consequence, we can suppose that the droplet does not bounce on a horizontal plane, but on the slope of the bath deformation. Therefore, the droplet bouncing generates an initial horizontal speed. While this term can be considered as negligible in other configurations such as the one in Section 6.1.4, the small forces involved in this study make this term non-negligible. The droplet initial speed when it leaves the vibrating bath can be calculated in the same way as in the previous Section (see Section 6.1.4) and projected on the horizontal axis by considering the slope of the bath deformation:

$$v_{0,x,2,b} = \frac{-g\tau_f}{2}\sin(\alpha) \tag{6.15}$$

where $g\tau_f/2$ is the initial speed of the droplet and $\alpha \approx h/r$ is the average angle of the liquid bath deformation (see Fig. 6.20).

The distance crossed by the droplet during one bounce $x(\tau)$ is plotted as a function of the distance between both droplets d in Fig. 6.21. The orange curve corresponds to the weakly charged droplet ($q = 32$ pC). The positive value of $x(\tau)$ indicates that two droplets close to each other tend to move away from each other. When the distance between droplets increases, the distance crossed by one droplet during one bounce decreases. For $d = 12$ mm, the distance crossed by one droplet becomes negative. Such a behavior indicates that both droplets invert their motion and tend to move closer to each other. As a consequence, the distance $d = 12$ mm can be considered as an equilibrium distance between droplets d_e. If droplets are artificially moved closer to each other, they tend to separate away. On the contrary, if both droplets are moved away from this equilibrium distance, they tend to move closer to each other. In practice, we observed such an equilibrium distance at $d_e \approx 7$ mm. We deduce from the comparison between the model and the experiment that the model correctly predicts the droplet behavior, even if it overestimates the equilibrium distance d_e. Note that the case of highly charged droplets (case 3, $q = 44$ pC) shows the same overestimation of the model compared to the experiment. Indeed, we observed an equilibrium distance $d_e \approx 9$ mm, while the model predicts an equilibrium distance $d_e = 17$ mm.

Once the droplets reach an equilibrium distance d_e, they remain more or less at the same equilibrium distance for several minutes. We showed in Section 4.2 that a bouncing droplet slowly loses its charge over time. Therefore, the electric repulsion

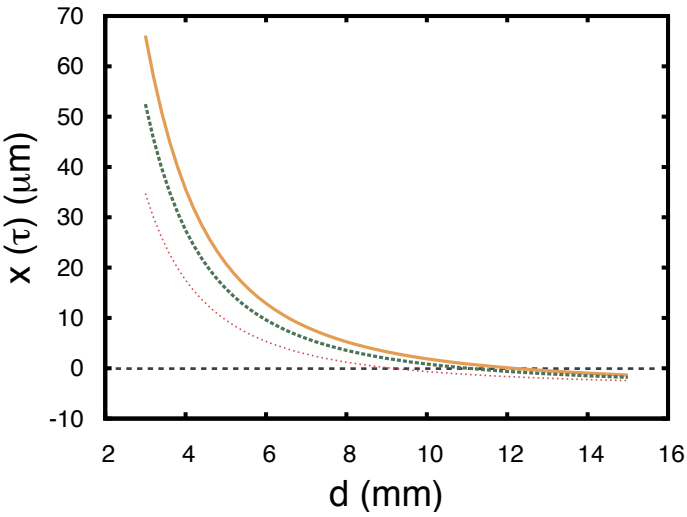

Figure 6.21: Distance crossed by a droplet during one bounce $x(\tau)$ as a function of the distance between droplets d. The orange line corresponds to a droplet with a charge $q = 32$ pC and a radius $r = 0.8$ mm. The green dashed line corresponds to a droplet with a charge $q = 29$ pC and a radius $r = 0.45$ mm (i.e. a weakly charged droplet after 800 s on the liquid bath). The red dotted line corresponds to a droplet with a charge $q = 24$ pC and a radius $r = 0.3$ mm (i.e. a weakly charged droplet after 1200 s on the liquid bath).

between droplets decreases over time. Naturally, the droplet radius also decreases over time. This reduction of the droplet radius generates a decrease of the bath deformation and consequently, a decrease of the capillary attraction. In order to be coherent with the observations, the model should predict the compensation between both the decrease of the electric repulsion and the decrease of the capillary attraction. In Fig. 6.21, we plotted the horizontal distance crossed by a charged droplet $x(\tau)$ by taking into account the charge and radius decrease after 800 s ($q = 29$ pC and $r = 0.45$ mm, green dashed curve) and 1200 s ($q = 24$ pC and $r = 0.3$ mm, red dotted curve). Note that only the decrease of the width of the bath deformations R was taken into account, given the absence of models on the influence on the droplet size on the depth of the deformation h. The results in Fig. 6.21 show that the equilibrium distance slightly decreases. Given the slight variation over time of the distance d in Fig. 6.15, this soft decrease of the equilibrium distance is difficult to confirm experimentally.

The overestimation of the equilibrium distance d_e can be explained by the simplifying hypothesis that were taken. Indeed, by neglecting the influence of the droplet deformation on the droplet displacement and by simplifying the shape of the liquid bath deformation, the influence of the electric repulsion may have been overestimated. In particular, the present model neglects the influence of the bath deformation generated during one droplet bounce on the next droplet bounce. In the case of charged

droplets influenced by an external homogeneous electric field (see Section 6.1.4), those hypothesis were justified by the importance of the forces involved. Indeed, the charged droplets were influenced by an external electric force $F_{el} \approx 10^{-5}$ N that generated a horizontal displacement during one bounce of $x(\tau) \approx 0.02$ mm. On the contrary, in the case of the interaction between two charged droplets, the applied forces and distances crossed are several orders of magnitude smaller (see Fig. 6.18 and 6.19). As a consequence, these simplifying hypothesis are less and less valid.

Given the number of hypothesis taken, this model should be treated cautiously. In order to confirm the present model, a precise description of the droplet motion during one bounce is needed. This could be achieved by imaging the droplet motion via a high-speed camera, in the same way as the microscopic observations in Section 6.1.3. Moreover, a precise description of the bath deformation would allow understanding in a deeper way the influence of the droplet-bath interaction on the droplet motion. Methods aiming at the characterization of liquid surface [106] could be used to achieve this goal.

In conclusion, we studied the interaction between two droplets bouncing on a vibrating bath. In the case of neutral droplets, both droplets are attracted toward each other. We deduced the attractive force between droplets from the measurement of the droplets position over time. The force was successfully modeled by supposing that the liquid bath deformation generates capillary attraction between droplets. In the case of two positively charged droplets, we observed that both droplets separate away until remaining at an equilibrium distance d_e. Even though the capillary force was found to be several orders of magnitude smaller than the electric repulsion, the model of the droplet motion during one bounce allowed explaining the presence of an equilibrium distance between droplets.

7

Electric charges influence on the Leidenfrost state

Contents

In this Chapter, we investigate the influence of electric charges on the Leidenfrost effect. Previous studies examined the influence of electric interactions on Leidenfrost drops levitating on heated solids [71]. We focus our attention on droplets in Leidenfrost state on a heated liquid pool. The experimental setup was described in Section 3.3.3.

In Section 4.3, we showed that electric charges decrease the surface energy of a droplet. In the first Section of this Chapter (see Section 7.1), we examine the influence of the surface energy decrease on the Leidenfrost droplet behavior. In particular, we study the shape of the droplet and the shape of the liquid bath as a function of the charge induced in the droplet.

In the second Section (see Section 7.2), we study the influence of electric charges on the stability of a Leidenfrost droplet on a liquid pool. We show that Leidenfrost droplets coalesce with the liquid pool at a given radius. Then, we attempt to model the critical radius leading to the extinction of the Leidenfrost effect as a function of the charge induced in the droplet.

7.1 Surface energy of a charged droplet in Leidenfrost state

As showed in Section 4.3, the surface energy γ^* of a charged droplet can be expressed as:

$$\gamma^* = \gamma - \frac{q_\sigma^2 r}{4\epsilon_0} \tag{7.1}$$

where γ is the droplet surface tension, q_σ is the droplet surface charge density, r is the droplet radius and ϵ_0 is the vacuum permittivity. In this Section, we show that this decrease in the surface energy influences the shape of a Leidenfrost droplet on a liquid pool and, as a consequence, the deformation induced by the droplet on the liquid pool.

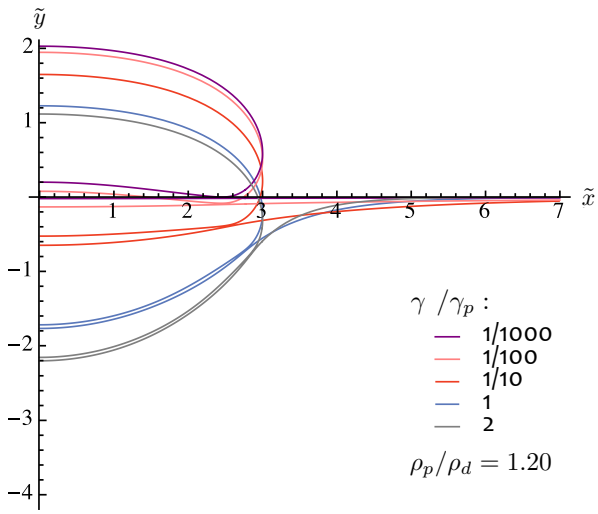

Figure 7.1: Study by Maquet et al [76] on the influence of the ratio of surface tensions γ_d/γ_p on Leidenfrost shapes. The droplet radius $\tilde{r} = 3$ and the density ration $\rho_p/\rho_d = 1.2$ are kept constant.

The Leidenfrost effect on a heated liquid bath has been previously studied by Maquet *et al* [76]. Among other things, they demonstrated that the droplet shape, while levitating on the liquid bath, depends on the droplet radius and surface energy. In the same way, they showed that deformation of the liquid pool due to the levitating droplet also depends on the droplet surface tension. Their theoretical study is shown in Fig. 7.1. The droplet and liquid pool shape are plotted as a function of the non-dimensional coordinates $\tilde{y}$ and $\tilde{x}$. Both coordinates are non-dimensionalized by the capillary length $l_c = \sqrt{\gamma/\rho g}$. They showed that for different ratios between the droplet surface tension γ and the liquid pool surface tension γ_p, the shape of the

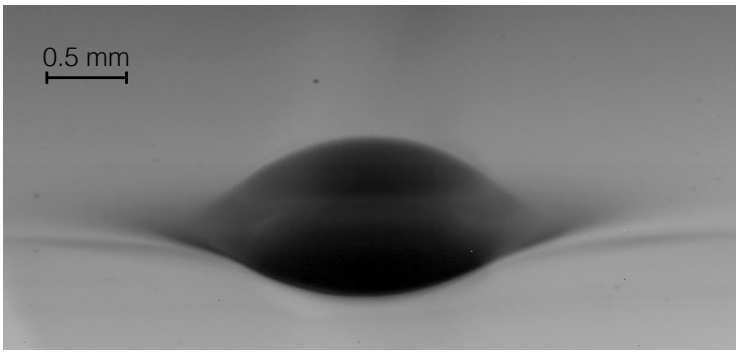

Figure 7.2: Image of the liquid pool deformation induced by the charged droplet. The droplet charge is q= 73 pC. The pool is at T_p = 100 °C while the boiling point of ethanol is T_{sat} = 78 °C. The maximum deformation depth corresponds to approximately 0.25 mm.

droplet and the shape of the liquid pool varies. The droplet radius $\tilde{r} = 3$ and the density ratio $\rho_p/\rho_d = 1.2$ were kept constant. We see in Fig. 7.1 that an increase in the surface tension ratio deepens the liquid pool deformation. On the opposite, the case of a very small surface tension ratio is similar to the case of a Leidenfrost droplet on a solid surface.

In order to compare the theory to measurements, we looked at the shape of the liquid surface as a function of the droplet electric charge. A typical image of the pool deformation due to the levitating droplet is shown in Fig. 7.2. The image is a side view of the droplet took under the surface of the liquid pool. The symmetry of the image is explained by the reflection of the deformation on each side of the liquid surface. Note that the influence of the charge on the droplet shape was not studied. This is explained by the difficulty to precisely measure the droplet shape while it is levitating on a liquid pool.

During the experiments we used a liquid bath composed of silicone oil 100 cSt heated at $T_p = 100$ °C and charged droplets composed of ethanol. The boiling point of ethanol is $T_{\mathrm{sat}} = 78$ °C, which means that the droplet was in Leidenfrost state when levitating on the pool. The temperature of the liquid pool was tracked thanks to a thermocouple positioned at the surface of the liquid pool. The charged droplet generator model A was used to charge droplets. The experiment was carried out with three different configurations: neutral droplets ($q = 0$ pC) and charged droplets (q =73.0 pC or q =110.7 pC). The shape of the liquid surface was obtained by using a high-speed camera (Phantom MIRO 310). The use of a high-speed camera was justified by the need of capturing a focused image of droplets freely moving at the surface of the heated liquid bath.

As explained in Section 3.1.2, the charged droplet generator influences the volume of the generated droplet. As a consequence, the droplet radius decreases with the

	q (pC)	r (mm)	γ^* (mN/m)	l_c (mm)
case 1	0	1.123	22.27	1.767
case 2	73.0	1.099	21.55	1.738
case 3	110.7	1.053	20.38	1.691

Table 7.1: The charge (q), the radius (r), the surface energy (γ^*) and the droplet capillary length (l_c) of the three experimental configurations used to study the influence of the electric charge on the shape of a droplet in Leidenfrost state on a liquid pool. With the increase in charge, the radius and the surface energy decrease.

droplet charge. The charge (q), the radius (r) and the surface energy (γ^*) of each configuration can be found in Tab. 7.1. We observe, as expected, that with the increase of charges induced in the droplet, the droplet radius and surface energy decrease. We were able to reduce the droplet surface energy by a maximum of 10 %.

As shown in Fig. 7.1, Maquet *et al* [76] were able to precisely model the shape of the droplet and the shape of the liquid interface. In order to demonstrate the influence of the charge on the droplet surface energy, we have to compare the liquid pool shape in Fig. 7.2 to their model. The Fig. 7.3 shows the shape of the liquid interface for the three cases studied. The $\tilde{y}$ and $\tilde{x}$ axis correspond respectively to the vertical and horizontal position of the liquid interface. The depth $\tilde{y} = 0$ corresponds to the position of the liquid interface when it is not deformed by the droplet. Both axes are normalized by the capillary length of the droplet $l_c = \sqrt{\gamma/\rho g}$. The value of the capillary length for each case studied is shown in Tab. 7.1. In Fig. 7.3, the green disks correspond to the measurements made from images such as the one in Fig. 7.2. These measurements were carried out just after the release of the charged droplet on the liquid pool. The red curve corresponds to the model from Maquet *et al* [76] only taking into account a radius variation and no surface energy variation. The orange curve corresponds to the model from Maquet *et al* [76] taking into account the influence of the charge on the surface energy and the droplet radius.

We see in Fig. 7.3 that the model correctly fits the experiments. Indeed, the orange curve, which takes into account the influence of the charge on the droplet radius and the droplet surface energy, is in good agreement with the green disks corresponding to the experiment. We only observe a small disagreement between the experiment and the model in the case 3, corresponding to a droplet highly charged. This contrast between the model and the experiment is explained by the difficulty to observe a highly charged droplet in Leidenfrost state on a liquid pool. We noticed during experiments that charged droplets prematurely coalesce with the liquid pool in comparison to neutral droplets. In the case 2, corresponding to a droplet moderately charged, the droplet early coalescence occurs several seconds after being dropped on the liquid pool. As a consequence, it did not affect the shape measurement performed few

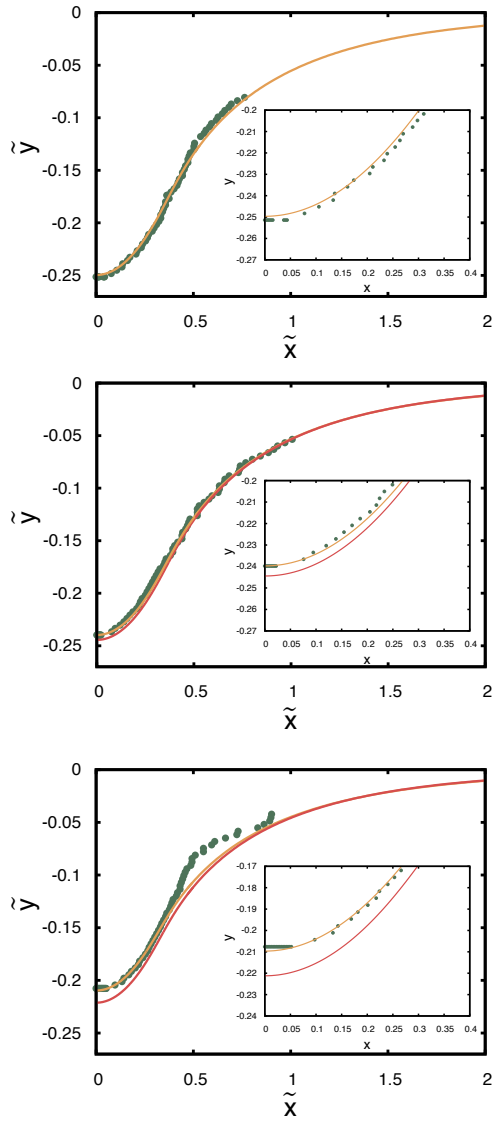

Figure 7.3: Shape of the liquid pool deformed by a charged droplet levitating on its surface via the Leidenfrost effect. The vertical ($\tilde{y}$) and horizontal ($\tilde{x}$) axes are normalized by the capillary length l_c. The green disks correspond to the measurements deduced from images such as Fig. 7.2. The red curve corresponds to the model of Maquet et al taking into account only a radius variation. The orange curve corresponds to the model of Maquet et al taking into account the influence of the charge on the radius and the surface energy density.

seconds after the droplet being dropped off. On the contrary, the case 3 corresponds to a droplet highly charged. In this case, the droplet coalesces with the liquid pool quickly after its drop-off. Therefore, It was difficult to record the droplet shape before its coalescence. Beyond the question of the influence of the charge on the droplet and the liquid interface shape, the question of the charged droplet early coalescence also needs to be addressed. Such a phenomenon is linked to the electric interaction between the droplet and the liquid bath. It will be discussed in the Section 7.2.

Regarding the influence of the charge on the droplet itself, we can affirm that the decrease of the droplet surface energy have to be taken into account in order to fully describe the system. However, the charge only slightly influences the shape of the liquid surface. Indeed, there is not a huge difference between the red curve (taking into account the surface tension corresponding to a neutral droplet) and the orange curve (taking into account the influence of the charge on the surface energy). The weakness of the shape modification is explained by the small change in surface energy density. Indeed, the Tab. 7.1 shows that the charge decreases the surface energy by only 10 percent. This limitation is explained by the difficulty to store a highly charged droplet on the liquid pool.

In conclusion, we showed that the electric charge of a droplet in Leidenfrost state on the liquid pool influences the liquid pool shape. While the influence of the charge on the shape of the liquid surface can be considered as a second order effect, the presence of electric charges also critically changes the behavior of the droplet. As we explained, we observed that the excess of electric charges generates an early coalesce of the droplet with the liquid pool. This significant variation in the droplet behavior is studied in the next Section.

7.2 Charged droplets in Leidenfrost state: Early coalescence

When a neutral droplet is dropped on a liquid pool heated above the droplet boiling temperature, it levitates on its own vapor. Over time, the droplet evaporates and its volume decreases. Once the droplet has reached a critical radius, the droplet no more levitates on its own vapor and coalesces with the liquid bath.

The Leidenfrost extinction for small neutral droplets was also observed by Celestini *et al* [107] for droplet in Leidenfrost state on solid surface. In the case of a solid surface, the droplet takes off at a critical radius. They showed that the Leidenfrost extinction was due to the breakdown of the lubrication regime. The same kind of mechanism should also occur for small droplets in Leidenfrost state on a liquid pool. However, the small critical radius at which the droplet coalesce ($r \approx 0.2$ mm) and the experimental setup makes it difficult to quantitatively measure the phenomenon.

By charging droplets in Leidenfrost state on a liquid pool, we observed that the

critical radius r_c at which the droplet coalesces with the liquid pool increases with the amount of charges induced in the droplet. In the next lines, we describe and attempt to model this observation. Our approach aims for two goals: (i) modeling the critical radius as a function of the droplet charge $r_c(q)$ allows deducing precisely the critical radius for a neutral droplet $r_c(q = 0)$. In other words, our approach allows studying precisely the underlying physics generating the Leidenfrost droplet extinction. (ii) Studying such a system give new insights on the influence of electric charges on the behavior of thin layers.

The droplet coalescence with the liquid bath is shown on the image sequence in Fig. 7.4. Images are separated by 3 ms. The charged droplet ($q = 60$ pC) composed of ethanol coalesces with the liquid bath at a critical radius $r_c = 9$ mm. The liquid pool was composed of silicone oil 20 cSt and heated at a temperature $T_p = 90$ °C.

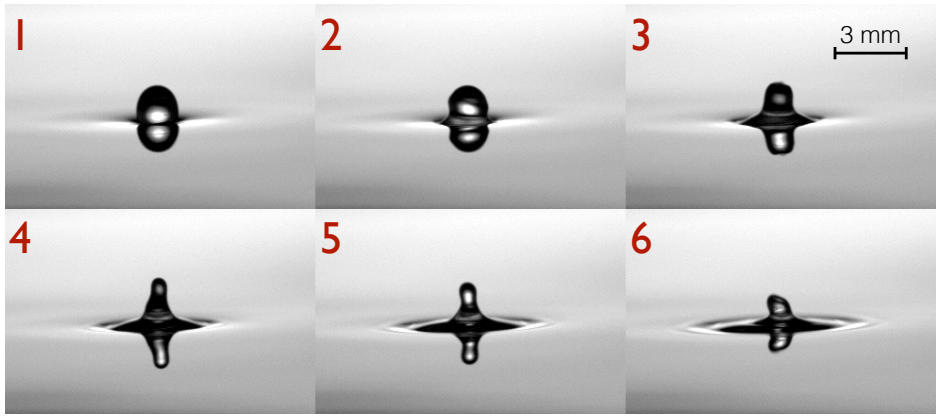

Figure 7.4: Image sequence of the coalescence of a charged droplet with the liquid pool. The images are separated by 3 ms. The droplet is composed of ethanol and has a charge of $q = 60$ pC. The liquid pool is heated at 90 °C.

In order to quantitatively describe the phenomenon, we studied the critical radius r_c at which the droplet coalesces with the liquid bath as a function of the charge induced in the droplet. Experiments were performed with droplets composed of ethanol and droplets composed of HFE. The ethanol and the HFE-7100 were chosen for their ability to easily levitate in Leidenfrost state and for their different properties. Indeed, the ethanol and the HFE-7100 possess quite different surface tensions, densities and thermal properties. Therefore, the influence of these parameters is highlighted. Contrarily to the ethanol, the HFE-7100 is less commonly used. The diminutive HFE stands for Hydrofluoroether. It is a complex organic solvent commonly used as a refrigerant or heat-transfer fluid. The surface tension γ, density ρ and temperature of boiling T_b are reported for both liquids in Tab. 7.2.

During the experiments, each charged droplet was generated by the charged droplet

	γ (mN/m)	ρ (kg/m^3)	T_b (°C)
Ethanol	22.27	789	78
HFE	13.6	1520	61

Table 7.2: Surface tension γ, density ρ and boiling temperature T_b of ethanol and HFE. The HFE has a smaller surface tension than the ethanol, but a larger density.

generator model A. The droplet radius before its coalescence with the liquid bath was measured thanks to a high-speed camera (Phantom Miro M-310). The initial droplet charge was known by the calibration of the charged droplet generator via a Faraday cup. The liquid pool was composed of silicone oil 20 cSt. The temperature of the liquid pool was measured by using a thermocouple dived in the silicone oil and positioned near the surface of the liquid pool. We performed three sets of experiments: (i) Ethanol droplets on a liquid pool at $T_p = 90$ °C, (ii) Ethanol droplets on a liquid pool at $T_p = 150$ °C and (iii) HFE droplets on a liquid pool at $T_p = 100$ °C.

The result of the measurements is shown in Fig. 7.5. The graph shows the critical radius r_c at which a droplet coalesces with the liquid pool as a function of its initial charge. The red crosses correspond to ethanol droplets in Leidenfrost state on a pool at a temperature $T_p = 90$ °C. The orange triangles corresponds to ethanol droplets in Leidenfrost state on a pool at $T_p = 150$ °C. The green disks corresponds to HFE-7100 droplets in Leidenfrost state on a pool at $T_p = 100$ °C. We observed that neutral droplets coalesce with the liquid bath at a critical radius between 0.1 and 0.2 mm. Then, the critical radius of coalescence linearly increases with the charge induced in the droplet. In the next lines, we attempt to model these observations.

In Fig. 7.4, the images were taken at the time when the droplet begins to coalesce with the liquid bath. The droplet destabilization begins at the bottom of the droplet. These images correspond to classic coalescence between a droplet and a liquid pool. From this observation, we conclude that the early coalescence of the charged droplet is due to the burst of the vapor layer between the droplet and the liquid pool. Two phenomena could explain the destabilization of the vapor layer, either the charged droplet destabilizes itself or the vapor layer becomes too thin to hold. These two scenarios are examined in the next lines.

The first interpretation would correspond to a Coulomb explosion. As expressed in the Section 2.2.1, the critical radius for a Coulomb explosion to occur, for a spherical droplet, corresponds to:

$$r_c = \left(\frac{q^2}{64\pi^2 \gamma \epsilon_0} \right)^{1/3} \tag{7.2}$$

The equation indicates a non-linear dependence of the radius with the charge, which is in disagreement with the observations. However, a droplet in Leidenfrost state on the liquid bath is slightly flattened, which could affect Eq. 7.2. In order

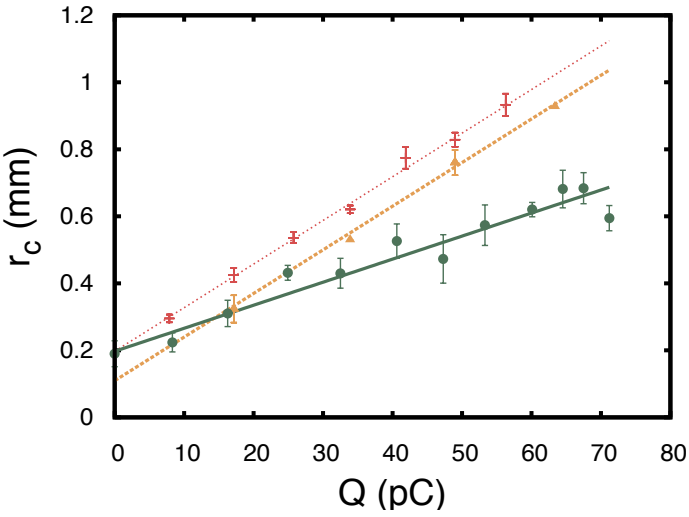

Figure 7.5: Critical radius at which a droplet coalesces with the liquid pool as a function of the droplet charge. The red crosses and orange triangles correspond to ethanol droplets on a liquid bath at a temperature of respectively $T_p = 90\,^\circ C$ and $T_p = 150\,^\circ C$. The green disks correspond to HFE-7100 droplets on a liquid bath at temperature $T_p = 100\,^\circ C$.

to force the linear dependence of the radius with the charge, we can perform a scale analysis of the system. If we suppose that the critical radius depends on the same variables as expressed in Eq. 7.2, we have:

$$r_c = \rho^\alpha g^\beta \epsilon_0^\delta \gamma^\eta q^1 \tag{7.3}$$

where α, β, δ and η are dimensionless numbers that need to be balanced in order to respect the units of each parameter. By applying the well-known Buckingham π theorem, we obtain:

$$r_c = (\rho g)^{1/4} \epsilon_0^{-1/2} \gamma^{-3/4} q \tag{7.4}$$

The Eq. 7.4 leads to a linear dependence between the charge and the radius. It also indicates that the critical radius decreases with the surface tension γ and increase with the density ρ. However, it is not what is experimentally observed. Indeed, HFE has a larger density and a smaller surface tension (see Tab. 7.2), which means that the slope of the HFE should be larger than the slope of the ethanol. In Fig. 7.5, the opposite is observed. As a consequence, the explanation of the early coalesce has to be found somewhere else.

If the droplet does not destabilize, the disruption of the vapor layer between the droplet and the liquid pool should be the reason why we observe the early coalescence. The vapor layer is schematized in Fig. 7.6. In the case of neutral droplet, the droplet

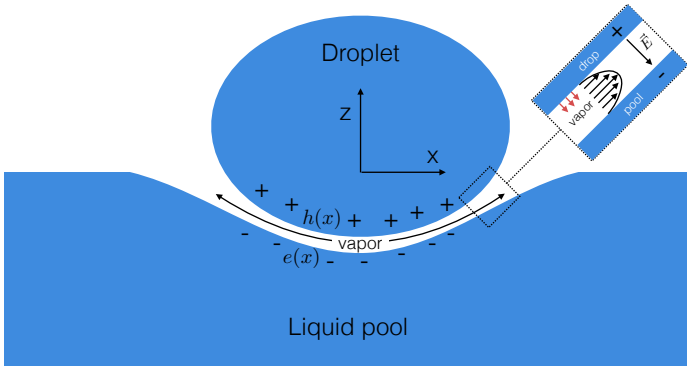

Figure 7.6: Schema of the charged droplet levitating on the heated liquid bath. To model the early coalescence of the droplet, we suppose that the electric charges in the droplet induce charge migration in the pool. The vapor layer is maintained by the equilibrium between, on one hand, the droplet evaporation and, on the other hand, the air lubrication due to the droplet weight, the droplet Laplace pressure and the electric attraction between the droplet and the pool.

levitation is explained by the equilibrium between the droplet vapor production and the vapor flux escaping from the zone between the droplet and the liquid surface. This vapor flux is controlled by the droplet weight and the droplet Laplace pressure. Given the electric field produced by a charged droplet, it is plausible to suppose that free charges in the pool are attracted toward the levitating droplet (negative charges are attracted toward the positively charged droplet in Fig. 7.6). Therefore, the presence of electric charges in the droplet adds an electric attraction between the droplet and the liquid pool. This electric attraction induces the thinning of the vapor layer and, eventually, its destabilization. This qualitative model could explain the early coalescence of a charged droplet.

In order to confirm this first draft, we examined models describing Leidenfrost droplets levitating on a liquid pool. To our knowledge, there is no simple model that describes the vapor layer of a droplet in Leidenfrost state on a liquid pool. Maquet *et al* [76] described in detail the vapor layer by studying the vapor mass conservation under the lubrication hypothesis. They supposed that the thickness of the vapor film is governed by the equilibrium between the local evaporation flux at the bottom droplet interface and a Stokes flow induced by the balance of forces normal to the

droplet surface. The equilibrium between both fluxes is expressed by:

$$\vec{\nabla} \cdot \vec{q_v} - \frac{\mathcal{J}}{\rho_v} = 0 \tag{7.5}$$

where $\vec{q_v}$ is the volumetric vapor flux, $\mathcal{J}$ is the evaporation flux and ρ_v is the vapor density. In the case of a neutral droplet, the excess of pressure in the air layer governs the volumetric vapor flux. Namely, we have:

$$\vec{q_v} = -\frac{\vec{\nabla} P_v}{12\mu_v}(h-e)^3 \tag{7.6}$$

where μ_v is the vapor dynamic viscosity, P_v is the excess pressure in the air layer, h is the vertical coordinate of the bottom of the droplet and e is the vertical coordinate of the liquid pool surface. Law [82] demonstrated that the charged droplet evaporation is influenced by its electric charges only for very small droplet radii ($r < 0.1$ μm). As a consequence, the only parameters influenced by the electric charges are the droplet surface tension and the balance of forces normal to the droplet surface. In order to resolve the Eq. 7.5, the first step is to take into account the adjusted droplet surface tension. The second step is to add to the pressure of a neutral droplet the electric pressure applied by the droplet on the volumetric vapor flux. For a neutral droplet, the excess pressure is due to the droplet Laplace and hydrostatic pressures:

$$P_v = \gamma\kappa_{\text{top}} + \rho g(z_{\text{top}} - h) - \gamma\kappa \tag{7.7}$$

where κ is the curvature of the droplet surface, κ_{top} is the curvature at the top of the drop, z_{top} corresponds to the vertical coordinate of the top of the droplet and h is the vertical coordinate of the bottom of the droplet.

For a charged droplet, the electric attraction between the droplet and the liquid pool has to be taken into account. In a first approximation, we can suppose that the attraction between the droplet surface and the liquid pool surface corresponds to a planar capacitor. In doing so, the excess of pressure due to electric attraction writes:

$$P_e = \frac{\epsilon_0}{2}\left(\frac{q_\sigma}{\epsilon}\right)^2 \tag{7.8}$$

where σ is the surface charge density and $\epsilon = \epsilon_r\epsilon_0$ is the relative permittivity. Once the Stokes flow (Eq 7.6) is calculated with both pressure ($P_v + P_e$), we can deduce the profile of the thickness of the vapor layer.

Once the profile defined from Eq. 7.5, we can investigate the critical thickness e_c as a function of the droplet radius and its charge. By computing the critical thickness e_c for each set of critical radius r_c and charge q measured, we could verify if the droplet coalescence is due to the disruption of the air layer.

In conclusion, we have seen here that the charge may have critical effects on the droplet behavior. In this case, the presence of electric charges induces an early coalescence of the droplet with the liquid pool. This early coalescence could be explained by the electric attraction between the charged droplet and the liquid bath. *A priori*, this attraction generates a thinning of the vapor layer between the droplet and the liquid pool. As a consequence, the droplet tends to coalesce with the liquid bath at bigger volumes.

8

General conclusion and perspectives

Conclusion

This thesis is a fundamental study of the influence of electric charges on millimetric isolated droplets. We investigated the intrinsic behavior of charged droplets as well as their interaction with electric fields.

In Chapter 1, we defined our subject: electrically charged droplets with a millimetric size. After this definition, we specified the environment in which this study is performed: the charged droplet is in contact only with gas.

In Chapter 2, we introduced the previous research necessary to understand the ins and outs of our study. We firstly described the different mechanisms generating an excess of electric charges in a droplet. Then, we examined previous research that studied how the charge influences the behavior of the droplet. We summarized the past discoveries made on the frequency shift, the Coulomb explosion and the motion of a charged droplet in an electric field. In the last Section of this Chapter, we described unresolved questions about charged droplets and explained the strategy adopted along this thesis. In particular, we showed that the lack of studies on millimetric droplets is due to the difficult to store them while avoiding charge leakage. In response to this issue, we chose to focus our attention on millimetric droplets in interaction with three different storage systems: the microgravity, the vibrating bath and the Leidenfrost effect.

In Chapter 3, we described the tools developed to study electrically charged droplets. We explained how the charge migration process can be easily used to induce a reproducible excess of charges inside droplets. A first model described how

the amount of charges induced in the droplet could be predicted and quantified. The design of three charged droplet generators was described according to their advantages and disadvantages. Once the charge mechanism described, we reported how the droplet charge was measured. Given the reproducibility of the charged droplet generators, we simply had to calibrate them by the use of a Faraday cup. We then described three storage methods that avoid the droplet contact with a solid or a fluid: the microgravity, the vibrating bath and the Leidenfrost effect. We firstly showed how it is possible to generate microgravity conditions by the use of parabolic flights. Secondly, we explained how the delayed coalescence could be exploited to store a droplet on a vibrating liquid bath. Thirdly, we explained how the Leidenfrost effect allowed us storing droplet on their own vapor. We compared each storing systems according to their own advantages. While the bouncing droplet is the more consistent storage mode, it forces the droplet motion in the vertical direction. On the opposite, the microgravity is reduced in time but does not influence by any way the droplet displacement. Finally, the Leidenfrost effect allows studying the influence of electric charges on two liquid surfaces near each other.

In the Chapter 4, we examined the influence of the electric charge on the droplet itself. We began by charging liquids with various chemical compositions. We showed that the important variable to take into account is the time to generate the droplet compared to the charge migration time. The charge migration time was found to depend on the liquid permittivity and conductivity. Once we understood how the charges are induced in the droplet, it was essential to understand how the charge could leave the droplet. We firstly summarized the previous models on charges leakage. We then brought for the first time measurements of the charge leakage from a millimetric charged droplet. We demonstrated that the droplet charge leakage could be modeled by the charge leakage of a capacitor. In a third Section, we investigated the influence of the charge on the surface energy density. From the well-known description by Lord Rayleigh of the charged droplet oscillation frequency, we studied the link between the electric charge and the droplet surface energy.

In the Chapter 5, we were interested in the interaction between two electrically charged droplets. We took advantage of the microgravity conditions to study the interaction between two charged droplets launched one in front of the other. The experiments showed that the coulomb interaction is enough to describe the trajectory of two charged droplets interacting with each other. During this set of experiments, impacts between droplets were also observed. We elaborated a sketch of the collision diagram between two charged droplets and compared it to the collision diagram of two neutral droplets. We concluded from this comparison that the droplet charge affects the possibility of a direct impact between droplets but also the nature of the droplet impact.

In the Chapter 6, we studied the displacement of a charged droplet on a vibrating bath. In a first experiment, we studied the horizontal motion of droplets bouncing

on a vibrating bath and influenced by a homogeneous electric field. We differentiated two sorts of droplet displacements. For small droplets influenced by a significant electric force, the droplet accelerates in the direction of its motion. For large droplets influenced by small electric force, we observed a droplet motion with a constant speed. This constant speed motion was explained by the interaction between the droplet and the liquid bath. Indeed, at the scale of one bounce, the droplet endures a go-stop horizontal motion. We developed a model that predicts the transition from a motion with a constant speed to an accelerated motion. Moreover, the experiment turned out to be a good way to micro-manipulate droplets by avoiding droplet pollution. In a second experiment, we studied the repulsion between two charged droplets of the same sign of charge stored on a vibrating liquid bath. We observed a weak attraction between droplets that could be connected to the cheerios effect. The measurements of the distance between droplets over time showed that droplets tend to stay at an equilibrium distance. The modeling of the motion of the bouncing droplet at the scale of one bounce allowed us to explain the observation of an equilibrium distance between droplets.

In the Chapter 7, we investigated the behavior of a charged droplet in Leidenfrost state on a liquid pool. In a first set of experiments, we studied the influence of the electric charge on the droplet shape. In particular, we linked the droplet surface energy decrease induced by the electric charge to the shape of the droplet and the shape of the liquid pool. In a second set of experiments, we examined the coalescence of Leidenfrost droplets with the liquid pool. We measured the increase of the critical radius at which the droplet coalesces with the liquid pool as a function of the droplet charge. Then, we attempted to explain the droplet coalescence with the liquid pool by looking at the vapor layer between the droplet and the liquid pool. Specifically, we added to the classic lubrication model an attraction between the Leidenfrost droplet and the liquid pool due to the droplet electric charges.

Perspectives

Naturally research topics are never closed subjects. Every experiment and every model always need to be improved. Of course, some subjects appear to be more important to study at specific times, depending on the general scientific interest or on the specific questions at which it could answer. In this Section, we indicate what could be studied in the extension of this thesis. This Section is addressed to anyone who wish to bring new answers to the study of charged drops.

Adding data to the collision diagram of charged droplets

Going back to the Chapter 5, we believe that the study of the impact between droplets needs to be extended. Indeed, the experiment performed in microgravity gave new insights on the influence of the charge on the collision between droplets. However, the microgravity sessions only allowed us exploring a part of the collision diagram comprised between We = 25 and We = 60. We believe that the rest of the diagram needs to be explored to deduce more general conclusions on the influence of the electric charge on the impact between droplets. In particular, the part of the diagram located below We = 25 needs to be explored in detail. Indeed, our study of the charged droplet trajectories demonstrated that the zone of low speed corresponds to the part of the diagram where the electric charges have the most important influence on the droplet motion. Moreover, the zone called bouncing zone, which corresponds to the bouncing between neutral droplets also needs to be studied in more details. One of our measurements showed that the bouncing between droplets is affected by their charges. Of course, one data is not enough to draw conclusion. However, given previous studies on the bouncing between droplets [65], this part of the diagram seems critically influenced by the electric charges and, as a consequence, needs to be studied in more details.

The part of the collision diagram that still needs to be explored has been highlighted by the hatched area in Fig. 8.1. Futures experiments may be performed in two different ways. Given the difficulty to perform experiments in microgravity configurations, a first step is to develop the same experiment in a classic laboratory. Even if we believe that aerodynamic forces applied on free falling droplets affect their collision, this phenomenon still has to be quantified. This second setup would allow explaining how important is the microgravity to study the influence of the electric charge on the droplet collision. Moreover, the laboratory being a more friendly environment, experiments could be performed with more precision and a more significant part of the diagram could be explored. Secondly, the microgravity setup could still be improved. By controlling in a more precise way the ejection of charged droplets in microgravity, it would be easier to accumulate data on the collision diagram. In the end, those two ways to accumulate new data would allow comparing in a deeper way our experiments to measurements made on thunderclouds.

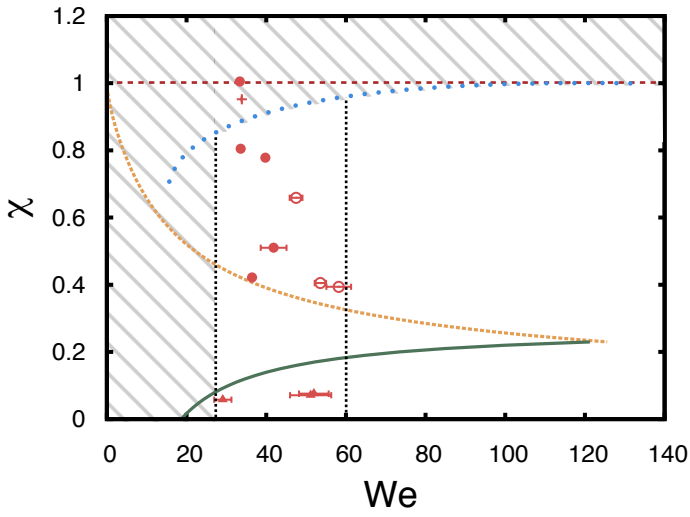

Figure 8.1: Collision diagram for the impact between two electrically charged droplets. The collision parameter χ is a function of the angle of collision between droplets while the Weber number We depends on the droplets relative speed and their size. The hatched area corresponds the zone of the diagram that still needs to be explored.

A step forward the micro-manipulation of electrically charged droplets

We showed in Chapter 6 that charged droplet bouncing on a vibrating bath could be manipulated by an external electric field. We modeled the droplet motion as a function of the electric field magnitude and the droplet volume. Furthermore, we demonstrated that charged droplets could be manipulated on the two dimensions of the liquid bath. Our study corresponds to the image on the left of the Fig. 8.2.

Naturally, this first study is not sufficient to proclaim that it is possible to perform complex lab-on-a-chip manipulations with droplets on vibrating bath. The system still needs to be improved. In particular, futures studies have to focus on optimizing the setup configuration to limit the droplet coalescence with the liquid bath and precisely control the droplet horizontal speed. This will be done by performing further experiments and improving the basic model developed in the Section 6.1.4. Furthermore, the interaction between several droplets and an external electric field has to be studied. These futures studies would allow understanding how to produce mixing between bouncing droplets. The study performed in Section 6.2 is a first answer to the question, but further studies on the droplet mixing are still needed.

In this sort of microfluidic system, the preservation of the droplet charge is also primordial. A first study in Section 4.2 gave a first answer to the question. However, we think the droplet charge leakage still needs to be studied as a function of the gas surrounding the droplet, especially as a function of the relative humidity.

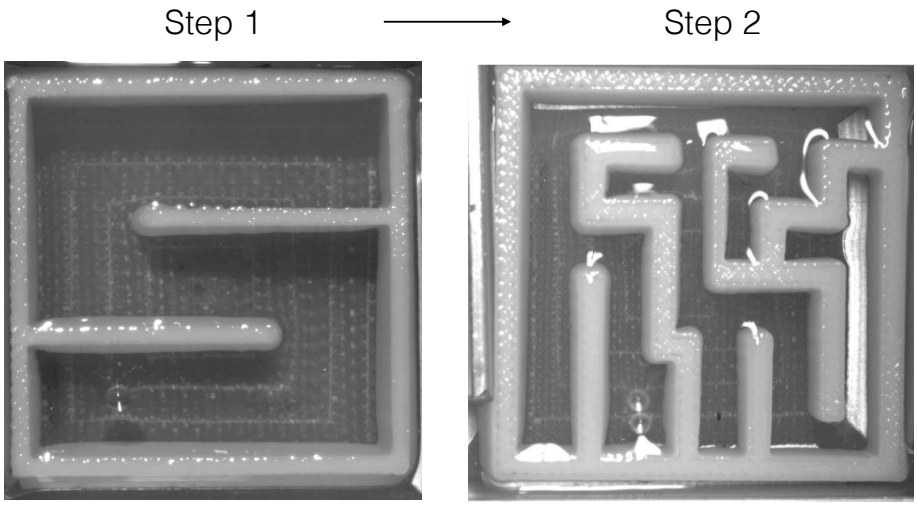

Figure 8.2: Images of the manipulation of charged droplets on a vibrating bath. Both images were taken from the top of the experiment. The future goal is to go from a basic manipulation (such as the image on the left) to a more complex and precise control of the droplet displacement (such as the image on the right).

A choice needs also to be made concerning the way to precisely control the droplet motion. Indeed, the droplet displacement could be controlled via the precise management of the electric field, but it could also be managed via the use of walls at the surface of the liquid. This last possibility is exhibited on the right image in Fig. 8.2. In this configuration, the droplet is less free to move on the liquid bath, but specific operation may be easier to perform.

Electrically charged walkers

In our study of charged droplets bouncing on a vibrating bath, we focused our attention on millimetric droplets bouncing on a viscous liquid bath at their reasoning frequency. However, it exists numerous other configurations of the system that lead themselves to specific droplet bouncing modes and interactions with the liquid bath. One of these specific behaviors is the walker.

In the world of bouncing droplets, walkers are small droplets ($r \approx 0.5$ mm) bouncing at half the forcing frequency on a low viscous silicone oil ($\mu \approx 20$ cSt) near the Faraday threshold of the oscillating liquid bath. When these conditions are gathered, the droplet moves of itself on the liquid bath. More precisely, the droplet generates the propagation of a wave on the liquid bath during its bouncing because of the proximity with the Faraday threshold. As a consequence, the droplet bounces on the slope of the wave emitted at its previous bouncing, which generates a horizontal motion.

This bouncing mode raised the interest of several research groups and led to several publications [61, 64]. One of the reasons of this enthusiasm is the parallel that can be made between the walker (a particle moving on its own wave) and the quantum physics. The addition of electric charges in walkers could provide new insights on the experiment. The electric charge could, for example, allow to control the droplet motion on its own wave in order to adjust the position of its bouncing on the wave. It could also be used as a tool to reproduce quantum experiments involving electric fields.

Naturally, the study of charged walkers requires developing specific tools to generate them and control them. During this thesis, we already developed a charged droplet generator that can produce walkers. The charged walker generator was called charged droplet generator model C in the Section 3.1.1. This charged droplet generator is a mixing between a neutral walker generator (described, for example, in [49]) and a charged droplet generator. It emits small droplets thanks to a piezoelectric crystal emitting droplets from a small hole in a metallic plate. A voltage between two metallic plates allows inducing charges in the ejected droplet. Such a charged droplet generator was found to create walkers properly. However, it still needs adjustments in order to eject droplets in an optimized way. Currently, the main limitation comes from the high speed of droplet ejection due to the electric force applied on the ejected droplet.

Note that the walkers have also been generated by a second method. By diving a charged metallic rod in the liquid oil and removing it quickly, we were able to generate walkers with an excess of electric charges. This method still needs to be quantified.

Even if a walker and the setup involving its creation are simple to describe, its experimental management may be difficult to master. As a consequence, we just had the occasion to perform preliminary experiments. We looked at the motion of a charged walker in an external electric field. The difficulty of the experiment is to produce a homogeneous electric field (to avoid dielectrophoresis) on a large scale (to measure the accelerations/decelerations on several bounces). As a consequence, we only accumulated data on droplet motion in non-homogenous electric fields. An example of a typical experiment is shown in Fig. 8.3.

We examined the motion of a walker between two charged electrodes. An electric field influenced the walker along its motion. The typical motion in the x and y directions (indicated in Fig. 8.3) are shown in Fig. 8.4. At this time, no conclusions have been drawn from these experiments, but we believe that the influence of the electric field on the walker displacement could be deduced from these measurements.

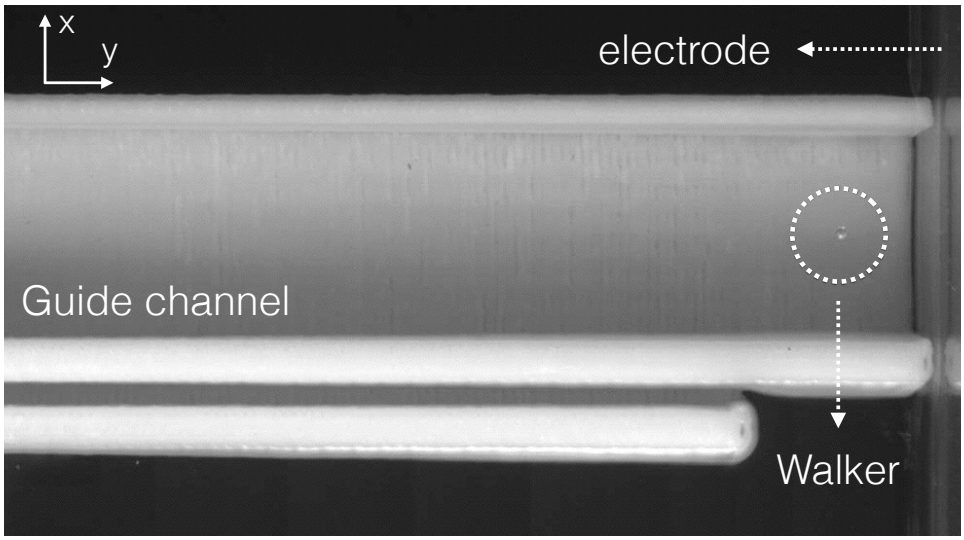

Figure 8.3: Image of the study of the motion of a walker. The image was taken from the top of the experiment. Two walls that pop out of the liquid bath guide the walker motion. The walker stored between the two walls is influenced by an electric field produced by two electrodes situated on each side of the liquid bath.

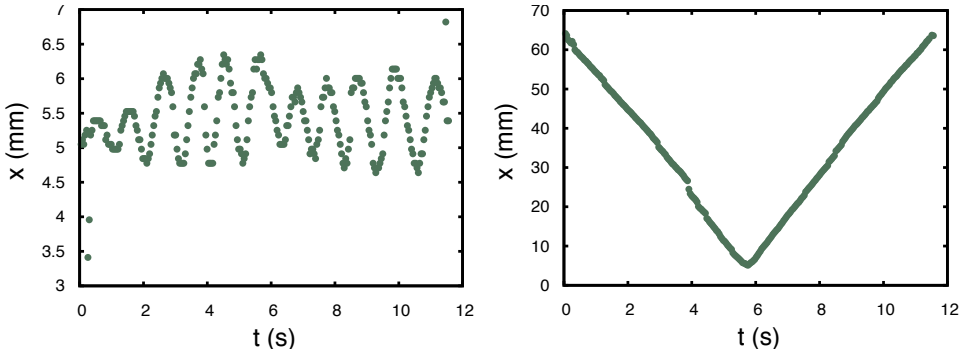

Figure 8.4: Displacement of a walker influenced by an external electric field over time. The graph on the left corresponds to its displacement along the direction x while the graph on the right corresponds to its displacement along the direction y.

A

Delayed coalescence of charged droplets

As explained in the Section 3.3.2, when a droplet falls on a liquid bath, it takes some times for the air layer between both liquids to drain out. The phenomenon is named delayed coalescence. The drainage of the air layer is due to the pressure applied by the droplet on the air cornered between the liquid interface and the droplet. Generally, electric charges, possibly influenced by electric fields, are found to increase the coalescence rate between liquid interfaces [109–111]. In Chapter 5, we also observed that electric charges in droplets can avoid the bouncing between impacting droplets. Recently, Ristenpart *et al* [65] showed that a charged droplet influenced by a significant electric field can contact a liquid interface without coalescing. To our knowledge, the study of Ristenpart *et al* corresponds to the only experimental setup in which electric charges in droplets are found to reduce the coalescence phenomenon. In the following experiment, we give an insight on how an external electric force applied on the droplet may further delay the droplet coalescence by reducing the pressure on the air layer.

The experiment is depicted in Fig. A.1. During one experiment, the charged droplet generator model A dropped off one droplet on a steady liquid bath. The liquid bath and the bottom electrode of the charged droplet generator were separated by a distance l =15 mm. The top electrode of the charged droplet generator was connected to an electrode dived in the liquid bath. The droplet and the liquid bath were composed of silicone oil 5 cSt with an addition of 1 percent of ethanol in order to insure the charge migration. Once dropped off, the droplet remained at the surface of the liquid bath until the air layer between both liquids interfaces was drained out. Two experimental configurations were studied.

In a first experiment, all the electrodes of the setup were connected to Earth. As a

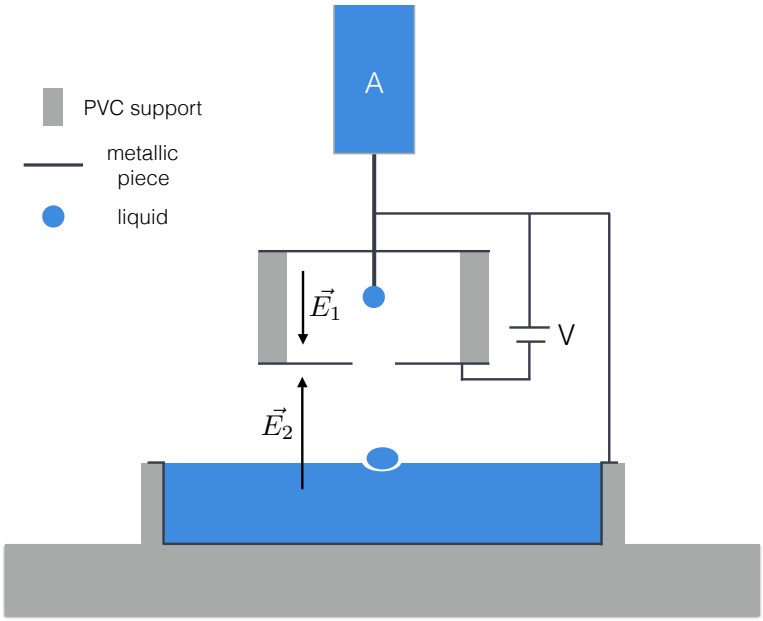

Figure A.1: Schema of the experimental setup. The charged droplet generator model A dropped off charged droplets on the steady liquid bath. The electric field induced between the liquid bath and the bottom part of the charged droplet generator allowed exerting an electric force F_e on the charged droplet.

consequence, the droplet remained neutral while being created by the charged droplet generator model A. Moreover, once dropped on the liquid bath, the droplet was not influenced by any external electric fields. In short, we studied the delayed coalesce of a neutral droplet on a liquid bath.

In a second experiment, A voltage $V = 3500$ V was induced between both electrodes of the charged droplet generator. As a consequence, the electric field $\vec{E}_1$ induced an excess of electric charges in the droplet. Moreover, given the connection between the charged droplet generator and the liquid bath, the charged droplet was influenced by an external electric field $\vec{E}_2$. The voltage polarization imposed an electric force on the charged droplet that was opposed to the gravity.

In both experiments, once the droplets were dropped on the surface of the liquid bath, their lifetimes before a coalescence with the liquid bath were measured. The Fig. A.2 is a picture of the delayed coalescence of a charged droplet on the liquid bath. The droplet remains at the same position until coalescing with the liquid bath. We observe that the droplet only slightly deforms the liquid bath.

In practice, we observed a large distribution of droplet lifetimes. Indeed, droplets, neutral or charged, may live on the liquid bath from only one second until several seconds before coalescing. As a consequence, the standard deviation is generally as large

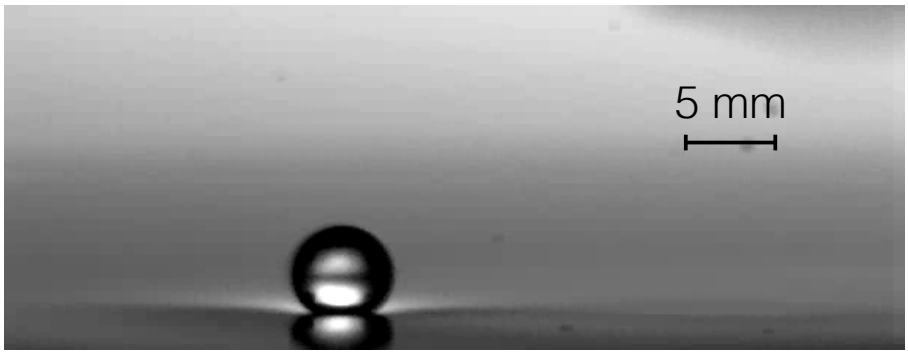

Figure A.2: Image of a typical experiment performed on the delayed coalescence of charged droplets influenced by an external electric field. The charged droplet only slightly deforms the liquid interface.

as the average droplet lifetime. In order to better report such a phenomenon, more precise statistical tools are generally used. In particular, the cumulative distribution function allows deducing the statistical distribution of a set of measures.

The cumulative distribution function $F_X(x)$ of a random variable X corresponds to the probability that X takes a value less than or equal to x, which is expressed as:

$$F_X(x) = P(X \leq x) \tag{A.1}$$

where $P(X \leq x)$ is the probability that the random variable X takes a value less than or equal to x. In practice, the cumulative distribution function is calculated as the following. First, the lifetime measurements t are ordered from the smaller to the larger. In this way, the smaller lifetime is named t_1 and the larger lifetime is named t_f. Then, the experimental cumulative distribution function at a time t_x is calculated by adding the lifetime measurements until the time t_x and normalizing the result by the addition of all the measured lifetimes:

$$F_X(t_x) = \frac{\sum_{i=1}^{t_x} t_i}{\sum_{i=1}^{t_f} t_i} \tag{A.2}$$

In Fig. A.3, the cumulative distribution function is presented for neutral droplets (red crosses) and charged droplets (green disks). We observe that charged droplets influenced by an external electric field possess a larger lifetime. To quantitatively describe this observation, the measured cumulative distribution function can be fitted by a continuous probability distribution. The Weibull distribution is commonly used to describe aging processes such as the delayed coalescence. The probability density

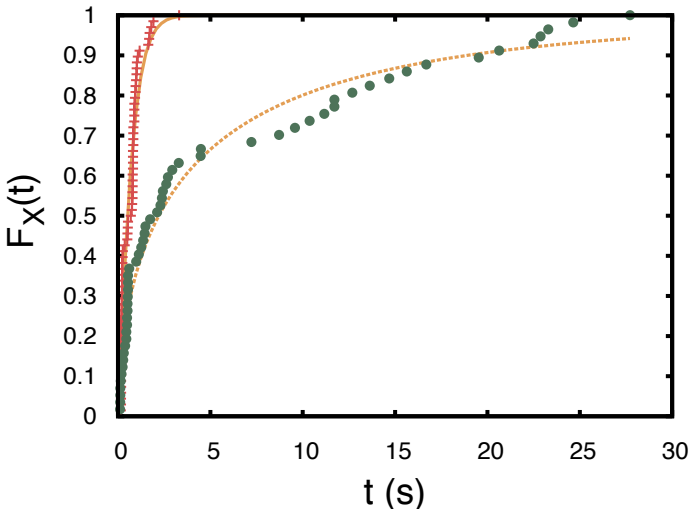

Figure A.3: Cumulative distribution functions $F_X(t)$ of the droplet lifetime on the liquid bath. The lifetime increases for charged droplets influenced by an external electric field compare to neutral droplets non-influenced by external electric fields. Both measurement was fitted by Eq. A.4.

function of a Weibull distribution is expressed by:

$$f(x;\lambda,k) = \begin{cases} \frac{k}{\lambda}\left(\frac{x}{\lambda}\right)^{k-1} e^{-(x/\lambda)^k} & x \geq 0, \\ 0 & x < 0, \end{cases} \tag{A.3}$$

where $k > 0$ is the shape parameter and $\lambda > 0$ is the scale parameter of the distribution. The cumulative distribution function of the Weibull function corresponds to:

$$F(x;k,\lambda) = 1 - e^{-(x/\lambda)^k} \tag{A.4}$$

Such a distribution generally describes a time to failure. If $k < 1$, the failure rate decreases over time. On the contrary, if $k > 1$ the failure rate increases with time. The particular case where $k = 1$ corresponds to a constant failure rate over time. In the case of droplet delayed coalescence, the failure rate is commonly supposed to increase with time, leading to Weibull distributions with $k > 1$. The average failure time of a Weibull distribution can be calculated via the following formula:

$$\mu = \lambda\Gamma(1 + 1/k). \tag{A.5}$$

where Γ is the Gamma function $\Gamma(t) = \int_0^\infty x^{t-1}e^{-x}\,dx$. In Fig. A.3, we fitted the measurements with Eq. 4.16. In Tab. A.1, we reported the fitted variables k and λ and the mean droplet lifetime μ calculated from the Weibull distribution. We observe

	k	λ	μ
$V = 0$ V	1.15	0.72	0.67 s
$V = 3500$ V	0.55	4.2	6.6 s

Table A.1: Fitting parameters and means of the Weibull distribution described by Eq. 4.16 and A.5.

that the charged droplet influenced by an external electric field has an average lifetime ten times greater than the neutral droplet.

The average lifetime calculated from the Weibull distribution confirms the increase of the droplet lifetime for charged droplets influenced by an external electric field. Such an experiment demonstrates that the external electric force applied on the droplet can be used to reduce the drainage of an air layer between two liquid interfaces. Unfortunately, our conclusions cannot go further than this observation. Indeed, we were not able to model the electric field $\vec{E}_2$ induced between the bottom electrode of the charged droplet generator and the liquid bath. Because of the hole in the bottom electrode of the charged droplet generator and the influence of the top electrode, the electric field $\vec{E}_2$ could not be reduced to a simple expression. As a consequence, the force applied on the charged droplet has to be modeled by simulations.

Rather than quantitatively describe the observations, we can elaborate an explanation of the discrepancy between the behavior of a charged Leidenfrost droplet and the present experiment. Indeed, in the case of a charged droplet in Leidenfrost state on a liquid bath, we observed a decrease of the droplet lifetime with the droplet electric charge (see Section 7.2). On the contrary, the present experiment shows an increase of the lifetime in the case of charged droplets. Naturally, the difference between both experiments resides in the presence of an external electric field. Our reasoning is schematized in Fig. A.4. In the case of the Leidenfrost droplet, the electric charges only generate an additional pressure on the vapor layer between the droplet and the liquid bath. In the present experiment, the external electric field generates a volumetric force on the droplet that is opposed to the droplet weight. Moreover, the charges inside the droplet migrate toward the top of the droplet because of the electric field. As a consequence, the droplet pressure on the air layer is reduced.

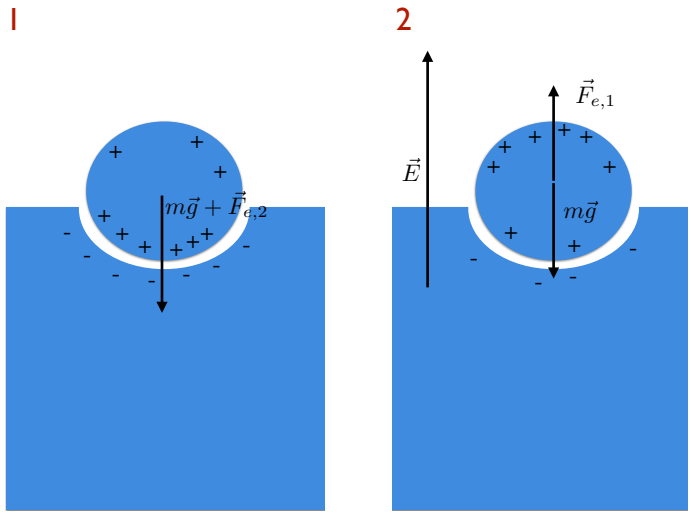

Figure A.4: Schema of the difference between a charged Leidenfrost droplet (1) and the delayed coalescence of a charged droplet influenced by a horizontal electric field (2). In the first case, the electric charges reduce the droplet lifetime. In the second case, the electric charges increase the droplet lifetime.

References

[1] E. P. Krider, *Benjamin Franklin and Lightning Rod*, Phys Today, **59**, 42 (2006).

[2] F. Leblanc, K.L. Aplin, Y. Yair, R.G. Harrison, J.P. Lebreton, and M. Blanc, *Planetary Atmospheric Electricity*, Space Sci. Rev. **137**, 1 (2008).

[3] A. Khain, V. Arkhipov, and M. Pinsky, *Rain Enhancement and Fog Elimination by Seeding with Charged Droplets. Part I: Theory and Numerical Simulations*, AMS **43**, 1513 (2004).

[4] M. Stolzenburg, and T. C. Marshall, *Charge Structure and Dynamics in Thunderstorms*, Space Sci Rev **137**, 355 (2008).

[5] K. V. Bread, H. T. Ochs, and S. Liu, *Collision between Small Precipitation Drops. Part III: Laboratory Measurements at Reduced Pressure*, AMS **58**, 13995 (2001).

[6] S. Chauzy, and S. Despiau, *Rainfall Rate and Electric Charge and Charge of Raindrops of Spring Showers*, AMS **37**, 1619 (1980).

[7] P. Lenard, *Über der Electrizität der Wasserfälle*, Ann. Phys. **46**, 584 (1892).

[8] D. C. Blanchard, *Electrically charged drops from bubbles in sea water and their meteorological significance*, J. Meteor **15**, 383 (1958).

[9] D. C. Blanchard, *Flow of Electrical Current From World Ocean to Atmosphere*, J. Geophys. Res. **90**, 9147 (1985).

[10] S. E. Law, *Agricultural electrostatic spray application: a review of significant research and development during the 20th century*, J Electrostat **52**, 25 (2001).

[11] P. Kebarle, and U. H. Verkerk, *On the Mechanism of Electrospray Ionization Mass Spectrometry (ESIMS), in Electrospray and MALDI Mass Spectrometry: Fundamentals, Instrumentation, Practicalities, and Biological Applications* Second Edition (ed R. B. Cole), John Wiley Sons, Inc., Hoboken, NJ, USA. (2010).

[12] R. J. Pfeifer, and C. D. Hendricks, *Parametric Studies of Electrohydrodynamic Spraying*, AIAA 66 (1967). Conference paper.

[13] D. J. Im, *Next generation digital microfluidic technology: Electrophoresis of charged droplets*, Korean J. Chem. Eng. **32**, 1001 (2015).

[14] D. Choi, H. Lee, D. J. Im, I. S. Kang, G. Lim, D. S. Kim, and K. H. Kang, *Spontaneous electrical charging of droplets by conventional pipetting*, Sci. Rep. **3**, 2037 (2013).

[15] L. Rayleigh, *On the Equilibrium of Liquid Conducting Masses Charged with Electricity*, Philos. Mag. **14**, 184 (1882).

[16] P. R. Brazier-Smith, M. Brook, J. Latham, C. P. R. Saunders, and M. H. Smith, *The Vibration of Electrified Water Drops*, Proc. R. Soc. Lond. A **322**, 523 (1971).

[17] C. P. R. Saunders, and B. S. Wonu, *Vibrational frequencies of freely falling chargedwater drops*, J. Atmos. Sol.-Terr. Phys. **36**, 707 (1974).

[18] R. J. A. Hill, and L. Eaves, *Shape oscillations of an electrically charged diamagnetically levitated droplet*, Appl. Phys. Lett. **100**, 114106 (2012).

[19] D. Duft, H. Lebius, B. A. Huber, C. Guet, and T. Leisner, *Shape Oscillations and Stability of Charged Microdroplets*, Phys. Rev. Lett. **89**, 084503 (2002).

[20] D. Duft, T. Achtzehn, R. Muller, B. A. Huber, and T. Leisner, *Coulomb fission - rayleigh jets from levitated microdroplets*, Nature **421**, 128 (2003).

[21] E. Giglio, B. Gervais, J. Rangama, B. Manil, B. A. Huber, D. Duft, R. Muller, T. Leisner, and C. Guet, *Shape deformations of surface-charged microdroplets*, Phys. Rev. E **77**, 036319 (2008).

[22] T. Achtzehn, R. Muller, D. Duft, and T. Leisnera, *The Coulomb instability of charged microdroplets: dynamics and scaling*, Eur. Phys. J. D **34**, 311 (2005).

[23] S. I. Betelu, M. A. Fontelos, U. Kindelán, and O. Vantzos, *Singularities on charged viscous droplets*, Phys. Fluids **18**, 051706 (2006).

[24] R. M. Thaokara, and S. D. Deshmukh, *Rayleigh instability of charged drops and vesicles in the presence of counterions*, Phys. Fluids **22**, 034107 (2010).

[25] Abbé Nollet, *Recherches sur les causes particulières des phénomènes électriques et sur les effets nuisibles ou avantageux qu'on peut en attendre* Paris (1752).

[26] M. Gamero-Castano, *The structure of electrospray beams in vacuum*, J. Fluid Mech. **604**, 339 (2008).

[27] R. A. Millikan, *On the elementary electrical charge and the avogadro constant*, Phys. Rev. **2**, 109 (1913).

[28] M. Jalaal, B. Khorshidi, and E. Esmaeilzadeh, *An experimental study on the motion, deformation and electrical charging of water drops falling in oil in the presence of high voltage D.C. electric field*, Exp. Therm. Fluid Sci. **34**, 1498 (2010).

[29] D. J. Im, J. Noh, D. Moon, and I. S. Kang, *Electrophoresis of a Charged Droplet in a Dielectric Liquid for Droplet Actuation*, Anal. Chem. **83**, 5168 (2011).

[30] M. Chiesa, J.A. Melheim, A. Pedersen, S. Ingebrigtsen, and G. Berg, *Forces acting on water droplets falling in oil under the influence of an electric field: numerical predictions versus experimental observations*, Eur. J. Mech. B-Fluid **24**, 717 (2005).

[31] J. Eggers, *Nonlinear dynamics and breakup of free-surface flows*, Rev. Mod. Phys. **69**, 919 (1997).

[32] M. A. Fontelos, U. Kindelán, and O. Vantzos, *Evolution of neutral and charged droplets in an electric field*, Phys. Fluids **20**, 092110 (2008).

[33] Sir G. Taylor, *Disintegration of Water Droplets in an Electric Field*, Proc. R. Soc. A **280**, 383 (1964).

[34] V. M. Ortega-Jimenez, and R. Dudley, *Spiderweb deformation induced by electrostatically charged insects*, Sci. Rep. **3**, 02108 (2013).

[35] Oleg.V. Salata, *Tools of Nanotechnology: Electrospray*, Curr. Nanosci. **1**, 25 (2005).

[36] A.B. Theberge, F Courtois, Y. Schaerli, M. Fischlechner, C. Abell, F. Hollfelder, and W.T.S. Huck, *Microdroplets in Microfluidics: An Evolving Platform for Discoveries in Chemistry and Biology*, Angew. Chem. Int. Ed. **49**, 5846 (2010).

[37] H. Zhouab, and S. Yao, *Electrostatic charging and control of droplets in microfluidic devices*, Lab Chip 13, 962 (2013).

[38] B. Ahn, K. Lee, R Panchapakesan, and K. W. Oh, *On-demand electrostatic droplet charging and sorting*, Biomicrofluidics **5**, 024113 (2011).

[39]] M. Gunji, and M. Washizu, *Self-propulsion of a water droplet in an electric field*, J. Phys. D **38**, 2417 (2005).

[40] A. H.C. Ng, B. B. Li,M. D.Chamberlain, and A. R. Wheeler, Digital Microfluidic Cell Culture Biomedical Engineering **17** 91 (2015).

[41] R. B. Fair, *Digital microfluidics: is a true lab-on-a-chip possible?*, Microfluid Nanofluidics **3**, 245 (2007).

[42] D. R. Link, E. Grasland-Mongrain, A. Duri, F. Sarrazin, Z. Cheng, G. Cristobal, M. Marquez, and D. A. Weitz, *Control of Droplets in MicrofluidicDevices*, Angew. Chem. Int. Ed. **45**, 2556 (2006).

[43] A. R. Thiam, N. Bremond, and J. Bibette, *Breaking of an Emulsion under an ac Electric Field*, PRL **102**, 188304 (2009).

[44] W. Thomson, *On a self-acting apparatus for multiplying and maintaining electric charges, with applications to the Voltaic Theory*, Proc. R. Soc. Lond. **16**, 67 (1867).

[45] A. R. Jones, and K. C. Thong, *The production of charged monodisperse fuel droplets by electrical dispersion*, J. Phys. D: Appl. Phys. **4**, 1159 (1971).

[46] D. B. Hibbert, *Introduction to electrochemistry*, MacMillan, Basingstoke, (1993).

[47] K. Choi, M. Im, J. Choi, and Y. Choi, *Droplet transportation using a pre-charging method for digital microfluidics*, Microfluid Nanofluidics 12, 821 (2012).

[48] Á. G. Marín, W. van Hoeve, P. García-Sánchez, L. Shui, Y. Xie, M. A. Fontelos, J. C. T. Eijkel, A. van den Berg, and De. Lohse, *The microfluidic Kelvin water dropper*, Lab Chip 13, 4503 (2013).

[49] D. Terwagne, F. Ludewig, N. Vandewalle, and S. Dorbolo, *The role of the droplet deformations in the bouncing droplet dynamics*, Phys. Fluids **25**, 122101 (2013).

[50] J. Hu, and J. L. Rovey, *Faraday cup with nanosecond response and adjustable impedance for fast electron beam characterization*, Rev. Sci. Instrum. **82**, 073504 (2011).

[51] S. Matsusaka, H. Maruyama, T. Matsuyama, and M. Ghadiri, *Triboelectric charging of powders: A review*, Chem. Eng. Sci. **65**, 5781 (2010).

[52] *Low Level Measurements Handbook - 7th Edition - Precision DC Current, Voltage, and Resistance Measurements*, Keithley, Tektronix.

[53] D. Kucerovsky, and Z. Kucerovsky, *Analysis of the dynamic Faraday cup*, J. Phys. D: Appl. Phys. **36**, 2407 (2003).

[54] M. Brandenbourger, *Gouttes chargées*, **Master thesis** (2012).

[55] D. Foresti, M. Nabavi, and D. Poulikakos, *On the acoustic levitation stability behaviour of spherical and ellipsoidal particles*, J. Fluid Mech. **709**, 581 (2012).

[56] Lord Rayleigh, *Investigations in Capillarity:—The size of drops.—The liberation of gas from supersaturated solutions.—Colliding jets.—The tension of contaminated water-surfaces*, Philos. Mag. **48**, 321 (1899).

[57] G. P. Neitzel, and P. Dell'Aversana, *Noncoalescence and nonwetting behavior of liquids*, Annu. Rev. Fluid Mech. **34**, 267 (2002).

[58] Y. Amarouchene, G. Cristobal, and H. Kellay, *Noncoalescing Drops*, Phys. Rev. Lett. **87**, 206104 (2001).

[59] K. R. Sreenivas, P. K. De, and J. H. Arakeri, *Levitation of a drop over a film flow*, J. Fluid Mech. **380**, 297 (1999).

[60] A. Duchesne, C. Savaro, L. Lebon, C. Pirat, and L. Limat, *Multiple rotations of a drop rolling inside a horizontal circular hydraulic jump*, EPL **102**, 64001 (2013).

[61] Y. Couder, E. Fort, C.-H. Gautier, and A. Boudaoud, *From Bouncing to Floating: Noncoalescence of Drops on a Fluid Bath*, Phys. Rev. Lett. **94**, 177801 (2005).

[62] T. Gilet, D. Terwagne, N. Vandewalle, and S. Dorbolo, *Dynamics of a Bouncing Droplet onto a Vertically Vibrated Interface*, Phys. Rev. Lett. **100**, 167802 (2008).

[63] S. Dorbolo, D. Terwagne, N. Vandewalle, and T. Gilet, *Resonant and rolling droplet*, New J. Phys. **10**, 113021 (2008).

[64] J. W. Bush, *The new wave of pilot-wave theory*, Phys. Today **68**, 47 (2015).

[65] W. D. Ristenpart, J. C. Bird, A. Belmonte, F. Dollar, and H. A. Stone, *Non-coalescence of oppositely charged drops*, Nature **461**, 377 (2009).

[66] R. T. Hilger, M. S. Westphall, and L. M. Smith, *Controlling Charge on Levitating Drops*, Anal. Chem. **79**, 6027 (2007).

[67] M. S. Westphall, K. Jorabchi, and L. M. Smith, *Mass Spectrometry of Acoustically Levitated Droplets*, Anal. Chem. **80**, 5847 (2008).

[68] J. Molacek, and J. W. M. Bush, *Drops bouncing on a vibrating bath*, J. Fluid Mech. **727**, 582 (2013).

[69] J. Leidenfrost, *De aquae communis nonnullis qualitatibus tractatus* Ovenius (1756).

[70] D. Quere, *Leidenfrost Dynamics*, Annu. Rev. Fluid Mech. **45**, 197 (2013).

[71] F. Celestini, and G. Kirstetter, *Effect of an electric field on a Leidenfrost droplet*, Soft Matter **8**, 5992 (2012).

[72] L. Maquet, M. Brandenbourger, B. Sobac , A. L. Biance, P. Colinet, and S. Dorbolo, *Leidenfrost drops: Effect of gravity*, EPL **110**, 24001 (2015).

[73] R. S. Hall, S. J. Board, A. J. Clare, R. B. Duffey, T. S. Playle, and D. H. Poole, *Inverse Leidenfrost Phenomenon*, Nature **224**, 266 (1969).

[74] M. Adda-Bedia, S. Kumar, F. Lechenault, S. Moulinet, M. Schillaci, and D. Vella, *Inverse Leidenfrost Effect: Levitating Drops on Liquid Nitrogen*, Langmuir **32**, 4179 (2016).

[75] M. Le Merrer, C. Clanet, D. Quéré, E. Raphaël, and F. Chevyd, *Wave drag on floating bodies*, PNAS **108**, 15064 (2011).

[76] L. Maquet, B. Darbois-Texier, A. Duchesne, M. Brandenbourger, B. Sobac, A. Rednikov, P. Colinet, and S. Dorbolo, *Leidenfrost drops on a heated liquid pool*, Accepted for publication in PRF (2016).

[77] P.N. Tshibangu, S. N. Ndwandwe, and E. Dixon Dikio, *Density, Viscosity and Conductivity Study of 1-Butyl-3-Methylimidazolium Bromide*, Int. J. Electrochem. Sci. **6**, 2201 (2011).

[78] H. Moretto, M. Schulze, and G. Wagner, *Ullmann's encycplopedia of industrial chemistry* Wiley, Weinheim (2012).

[79] M. I. Newton, D. L. Herbertson, S. J. Elliott, N. J. Shirtcliffe, and G. McHale, *Electrowetting of liquid marbles*, J. Phys. D: Appl. Phys. **40**, 20 (2007).

[80] D. B. Hibbert, *Introduction to electrochemistry* MacMillan, Basingstoke (1993).

[81] J. F. Mora, G. J. Van Berkel, C. G. Enke, R. B. Cole, M. Martinez-Sanchez, and J.B. Fenn, *Electrochemical processes in electrospray ionization mass spectrometry*, J. Mass Spectrom. **35**, 939 (2000).

[82] S. E. Law, *Charge and Mass Flux in the Radial Electric Field of an Evaporating Charged Water Droplet: An Experimental Analysis*, IEEE Trans. Ind. Appl. **25**, 1081 (1989).

[83] J. V. Iribarne, and B. A. Thomson, *On the evaporation of small ions from charged droplets*, J. Chem. Phys. **64**, 2287 (1976).

[84] C. J. Hogan, P. Biswas, and D. Chen, *Charged Droplet Dynamics in the Submicrometer Size Range*, J. Phys. Chem. B **113**, 970 (2009).

[85] C. B. Moore, and B. Vonnegut, *Measurements of the electrical conductivities of air over hot water*, J. Atmos. Sci. **45**, 885 (1987).

[86] D. Retalis, A. Pitta, and P. Psallidas, *The Conductivity of the Air and Other Electrical Parameters in Relation to Meteorological Elements and Air Pollution in Athens*, Meteorol. Atmos. Phys. **46**, 197 (1991).

[87] W. C. Swinbank, *Collisions of Cloud droplets*, Nature **159**, 850 (1947).

[88] M. H. Davis, and J. D. Sartor, *Theoretical Collision Efficiencies for Small Cloud Droplets in Stokes Flow*, Nature **215**, 1371 (1967).

[89] F. Y. Testik, *Outcome regimes of binary raindrop collisions*, Atmos. Res. **94**, 389 (2009).

[90] K. V. Bread, H. T. Ochs, and S. Liu, *Collision between Small Precipitation Drops. Part III: Laboratory Measurements at Reduced Pressure*, AMS **58**, 13995 (2001).

[91] C. N. Franklin, P. A. Vaillancourt, M. K. Yau, and P. Bartello, *Collision Rates of Cloud Droplets in Turbulent Flow*, AMS **62**, 2451 (2005).

[92] N. Ashgriz, and J. Y. Poo, *Coalescence and separation in binary collisions of liquid drops*, J. Fluid Mech. **221**, 183 (1990).

[93] J. Qian, and C. K. Law, *Regimes of coalescence and separation in droplet collision*, J. Fluid Mech. **331**, 59 (1997).

[94] C. Gotaas, P. Havelka, H. A. Jakobsen, and H. F. Svendsen, *Evaluation of the impact parameter in droplet-droplet collision experiments by the aliasing method*, Phys. Fluids **19**, 102105 (2007).

[95] K. V. Beard, R. I. Durkee, and H. T. Ochs, *Coalescence Efficiency Measurements for Minimally Charged Cloud Drops*, JAS **59**, 233 (2002).

[96] J. C. Bird, W. D. Ristenpart, A. Belmonte, and H. A. Stone, *Critical Angle for Electrically Driven Coalescence of Two Conical Droplets*, PRL **103**, 164502 (2009).

[97] J. Wang, B. Wang, and H. Qiu, *Coalescence and Breakup of Oppositely Charged Droplets*, Sci. Rep. **4**, 7123 (2014).

[98] K. Okumura, F. Chevy, D. Richard, D. Quéré, and C. Clanet, *Water spring: A model for bouncing drops*, Europhys. Lett. **62**, 237 (2003).

[99] D. Terwagne, F. Ludewig, N. Vandewalle, and S. Dorbolo , *The role of the droplet deformations in the bouncing droplet dynamics*, Phys. Fluids **25**, 122101 (2013).

[100] Lord Rayleigh, *On the Capillary Phenomena of Jets*, Proc. R. Soc. London **29**, 71 (1879).

[101] P. Drude, *Zur Elektronentheorie der metalle*, Annalen der Physik. **306**, 566 (1900).

[102] P. Drude, *Zur Elektronentheorie der Metalle; II. Teil. Galvanomagnetische und thermomagnetische Effecte*, Annalen der Physik. **308**, 369 (1900).

[103] D. Terwagne, N. Mack, S. Dorbolo, T. Gilet, J.-Y. Raty, and N. Vandewalle, *The mayonnaise droplet*, CHAOS **19**, 041105 (2009).

[104] M.M. Nicolson, *The interaction between floating particles*, Proc. Cambridge Philos. Soc. **45**, 288 (1949).

[105] P. A. Kralchevsky, and K. Nagayama, *Capillary interactions between particles bound to interfaces, liquid films and biomembranes*, Adv. Colloid Interface Sci. **85**, 145 (2000).

[106] F. Moisy, M. Rabaud, and K. Salsac, *A synthetic Schlieren method for the measurement of the topography of a liquid interface*, Exp Fluids **46**, 1021 (2009).

[107] F. Celestini, T. Frisch, and Y. Pomeau, *Take Off of Small Leidenfrost Droplets*, PRL **109**, 034501 (2012).

[108] T Umeki, M Ohata, H Nakanishi, and M Ichikawa, *Dynamics of microdroplets over the surface of hot water*, Sci. Rep. **5**, 8046 (2015).

[109] J. C. Ahern, *The Influence of Electric Charge and Electric Fields on the Formation and Duration of Water Boules*, **PhD Thesis** (2003).

[110] Lord Rayleigh, *The influence of electricity on colliding water drops*, Proc. R. Soc. Lond. **28**, 405 (1879).

[111] R. S. Allan, and S. G. Mason, *Effect on electric fields on coalescence in liquid+liquid systems*, Trans. Faraday Soc. **57**, 2027 (1961).